The axonal ER couples translation and secretion machineries for local delivery of axonal transmembrane proteins to promote axonal development

Ha H. Nguyen[1], Noortje Kersten[1], Chun Hei Li[1], Huey de Jong[1], Tanuj Arora[1], Themistoklis Liolios[1], Dan T. M. Nguyen[1], Maarten P. Bebelman[1], Maarten Altelaar[2], Max Koppers[3], Ginny G. Farías[1,4*]

[1] Cell Biology, Neurobiology and Biophysics, Department of Biology, Faculty of Science, Utrecht University, 3584 CH Utrecht, the Netherlands

[2] Biomolecular Mass Spectrometry and Proteomics, Bijvoet Center for Biomolecular Research and Utrecht Institute for Pharmaceutical Sciences, Utrecht University, 3584 CH Utrecht, the Netherlands

[3] Center for Neurogenomics and Cognitive Research, Department of Functional Genomics, Vrije Universiteit Amsterdam, 1081HV Amsterdam, the Netherlands

[4] Lead Contact;

[*] Correspondence: g.c.fariasgaldames@uu.nl (G.G.F.).

HIGHLIGHTS

- Transmembrane proteins (TMPs) are locally translated and secreted within the axon
- Axonal ER-associated ERES components mediate unconventional secretion
- HDLBP and NRZ-SEC22B complex couple local translation and secretion to PM via ERES
- Local TMP translation and secretion are essential for axonal development

SUMMARY

Proper neuronal development and function rely on the polarized sorting of transmembrane proteins (TMPs) to their distinct somatodendritic or axonal domains. Most TMPs follow a conventional secretory pathway confined to the cell soma, where they are translated at the rough ER, exit through ER exit sites (ERES) to reach the Golgi apparatus (GA), prior to their delivery to the plasma membrane (PM). Intriguingly, we recently found that many mRNAs encoding TMPs are associated with the axonally-enriched ER-protein P180, which facilitates axonal ER-ribosome interaction and regulates local translation. Given the absence of the GA in the axon, it remains unknown how locally synthesized TMPs leave the ER and reach the axonal PM. Here, we visualized the translation of different axonal TMPs within the axon and followed their trafficking from the ER. We found that a fraction of neosynthesized cargos follow an unconventional route, exiting the axonal ER and reaching the PM independent of the GA. Notably, we identified axonal ERES components tightly associated with the axonal ER. Removal of these components prevents TMP exit from the axonal ER, while addition of external cues increases the number of axonal ERES and Golgi-bypassing cargos. Moreover, we identified the ER-translation regulator HDLBP and the NRZ-SEC22B vesicular tether complex associated with axonal ERES and involved in unconventional secretion. Local removal of axonal ERES components or depletion of these identified players causes defects in axon growth and bouton assembly. We propose a novel mechanism coupling local TMP translation and secretion to the PM at the axonal ER, which is essential for neuronal development.

KEYWORDS: Neurons, unconventional secretion, Golgi-bypass, local translation, ER exit sites, axonal ER, HDLBP, SEC22B, NRZ tethering complex, axon development, pre-synaptic bouton assembly

INTRODUCTION

Neurons are highly polarized and morphologically complex cells, serving as the fundamental functional units of the nervous system. They consist of a cell body from which thick, branched dendrites and a long, thin axon emerge. These different neuronal compartments exhibit distinct molecular components and functions, which are important for neurons as signal integration centers. In humans, axons can extend up to one meter in length, resulting in a total surface area that may be thousands of times larger than that of the soma. This large surface area demands substantial amounts of membranes and proteins in the axon.[1,2] Additionally, during development and synaptic activity, axons need to grow extensively and respond quickly to intracellular signals and ongoing changes in their external environment.[3–5] Therefore, to ensure proper neuronal growth and maintain axonal function, precise spatiotemporal regulation of the axonal proteome is required.

RNA localization and local translation allow axons to regulate their proteome in response to local demand, playing a vital role during axonal development and synaptic activity.[6] Axons possess the necessary translational machinery[7–9] and studies employing compartment-specific transcriptome and translatome analyses have identified thousands of mRNAs localized and translated within axons.[8,10,11] Interestingly, a significant portion of these are mRNAs encoding transmembrane proteins (TMPs).[8,12–14] These include neuronal cell adhesion molecules, guidance and signaling receptors, and synaptic proteins, suggesting that translation of TMPs occurs along the axon and has an impact during different stages of neuronal development. Most TMPs follow a conventional secretory pathway, where they are translated at the rough endoplasmic reticulum (ER), exit through ER exit sites (ERES) and sorted to the Golgi apparatus (GA), before being delivered to their target locations at the plasma membrane (PM). However, major components of the secretory pathway including the rough ER and the GA are restricted to the somatodendritic domain in CNS neurons,[15,16] raising fundamental questions about local TMP biogenesis and trafficking in axons, which lack these conventional secretory organelles. Notably, axons harbor extensive ER tubules that associate with ribosomes to regulate local translation in an extrinsic cue-dependent manner.[17] Many mRNAs encoding TMPs are associated with P180/RRBP1, an axonally-enriched ER protein that facilitates the interaction of ribosomes with the axonal ER to regulate local translation.[17] Yet, how axonally synthesized TMPs exit the ER and whether the axon has the capacity for local secretion of neosynthesized TMPs to the PM remain elusive.

In this study, we demonstrate that TMPs such as adhesion molecules and synaptic proteins can be locally synthesized within developing axons. We find a fraction of neosynthesized cargos following an unconventional route, exiting the axonal ER and reaching their target locations at the PM, independent of the GA. Interestingly, we identify the ERES protein complex along the axon, tightly associated with the axonal ER. Depletion of axonal ERES components results in retention of nascent TMPs in the axonal ER, while neuronal stimulation increases ERES formation and promotes the secretion of Golgi-bypassing cargos. Moreover, we uncover key molecular components proximal to axonal ERES, including the ER-associated translation regulator HDLBP and the NRZ-SEC22B vesicle tethering complex, which facilitate this unconventional trafficking route. Local removal of axonal ERES components or depletion

of identified proteins involved in unconventional secretion causes defects in axonal growth and bouton assembly. We propose a novel mechanism coupling axonal translation and secretion of TMPs to the PM, which is critical for axon development.

RESULTS

Axonal TMPs are locally synthesized in the axon of primary rat and iPSC-derived human neurons

Many mRNAs encoding TMPs have been identified in axonal transcriptome and translatome datasets.[8,11,12,14] It remains unknown where translation for TMPs takes place along the axon. To visualize translation of TMPs in the axon, we performed puromycin labeling coupled with a proximity ligation assay (puro-PLA) (**Figure 1A**).[18] In short, two antibodies, one targeting puromycin and another one targeting a TMP (POI) were used. If they bind to the same molecule, a bridge between them will be formed by hybridization of oligonucleotide secondary probes, allowing for further signal amplification, indicating translation sites of the POI. We set out to visualize the axonal translation of the synaptic protein Synaptotagmin-1 (SYT1), and the adhesion molecules Neurexin-1 (NRXN1α) and L1CAM in primary rat hippocampal neurons and iPSC-derived human cortical neurons. These proteins play critical roles in axonal development and maintenance.[19–21] Although SYT1 and NRXN1α proteins are actively produced in the cell soma, we found that they can also be locally translated in the axon of rat hippocampal neurons at day in vitro (DIV) 10 (**Figures 1B, D**) The number of Puro-PLA puncta along the axon was normalized to total axon area using the axonal neurofilament marker SMI-312 (**Figures 1B-E**). There was a significant difference between neurons treated with puromycin for 10 minutes compared to those pre-treated with the translation inhibitor anisomycin, indicating the specificity of this assay (**Figures 1B-E**). Since external cues have been shown to increase local protein synthesis and neuronal activity,[9,22–24] we stimulated neurons with BDNF for 30 minutes before puromycin labeling. Interestingly, upon BDNF stimulation, there was a significant increase in local SYT1 translation (from 2.679 to 3.407 puncta per 100 μm^2), indicating that translation of SYT1 can be cue-induced (**Figures 1B, C**). On the other hand, BDNF stimulation caused only a slight increase in the number of nascent NRXN1α protein (**Figures 1D, E**). We observed a higher number of newly synthesized SYT1 (±2.679 puncta) compared to NRXN1α (±1.08 puncta) in 100um^2 axon area, suggesting a higher translational rate for SYT1 along the axon (**Figures 1C, E**). We also observed SYT1 being synthesized at branching points and axon tips (**Figure 1F**), consistent with ER-ribosome interactions enriched in these axonal sub-compartments.[17,25,26] Moreover, we found that axonal synthesis of TMPs is not restricted to rat hippocampal neurons, as we also observed local translation for SYT1, NRXN1α and L1CAM in axons of human cortical iNeurons at DIV24, with similar abundance to rat neurons (**Figures 1G-L**). These results show that different TMPs can be locally synthesized in axons, including in axon branches and axon tips, and that their translation increases upon neuronal stimulation.

Newly synthesized TMPs undergo unconventional secretion from the axonal ER

Since we observed translation of TMPs occurring along the axon, we wondered whether these could be locally secreted. Consistent with previous findings, we confirmed that the GA and derived Golgi outposts are absent in the axon (**Figures S1A, B**).[15,16,27] To determine whether these newly synthesized proteins have the capability to be secreted from the axonal ER, we used the Retention Using Selective Hook (RUSH) system. This method allows the retention of POIs in the ER and their synchronous release upon the addition of biotin, to follow their

sorting.[28] We first used the ER retention sequence KDEL or the invariant chain of class II MHC as a hook coupled to Streptavidin, and our protein of interest (SYT1, NF186 and L1CAM) coupled to a Streptavidin binding peptide (SBP) and an mNeonGreen (mNG) fluorescent tag in its cytoplasmic domain for cargo visualization (**Figure 2A**). We found that at timepoint 0 (no biotin), our cargos are properly retained at the ER, with an enrichment in the somatodendritic domain (**Figures S2A-C**). Upon addition of biotin for 15 minutes, we observed their sorting to the somatic GA, followed by their localization to specific compartments after 24h. SYT1 properly reached synaptic vesicles and the PM, NF186 localized to the axon initial segment PM, and L1CAM distributed along the axonal PM (**Figures S2A-C; Video S1A, B**). To study unconventional secretion, independent of somatodendritic ER-GA sorting, we used Brefeldin A (BFA). BFA targets Arf1 GTPase, preventing COP-I binding to the GA, which eventually leads to overall ER-GA trafficking defects and GA fragmentation (**Figures S3A, B**).[29] The COPI components α - and β-COP were restricted to the somatodendritic domain in control and BFA-treated cells (**Figures S3C, D**). For the RUSH system, BFA was added to the culture medium for 30 minutes, immediately followed by the addition of D-biotin for 4 hours (**Figure 2B**). Release of SYT1 from the ER after 4 hours of biotin addition showed the distribution of SYT1 vesicles along the axon, with an average of 33 SYT1-positive vesicles per 100 µm axon (**Figure 2C, D; Figure S3E**). Upon BFA treatment, we found that most SYT1 signal was detected in the somatic ER (**Figure S3F**). Interestingly, we observed a portion of SYT1 secreted independently of the Golgi, with an average of 15 vesicles per 100 µm axon (**Figure 2C, D; Figure S3F**). Similar results were observed for NF186 and L1CAM (**Figures S3E, F**). Since local translation of SYT1 in the axon increased upon BDNF stimulation (**Figures 1B, C**), we wondered if this also promotes local secretion of SYT1 in the axon. We stimulated neurons pretreated with BFA during biotin release for 4 hours, and indeed, this led to an increase in the number of Golgi-bypassing cargos, from ± 15 cargos to ± 27 cargos per 100 µm axon (**Figure 2C, D**). The presence of cargos along the axon was not due to inefficient ER-Golgi trafficking blockage, as the somatodendritic transferrin receptor (TfR) was efficiently blocked (**Figure S3G**). Live cell imaging during BFA incubation showed no clear translocation of Golgi bypassing vesicles from soma to axon, suggesting cargo release from the axonal ER (**Video S1C, D**). To further confirm that unconventional secretion occurs from the axonal ER, without blocking conventional secretion, we utilized a truncated version of the axonally-enriched ER-protein P180 as a hook (Strep-P180ΔCC) (**Figure 2E**).[30] Live cell imaging for SBP-SYT1-mNG revealed initial tubular ER signal in the axon and the appearance of newly secreted proteins confined to brighter vesicular compartments within 30 minutes of biotin addition (**Figure 2F; Video S2A**). We observed ER bending and cargo budding from the ER in the distal axon after biotin addition (**Figure 2G**). Some SYT1 vesicles became diffusive, while others underwent transport or remained stably attached to the ER (**Figure 2G; Video S2B**). To verify that vesicles present along the axon can be locally secreted from the axonal ER, we performed axon cutting with a 355nm photoablation laser prior to biotin-induced ER release (**Figure 2H**; **Figures S4A, B**). Similar to intact axons, we observed local TMP secretion from the ER in desomatized axons (**Figures 2I, J; Video S3**). These different assays provide evidence that TMPs can be locally secreted from the axonal ER in a GA-independent manner.

Axonal ERES, tightly associated with the axonal ER, are required for unconventional secretion

We next sought to gain insight into how locally secreted proteins exit the ER. Although the GA or Golgi outposts are excluded from CNS axons,[15,16,27] a previous study found the ERES

component SAR1 enriched along the forming axon during neuronal polarization.[31] However, it remains unknown if all ERES components are present along the axon in polarized neurons and if axonal ERES participate in unconventional protein secretion. We found different ERES components in the axon of rat hippocampal neurons at different stages of development (**Figure 3A; Figures S5A-D**). Endogenous staining of SEC31A protein and overexpression of V5-tagged SEC31A showed a similar abundance of axonal ERES puncta (**Figures S5E, F**). We found that ERES components highly colocalized with each other in the axon, suggesting they form a complex (**Figures 3A, B**). To determine if these ERES components are indeed associated with the ER and are not COPII-decorated vesicles, we performed live cell imaging for the ERES marker GFP-SEC23A. Most puncta exhibited little mobility along the axon (**Figures S5G-I**). Importantly, BFA treatment did not interfere with the presence of ERES components in the axon or their dynamics (**Figures S5J-L**). Using a SoRa spinning disk super-resolution microscope, we further observed ERES stably associated with tubular axonal ER and some short-range ERES movement associated with tubular ER rearrangement (**Figure 3C; Video S4**). To examine whether the axonal ER is required for distribution of ERES along the axon, we removed the ER from the axon. For this, we used an established Strep/SBP heterodimerization system that relocates the axonal ER to the somatodendritic domain via the minus-end directed KIFC1 motor (**Figure 3D**).[17,30,32] ER tubule removal from the axon resulted in removal of axonal ERES, indicating that axonal ERES components are tightly associated to the axonal ER (**Figures 3E, F**).

We then assessed the requirement of axonal ERES for unconventional cargo release. We first expressed a SAR1B-H79G mutant together with the RUSH-SYT1 construct. This SAR1B-GTP mutant (H79G) directly inhibits ERES complex function.[33,34] Expression of SAR1B-H79G in neurons impaired ERES and cargo distribution along the axon (**Figure S5M-O**). To determine whether local ERES are required for axonal unconventional secretion, we developed a rapalog-induced FKBP/FRB heterodimerization system to remove axonal ERES components by coupling SEC23A to the KIFC1 motor (**Figure 3G**). We first confirmed that SEC23A was efficiently removed from the axon (**Figure 3H,** see also related **Figure 6A-G**). Then, neurons were transfected with RUSH-SYT1, together with FKBP-SEC23A and KIFC1-FRB. Rapalog or vehicle were added to culture medium immediately after transfection for 16 hours to allow for efficient removal of axonal ERES components. BFA was added to the medium for 30 minutes, followed by biotin-induced cargo release for 4h together with BDNF. Removal of ERES complexes from the axon significantly reduced the number of RUSH-SYT1 Golgi-bypassing cargos, indicating that axonal ERES mediate TMP exit from the ER (**Figures 3I, J**).

We observed BDNF-induced local translation (**Figure 1**) and increased Golgi-bypassing cargos (**Figure 2**) along the axon. Previous evidence has shown that BDNF induces insertion of some TMPs at the dendritic PM for proper neuronal response.[35,36] Thus, we wondered if BDNF could reorganize axonal ERES to promote fusion of neosynthesized TMPs with the PM upon this increased demand. We observed more ERES along the axon after cue stimulation, suggesting they increase in number to accommodate increased cargo demands at the axonal PM (**Figures 3K, L**). To determine whether these cargos are inserted at the PM, we performed HA live surface labeling with RUSH-SYT1-mNG, which contains an HA tag in the luminal/extracellular domain of SYT1 (**Figure 3M**). We found that under BFA treatment, newly secreted SYT1 could still reach the PM, although to a lesser extent than conventional cargos (**Figures 3N, O**). Interestingly, BDNF stimulation increased Golgi-bypassing cargos fusing with the PM (**Figures 3N, O**).

Together, these results show that the ERES complex, which is tightly associated with the axonal ER, supports cue-induced unconventional cargo sorting to the axonal PM.

Identification of translation and secretion machineries associated with axonal ERES

We next aimed to identify potential key players involved in unconventional protein secretion in the axon. We combined the proximity labeling APEX2 system[37] with proteomics to study the interactome of neuronal ERES (**Figure S6A**). We employed the ERES component SEC13 as bait (APEX2-V5-SEC13). We first validated SEC13-dependent proximal biotinylation by imaging and western blot (**Figures S6B, C**). In our mass spec data from rat neurons, we found known interactors of SEC13, including other COPII components and ER and Golgi proteins (**Figures S6D, E**). Moreover, we found several interesting proteins enriched near SEC13, which could have potential roles at different stages of the unconventional secretion pathway (**Figure 4A**). Among these candidates, HDLBP stood out as particularly interesting for various reasons. HDLBP is an RNA-binding protein recently found to predominantly bind to ER-targeted mRNAs, promoting synthesis of transmembrane and secretory proteins.[38] Intriguingly, HDLBP interacts with the ER-associated P180/RRBP1 protein[39], which we previously found to be enriched along the axon and involved in axonal translation (**Figure S6F)**.[17,30] This suggests a possible link between translation and secretion. These processes are well segregated in the conventional pathway, where secretion at ERES takes place in ribosome-free regions.[40,41] To determine whether axonal translation and ERES machineries can be in proximity, we first visualized SYT1 translation sites with the Puro-PLA system and their co-distribution with the ERES marker SEC23A in the axon. We observed instances of close proximity between translation sites and ERES in axon shafts and branching points (**Figure 4B**). We then assessed the distribution of endogenous HDLBP along the axon and similarly observed its presence along the axon and enrichment in branching points and axonal tips (**Figure 4C**). These results suggest the coupling of TMP translation and ERES machineries along the axon.

Another interesting set of candidates enriched in our APEX2-SEC13 mass spec data was the NRZ tethering complex (NBAS, RINT1 and ZW10) and the SNARE SEC22B, which could mediate cargo exit from the axonal ER and/or fusion with the PM. The NRZ complex is tethered to the ER via its interaction with SEC22B[42] (**Figure S6F**). Recent work has also linked both the NRZ complex and SEC22B to ERES-dependent secretion.[43–45] We first looked at the localization of these proteins in the axon in control condition and under BFA treatment. We found them present in the axonal shaft, in axonal branching points and axonal tips (**Figure 4D**). The distribution of all candidate proteins remained unchanged after BFA treatment (**Figure 4D**). To determine whether these tethering proteins are in proximity to ERES, we visualized ZW10, NBAS and SEC22B together with SEC23A. Though the signal of ZW10 was mostly continuous along the axon, we observed enrichment of this protein next to SEC23A (**Figures 4E, F**). NBAS and SEC22B puncta were also found near SEC23A (**Figures 4G-J**). Interestingly, we found SEC22B colocalizing with Golgi-bypassing cargos after BFA treatment, suggesting its possible involvement in cargo secretion (**Figures 4K, L**). We observed the co-movement of SYT1 Golgi-bypassing cargos and SEC22B in a slow bi-directional, short movement along the axon, similar to that of axonal ERES (**Figure 4M; Video S5**). When visualized together with either ZW10 or NBAS, a portion of SEC22B puncta also colocalized with these proteins and had similar movement in the axon (**Figures 4N, O; Video S5**). This suggests that HDLBP and the NRZ-SEC22B tethering complex could function in concert with ERES to coordinate translation and secretion for unconventional cargo delivery to the PM.

Coupling of translation and secretion machineries promotes unconventional cargo secretion via HDLBP and NRZ-SEC22B tethering complex

Since HDLBP has been shown to bind to RNA and regulate translation of TMPs in non-neuronal cells,[38] we wondered if HDLBP is also involved in axonal TMP translation. We first validated a shRNA targeting HDLBP by qPCR (**Figure S7A**). We then performed knockdown of HDLBP in combination with SYT1 Puro-PLA assay to visualize SYT1 axonal translation. Compared to our scramble shRNA control, HDLBP knockdown led to reduced SYT1 translation, from ±14 translation sites/100 µm in scramble shRNA control to ±9 sites/100 µm in HDLBP knockdown condition (**Figures 5A, B**). As we observed close proximity between TMP translation sites and ERES (**Figures 4B**), we wondered whether HDLBP-dependent translation and cargo exit from the ER are functionally coupled. To investigate this, we visualized RUSH-SYT1-mNG unconventional secretion in the presence of scrambled or HDLBP shRNA. Briefly, neurons were transfected with shRNA together with RUSH-SYT1-mNG construct for 4 days, and biotin and BDNF were added to the medium after 30-min BFA incubation as in **Figure 2B, C**. Interestingly, we found that HDLBP knockdown impaired unconventional cargo secretion in the axon, indicating axonal TMP translation and ER exit are coupled (**Figures 5C, D**).

The SNARE SEC22B recycles between the ER and acceptor membrane, and binds SEC23/24 at ERES in its unassembled form prior to SNARE complex assembly-dependent membrane fusion [44,45]. On the other hand, the SEC22B-interacting NRZ tethering complex has been suggested to recruit acceptor membranes to ERES for cargo exit.[43,45] Given the co-distribution of SEC22B and NRZ complex with each other and with axonal ERES (**Figure 4E-O**), we wondered if they could play a role during unconventional secretion of TMPs along the axon. Thus, we transfected neurons with shRNAs targeting SEC22B, ZW10, and NBAS together with RUSH-SYT1-mNG as described above. The efficiency of these shRNAs was also validated by qPCR (**Figures S7B-D**). We observed a similar reduction in the number of SYT1 Golgi-bypassing cargos for the knock-down of SEC22B and NRZ complex proteins, compared to control (**Figures 5C, D**). This indicates that these proteins play a key role in cargo exit at axonal ERES.

We then wondered whether the NRZ-SEC22B complex could also regulate the insertion of TMPs at the PM after ER exit. To investigate the role of HDLBP, ZW10, NBAS and SEC22B in regulating the fusion of Golgi-bypassing cargos with the PM, we knocked them down and visualized the total RUSH-SYT1 vesicular pool with mNG and its surface pool with HA surface labelling, as in **Figures 3M-O**. We quantified the percentage of Golgi-bypassing cargos that were also positive for HA staining, indicating their fusion with the PM. As expected, knockdown of HDLBP did not change the ability of SYT1 to reach the PM (**Figures 5E, F**). Interestingly, we found that knock-down of either ZW10, NBAS, or SEC22B resulted in a reduced percentage of unconventional cargos reaching the PM (30% of cargos for ZW10, 22.4% for NBAS, and 22.5% for SEC22B, with respect to 42% in control) (**Figures 5E, F**). These results, together with their co-distribution and co-dynamics (**Figure 4E-O**), suggest that an NRZ-associated compartment might be recruited at ERES by SEC22B, for SEC22B and cargo exit at ERES. This NRZ-associated compartment could then target cargos to the PM (**Figure 5G**).

Altogether, these results show that HDLBP is involved in axonal TMP translation and ER-exit, but not in TMP delivery to the PM. ZW10, NBAS and SEC22B, on the other hand, are involved in both cargo exit from the ER and further delivery to the axonal PM.

Unconventional TMP secretion promotes axon growth and synaptic bouton maturation during axonal development

TMPs such as adhesion molecules and synaptic proteins shown here, undergoing axonal translation and unconventional secretion, have essential roles in axon development and maintenance.[19,46–48] Therefore, we wondered if perturbation of local unconventional secretion results in defects in axon development and maintenance. To study this, we developed a Strep-SBP heterodimerization tool for long-term local removal of axonal ERES components. In this system, the ERES protein SEC23A is coupled to SBP and the KIFC1 motor is coupled to Strep (**Figure 6A**). Removal of SEC23A from the axon efficiently depleted V5-SEC13 and endogenous SEC31A from the axon (**Figures 6B-E**), confirming that the ERES complex was removed, while the axonal ER was still present (**Figures 6F, G**). We first investigated whether unconventional axonal secretion is required during early stages of development. Previous studies have depleted the ERES component SAR1 but found conflicting results regarding its contribution to axon growth.[31] Here, we transfected neurons at DIV2 with our axonal ERES heterodimerization tool and fixed them at DIV4. We observed that by removing the ERES complex from the axon, the primary axon length was significantly reduced, from ± 331 µm in control to ± 282 µm (**Figures 6H, I).** We also found that the total axon arborization was reduced, from ± 890 µm in control to ± 692 µm, indicating a decrease in overall axon growth **(Figures 6H, J)**. These results support a local role of ERES in axon development.

To study the role of identified proteins involved in unconventional secretion on axon development, we transfected DIV1 neurons with scramble shRNA control, or shRNAs targeting HDLBP, ZW10, NBAS, or SEC22B. Similar to what was observed for the removal of axonal ERES components, knockdowns of these proteins resulted in shorter primary axons (from ±475 µm in control to ±323 µm in HDLBP, ±372 µm in ZW10, ±398 µm in NBAS, and ±356 µm in SEC22B knockdown conditions) **(Figures 6K, L)** and total axon arborization (from ±2059 µm in control to ±1048 µm in HDLBP, ±1208 µm in ZW10, ±1243 µm in NBAS, and ±1476 µm in SEC22B knockdown conditions) **(Figures 6K, M).** This suggests that unconventional secretion from axonal ERES, regulated by HDLBP and NRZ-SEC22B complex, is essential for axon growth.

During neurodevelopment, after axon elongation and branching, the assembly of presynaptic boutons and eventually functional synapses is of great importance. Synapse formation and maintenance is a complex process that requires many TMPs to be recruited and assembled in pre- and post-synapses.[49–51] Local protein synthesis is critical for the development and function of these synapses, especially under stimulation.[9,52] Therefore, we wondered whether unconventional secretion of newly synthesized proteins in the axon plays a role in pre-synaptic bouton assembly. We first performed local removal of axonal ERES components using our Strep-SBP heterodimerization tool (**Figure 6A**). Neurons were transfected on DIV14 with SEC23A-SBP and KIFC1-Strep heterodimerization system. Co-expression of a fluorescent protein (fill) was used to identify pre-synaptic boutons in transfected axons. DIV17-18 neurons were then fixed and stained for the peripherally synaptic vesicle-associated protein Synapsin-I (SYN1) to identify mature presynaptic boutons. Removal of axonal ERES components led to a lower number of boutons that were positive for SYN1, from ±5.2 boutons in control to ±3.1 boutons after removal, suggesting that local secretion is required for synapse assembly (**Figures 7A, B**).

Next, we studied the role of ERES-associated proteins involved in unconventional secretion in pre-synaptic bouton assembly. We transfected DIV12-14 neurons with a fluorescent fill and scrambled shRNA control, or shRNAs targeting HDLBP, ZW10, NBAS, or SEC22B. Neurons were then fixed at DIV16-18 and stained for Synapsin-I, as described above. Knockdown of

these proteins led to similar results as for the removal of ERES components. We found a reduction in the number of mature boutons, from ±6.2 boutons in scrambled control to ±2.8 boutons in HDLBP, ±3 boutons in ZW10, ±2.6 boutons in NBAS, and ±2.6 boutons in SEC22B knockdown conditions (**Figures 7C, D**).

Together, these results indicate that unconventional secretion, via local ERES and key interacting machineries, is essential for axon development and pre-synaptic bouton assembly.

DISCUSSION

For many years, it has been believed that the supply of TMPs to the axon strictly depends on their production and trafficking from the soma. In this study, we show that TMPs can be locally translated and secreted in axons. TMPs exit the ER via local ERES complexes tightly associated with the axonal ER. Depletion of axonal ERES components leads to the retention of unconventionally secreted cargos at the ER, while cue stimulation leads to concomitant increase in local ERES number and cargo insertion at the PM. We further identified the ER-translation regulator HDLBP, and the membrane tethering NRZ-SEC22B complex associated with axonal ERES. We propose a mechanism in which the axonal ER couples translation and secretion machineries via ERES to control local cue-induced TMP delivery to the axonal PM (**Figure 7E**). This axonal unconventional protein secretion plays a key role during axon growth and pre-synaptic bouton assembly (**Figure 7E**).

Several translatomic studies have shown local synthesis of TMP mRNAs in isolated axons.[8,11,53] Consistent with these findings, we found several TMPs locally translated in the axon of primary rat hippocampal neurons and iPSC-derived human cortical neurons by imaging using the Puro-PLA assay. These include synaptic vesicle proteins and adhesion molecules involved in axon pathfinding and elongation,[46,47,54] and in synapse formation and maintenance.[19,48,55] These newly synthesized TMPs were distributed along the axon shaft and present in axon branching points and axon tips. Interestingly, upon BDNF stimulation, we observed an increase in the synthesis of SYT1, consistent with previous studies showing cue-induced axonal translation.[22–24] This cue-induced TMP translation regulation could provide a fast response to local and temporal requirements at the axonal PM.

By using multiple methods, we have shown that axonal TMPs can be secreted, independently of the GA, from the axonal ER to the PM. In dendrites, some neosynthesized TMPs are confined to dendritic ER sheets,[56] sorted to ER-Golgi intermediate compartments (ERGICs) and then to Golgi outposts (GO)[15,57] or Golgi satellites (GS)[58–61] prior to delivery to the PM, independent of the GA. This could serve as a local machinery that allows dendritic TMPs to be secreted in distal branches without traversing the GA in the soma. In PNS axons, which also contain ER sheets,[62] it has been shown that the TMP TRPM8, at steady state, utilizes a pGolt/TGN38/RAB6-positive GS, to reach the axonal PM.[63] This local trafficking route is highly dependent on the presence of GBF1, an ARF1-GEF that is essential for COPI vesicle formation.[63] In line with previous observations in CNS axons, we detected no cis- or trans-Golgi markers within the axon.[15,27,57] This points to a Golgi-bypassing mechanism that operates independently of Golgi-derived structures in CNS axons. Consistent with this, COPI components were notably absent from the axon, and upon disruption of ER-Golgi transport with BFA, a subset of TMPs was still able to exit the axonal ER and reach the PM. It remains unknown whether core-glycosylated TMPs exiting the axonal ER can be locally processed by glycosidases and glycosyltransferases prior to their insertion at the PM. Interestingly, previous studies have shown that many core-glycosylated dendritic and axonal TMPs are sorted to the

PM, without being processed at the GA.[64–66] These proteins maintain their functionality, indicating that further glycosylation steps are not strictly required for TMP function.

The ERES complex plays an essential role in the conventional secretory pathway, enabling cargos to exit the ER for sorting to the GA or related GO and GS.[60,67,68] However, whether ERES contributes to unconventional TMP secretion remained unknown. Interestingly, the ERES component SAR1 has been found enriched along the forming axon during axon specification at DIV2-3 in CNS neurons.[31] Here, we found that the different ERES components are present along the axon of polarized neurons across developmental stages. These ERES components colocalized, forming ERES complexes that were stable even after BFA treatment. ERES components remained tightly associated with the axonal ER, with no clear evidence of dynamic COPII-coated vesicles, which is consistent with recent evidence showing that COPII components remain associated with the ER membrane rather than translocating with the cargo to acceptor membranes.[69] Importantly, axonal removal of ERES components impaired Golgi-bypassing cargo exit from the ER. Consistent with our observation of increased TMP axonal translation upon cue stimulation, we found an increased number of Golgi-bypassing cargos reaching the PM. Concomitantly, we observed an increase in the number of ERES, which likely supports a higher demand for specific TMPs at the axonal PM. The mechanism behind ERES number increase remains unknown. It is unlikely that cytosolic ERES components diffuse or are transported from the soma, as this would not allow for a rapid, localized response to meet spatiotemporal demands. Instead, we suggest that cytosolic ERES components are already distributed along the axon and assembled locally on the ER membrane within subdomains for local and fast delivery of newly synthesized TMPs to the PM.

Given that axonal length and area far exceed those of the soma, it is unlikely that the molecular machineries for translation, ER exit, and secretion are spatially segregated. Our APEX-SEC13 proximity labeling combined with proteomic analysis in primary rat neurons revealed a set of candidate proteins localized in close proximity to ERES. These candidates may play crucial roles in coordinating translation and secretory processes within the axon. One such protein is HDLBP, an RNA-binding protein that selectively binds to ER-targeted mRNAs and interacts with the ER-resident and axon-enriched protein P180.[38,39] We previously found that P180 binds TMP mRNAs and is essential for axonal translation regulation.[17] Here, we found that HDLBP knockdown significantly reduced SYT1 synthesis in the axon, further supporting the existence of an axonal ER-associated translation machinery responsible for local TMP production. Notably, we found TMP translation sites near axonal ERES, suggesting coupling of TMP translation and ER exit along the axon. Indeed, we found that HDLBP knockdown also impaired the release of cargo from the axonal ER.

The close spatial association between translation and ER exit machineries likely facilitates their functional coupling. However, a question remains as to how cargos subsequently reach the PM. Vesicle tethering proteins are critical mediators of membrane fusion events between donor and acceptor compartments.[70,71] In our proteomic analysis, we identified components of the NRZ vesicle tethering complex as well as the SNARE SEC22B. In this study, we observed these components distributed along the axon and they were required for cargo exit and subsequent targeting to the axonal PM. The NRZ complex, composed of NBAS, RINT1, and ZW10, has traditionally been implicated in Golgi-to-ER retrograde transport.[42] SEC22B facilitates membrane fusion and is involved in different steps of vesicular transport.[45] In anterograde trafficking, SEC22B, in its unassembled form, interacts with the SEC23A/SEC24A complex, allowing for its trafficking from the ER to acceptor compartments.[45] The NRZ complex interacts with and stabilizes the ER-resident SNARE complex, consisting of SEC22B, BNIP, STX18, and USE1.[42] Together, the NRZ - ER SNARE

complex is conventionally shown to receive COPI-coated vesicles from the Golgi to the ER.[42] Indeed, a recent study showed that the NRZ complex tethers and recruits ERGIC membrane to ERES,[43] creating a tunnel between the ER and Golgi for collagen export.[72] Besides its role in ER-Golgi protein trafficking, emerging evidence has linked this complex to non-canonical secretory pathways[73] Building on these findings, in the narrow confines of the axon, the NRZ complex could facilitate a similar mechanism by tethering the ERES to a vesicular compartment for SEC22B and cargo exit from the ER and targeting to the PM (**Figure 5G**). Thus, the unique properties of the NRZ-SEC22B complex, its ability to bridge organelles and recruit membranes, enable a pathway by which locally translated TMPs can bypass conventional somatic trafficking to achieve rapid, targeted delivery to the axonal surface.

We further studied the role of axonal ERES and its coupling to translation and secretion machineries in axon elongation and pre-synaptic bouton assembly. During early development, axons navigate through their environment via dynamic responses and interactions with extracellular cues at axonal growth cones or tips. These interactions are created and maintained by TMPs such as specialized cell adhesion molecules (CAMs), receptors, ion channels at the axon tip.[4,46,47,74] Similarly, in later stages of development, the localization and function of these TMPs play significant roles in synapse formation and maintenance, where the complex and intricate assembly of molecules in the pre-and post-synaptic compartments is tightly regulated.[19,48,55] Here we show that removal of axonal ERES components or knockdown of HDLBP and NRZ-SEC22B complex at different developmental stages caused reduced primary axon length, total arborization, and impaired pre-synaptic bouton assembly. Our results demonstrate that the local and coupled TMP translation and secretion in axons plays a key role during axonal development. These findings open new questions for future research. For instance, how does this local axonal machinery for TMP production and secretion contribute to the axonal proteome? Do local translation and secretion diversify TMP and neuron functioning? Finally, considering mutations in ER-resident proteins that alter axonal ER organization also cause Hereditary Spastic Paraplegia (HSP) and Amyotrophic Lateral Sclerosis (ALS), what is the contribution of axonal ER-associated translation and secretion defects to disease?

Altogether, our findings reveal a Golgi-independent, axon-intrinsic secretory pathway that enables the local translation, ER export, and PM insertion of TMPs in CNS axons. This process is mediated by local ERES and associated translation and secretion machineries. Its response to external cues further supports the adaptability of this pathway to meet spatiotemporal axonal needs. Although it is unclear to what extent this pathway can be applied, we found its significance at different stages of neuronal development, underscoring the physiological importance of localized TMP translation and trafficking for proper neuronal development and maintenance.

ACKNOWLEDGEMENTS

We thank Derk Draper (Farías Lab) for providing the SBP-HA-APPwt-mNeonGreen construct and Professor Dr. Judith Klumperman (University Medical Center Utrecht, NL) for providing the pIRES-neo3-Strep-Ii-LAMP2-SBP-FKBP-GFP construct. We thank Professor Dr. Anna Akhmanova (Utrecht University, NL) for providing critical feedback and discussion during the project. This work was supported by the European Research Council (ERC-StG 950617) to G.G.F., Target ALS Foundation (NI-2024-NAI-S5) to G.G.F., and European Research Council (ERC-StG 101163280) to M.K.

AUTHOR CONTRIBUTIONS

H.H.N. designed and performed experiments, analyzed data, and wrote the manuscript. N.K. designed, cloned constructs and performed experiments to validate the ERES pulling assay. C.H.L. performed mass spectrometry experiments and was supported by M.A. H.J. designed constructs and performed experiments related to axon morphology with heterodimerization system. T.A. and T.L. designed, cloned constructs and performed initial optimizations. D.T.M.N. performed experiments and analyzed qPCR data related to shRNA knockdown. M.B. established human iPSC culture and neuron differentiation protocols and provided iNeurons. M.K. provided feedback and edited the manuscript. G.G.F. designed experiments, supervised the research, coordinated the study, and wrote the manuscript.

DECLARATION OF INTERESTS

The authors declare no competing interests.

MAIN FIGURE TITLES AND LEGENDS

Figure 1. Axonal TMPs are locally synthesized in the axon of primary rat and iPSC-derived human CNS neurons

(A) Schematic representation of puro-PLA assay.

(B-E) Representative images of SYT1 (B) and NRXN1α (D) translation sites in DIV10 primary rat hippocampal axons labelled with SMI-312, under only puromycin labeling, anisomycin pretreated, or BDNF pretreated conditions. Quantification of newly synthesized SYT1 (C) and NRXN1α (E) per 100 μm^2 axon.

(F) Representative images of SYT1 translation sites in branching points or axon tips, indicated by white arrow heads.

(G-L) Representative images of SYT1 (G), NRXN1α (I), and L1CAM (K) translation sites in DIV24-26 iPSC-derived human cortical neurons under only puromycin labeling or anisomycin pretreated conditions. Quantification of SYT1 (H), NRXN1α (J) and L1CAM (L) translation sites per 100 μm^2 axon.

Data are presented as box-and-whisker plots in (C, E, H, J, L). Individual data points each represent an axon area and each color per condition represents an independent experiment. ns = non-significant, **$p < 0.01$, ***$p<0.001$, ****$p<0.001$ comparing conditions with control using ordinary one-way ANOVA test, followed by a Dunnett's multiple comparisons test (C), Kruskal-Wallis test followed by Dunn's multiple comparisons test (E), or Mann-Whitney tests (H, J, L). Scale bars represent 20 μm in (B, D, G, I, and K) and 5 μm in (F).

Figure 2. Locally translated TMPs undergo unconventional secretion from the axonal ER

(A) Schematic representation of the RUSH system to track cargo trafficking from the ER. Upon biotin addition, cargos are released, accumulated at the GA and sorted to the PM (upper panel). BFA treatment is used to block ER-GA trafficking and to assess if cargo can exit the ER and reach the PM (lower panel).

(B-D) Schematic showing the timeline of different treatments before fixation (B). Representative images of RUSH-SYT1 cargo distribution in DIV10-11 axons at timepoint 0, 4h biotin release, 4h biotin release with BFA, and 4h biotin release with BFA and BDNF (C).

Quantification of RUSH-SYT1 cargo numbers per 100 μm axon (D). See also Figure S2, S3 and Video S1.

(E-G) Schematic representation of the RUSH system with axonal ER hook (E). Time series from Video S2A showing the ER retention and release of RUSH-SYT1 with P180ΔCC hook over 60 minutes at 20-second intervals (F). Time series from Video S2B showing RUSH-SYT1 exit from the ER in the distal axon at 1-minute intervals for 120 minutes (G).

(H-J) Schematic representation of the RUSH system with axonal ER hook in combination with axon severance by photo ablation using 355nm laser (H). Representative image of a neuron expressing the RUSH-P180ΔCC-SYT1 system after axon cutting. The blue arrow points to ablation site (I). Time series from Video S3 showing two axon segments imaged at 20-second intervals for 60 minutes. Arrowheads point to new cargo exiting the axonal ER (J). See also related Figure S4.

Data are presented as box-and-whisker plots (D). Individual data points each represent a neuron, and each color per condition represents an independent experiment. **$p < 0.01$, ****$p<0.001$ comparing conditions using ordinary one-way ANOVA test followed by a Tukey's multiple comparisons test (D). Scale bars represent 10 μm in (C, F, I, and J) and 2 μm in (G).

Figure 3. ERES components are tightly associated with the axonal ER and are required for unconventional secretion

(A-B) Representative images of DIV9-10 axons expressing SEC23A together with SEC24D, SEC31A or SEC16B (A). Quantification of colocalization between SEC23A and SEC24D, SEC31A or SEC16B (B).

(C) Representative still and time-lapse from zoomed regions showing the tight association between SEC23A and the axonal ER labelled with SEC61β. Images were acquired at 1-second intervals for 80 seconds. See Video S4.

(D-F) Schematic showing the Strep-SBP heterodimerization system using Strep-KIFC1 and SBP-RTN4 to relocate axonal ER to the soma (D). Representative images of SEC23A and RTN4 in DIV10 neurons in the absence (control) or presence of KIFC1 motor (pulled) (E). Quantification of SEC23A number from conditions in (E) in 100 μm axons (F).

(G-J) Schematic showing the FKBP-FRB heterodimerization system using KIFC1-FRB and FKBP-SEC23A to relocate axonal ERES components to the soma (G). Representative images of SEC23A treated with ethanol (vehicle, control) or Rapalog for 16h (H). Representative images of RUSH-SYT1 cargos in neurons treated as in (H) for 16h, prior biotin addition for 4h in the presence of BFA and BDNF (I). Quantification of RUSH-SYT1 cargo number from conditions in (I) in 100 μm axons (J).

(K-L) Distribution of SEC23A in the axon in control BSA and after 30 min BDNF stimulation (K). Quantification of SEC23A puncta number per 100 μm axon (L).

(M-O) Schematic showing the timeline of different treatments before fixation (M). Representative images of DIV10-11 neurons expressing RUSH-SYT1 after 4h biotin release, 4h biotin release and pre-treated with BFA alone, or 4h biotin release together with BFA and BDNF. Live cell surface labeling for HA-tag inserted in the luminal/extracellular domain of RUSH-SYT1, allows for the visualization of SYT1 fusion with the PM (N). Quantification of the percentage of released cargos fusing with the PM (O).

See also related Figure S5.

Data are presented as box-and-whisker plots in (B, F, J, L, O). Individual data points each represent a neuron, and each color per bar represents an independent experiment. *$p < 0.05$, **$p < 0.01$, *** $p < 0.001$, ****$p<0.001$ comparing conditions using unpaired t-test in (F, J, L) or ordinary one-way ANOVA test followed by Tukey's multiple comparisons test in (O). Scale bars represent 10 μm in (A, E, H, I, K, N), 5 μm in the overview image, and 1 μm in cropped images in (C).

Figure 4. Identification of translation and secretion machineries associated with axonal ERES

(A) Volcano plot showing the interactome of SEC13 in neurons. Proteins that are enriched near SEC13 are in yellow and potential key candidates are highlighted in magenta.

(B) Representative images of SYT1 translation sites with Puro-PLA assay in close proximity to SEC23A in the axon.

(C-D) Distribution of endogenous HDLBP (C), and endogenous HDLBP, NBAS and ZW10 and low expression of SEC22B in axons from neurons treated or not with BFA (D).

(E-J) Localization and enrichment of ZW10 (E), NBAS (G) and SEC22B (I) near SEC23A in DIV10 axons and magnifications of merged images. Intensity profile lines from magnified merged images are shown in (F, H and J).

(K-L) Localization of SEC22B near Golgi-bypassing RUSH-SYT1 cargos after 4h biotin release in DIV10 axons, treated with BFA and BDNF. Intensity profile line from magnified merged image is shown in (L).

(M-O) Time series showing colocalization and co-movements of SEC22B with Golgi-bypassing RUSH-SYT cargos after BFA treatment for 30 minutes (M), ZW10 (N) or NBAS (O). Images were acquired at 1-second intervals for 3 minutes. Arrowheads point to the colocalized regions.

See also related Figure S6 and Video S5.

Scale bars represent 5 μm in (B, E, G, I, K, M, N, O), 1 μm in magnified images in (E, G, I, K), and 10 μm in (C, D).

Figure 5. Coupling of translation and secretion machineries promotes unconventional cargo secretion via HDLBP and NRZ-SEC22B tethering complex

(A-B) Representative images of SYT1 translation sites using the Puro-PLA assay in axons of DIV9-10 neurons expressing scramble shRNA (control) or shRNA targeting HDLBP (A). Quantification of newly synthesized SYT1 number per 100 μm axon (B).

(C-D) Representative images of DIV11 neurons expressing RUSH-SYT1, together with shRNA scramble or shRNAs targeting HDLBP, ZW10, NBAS or SEC22B. Neurons were treated with BFA, biotin and BDNF for 4h (C). Quantification of Golgi-bypassing cargo number for conditions in (C) in 100 μm axon (D).

(E-F) Representative images of DIV11 neurons transfected as in (C). Live cell surface labeling for HA-tag incorporated to the luminal/extracellular side of RUSH-SYT1. Arrowheads point to RUSH-SYT1 cargos that are also positive for HA labeling (E). Quantification of the percentage of Golgi-bypassing cargos fusing with the PM (F).

(G) Model schematic for the coupling of translation and secretion machineries at local ERES in axon via HDLBP and NRZ-SEC22B tethering complex.

See also related Figure S7.

Data are presented as box-and-whisker plots in (B), or as mean values ± SEM in (D, F). Individual data points each represent a neuron, and each color per condition represents an independent experiment. ns = non-significant, *$p < 0.05$, *** $p < 0.001$, ****$p<0.001$ comparing conditions using Mann-Whitney test in (B), Kruskal-Wallis test followed by Dunn's multiple comparisons test in (D), or ordinary one-way ANOVA test followed by Dunnett's multiple comparisons test in (F). Scale bars represent 10 μm in (A, C, E).

Figure 6. Unconventional secretion of TMPs promotes axon growth

(A-C) Schematic showing the Strep-SBP heterodimerization system using Strep-KIFC1 and SBP-SEC23A to relocate axonal ERES components to the soma (A). Representative images of neurons DIV9 co-transfected with SBP-SEC23A and V5-SEC13 in the absence (control) or presence of Strep-KIFC1 (pulled) (B). Quantification of SEC23A and SEC13 puncta in axon (C).

(D-E) Representative images of neurons transfected with SBP-SEC23A alone or with Strep-KIFC1 and stained for endogenous SEC31A (D). Quantification of SEC23A and endogenous SEC31A puncta in the axon (E).

(F-G) Representative images of neurons transfected with SBP-SEC23A alone or with Strep-KIFC1 and stained for endogenous RTN4 for axonal ER labeling (F). Quantification of average ER intensity in the axon (G).

(H-J) Representative images of DIV4 neurons transfected with a fill and the Strep-SBP heterodimerization system for the removal of axonal ERES components (H). Quantification of primary axon length (I) and total axon arborization (J). Arrowheads point to axons.

(K-M) Representative images of DIV4 neurons transfected with a fill and scramble shRNA or shRNAs targeting HDLBP, ZW10, NBAS or SEC22B (K). Quantification of primary axon length (L) and total axon arborization (M). Arrowheads point to axons.

Data are presented as mean values ± SEM in (C, E, G, I, J, L, M). Individual data points each represent a neuron, and each color per condition represents an independent experiment. ns = non-significant, **$p < 0.01$, ***$p < 0.001$, ****$p<0.001$ comparing conditions to control using Mann-Whitney test in (C, E (SEC23A), G, I) or unpaired t-test in (E(α-SEC31A), J), or Kruskal-Wallis test followed by Dunn's multiple comparisons test in (L, M). Scale bars represent 10 μm in (B, D, F), 100 μm in overview images in (H, K), and 20 μm in axon crops in (H).

Figure 7. Unconventional secretion of TMPs promotes pre-synaptic bouton assembly

(A-B) Representative images of DIV17 neurons transfected with a fill and SBP-SEC23A (control) or with Strep-KIFC1 (SEC23A pulled) as described in Figure 6A. Staining for endogenous Synapsin-I was performed to label mature pre-synaptic boutons. Arrowheads point to boutons positive for Synapsin-I (A). Quantification of mature bouton number in 50 μm axon length (B).

(C-D) Representative images of DIV17 neurons transfected with a fill and scramble shRNA or shRNAs targeting HDLBP, ZW10, NBAS, or SEC22B (C). Quantification of mature bouton number in 50 μm axon length (D).

(E) Coupling of local translation and secretion in the axon. Locally translated TMPs exit the ER via axonal ERES, followed by their delivery to the PM. This process is dependent on the translation regulator HDLBP and NRZ-SEC22B tethering complex and is enhanced upon cue stimulation. Removal of axonal ERES components or KD of proteins involved in unconventional secretion results in reduced axon growth and impaired pre-synaptic bouton assembly.

Data are presented as mean values ± SEM in (B, D). Individual data points each represent an axon segment, and each color per condition represents an independent experiment. ****$p<0.001$ comparing conditions to control using unpaired t-test in (B) or Kruskal-Wallis test followed by Dunn's multiple comparison test in (D). Scale bars represent 10 µm in (A, C).

SUPPLEMENTAL INFORMATION

Supplemental figure titles and legends

Figure S1. (Related to Figure 2). The Golgi apparatus (GA) and derived Golgi structures are absent from the axon

(A-B) Representative images of neurons DIV9 expressing a fill and stained for endogenous cis-GA marker GM130 (A) or trans-GA (B) marker in the soma and their absence in the axon (B).

Scale bars represent 10 µm in (A, B).

Figure S2. (Related to Figure 2). ER retention and tracking of RUSH cargo trafficking to the PM

(A-C) Representative images of neurons DIV10-11 expressing RUSH-SYT1 (A), RUSH-NF186 (B), or RUSH-L1CAM and their retention at timepoint 0, accumulation at the GA after 15 min and localization in target membranes after 24h. SYT1 localized to synaptic vesicles and PM, NF186 enriched at the axon initial segment (AIS) and L1CAM enriched along the axonal PM.

Scale bars represent 20 µm in (A-C).

Figure S3. (Related to Figure 2). Effects of Brefeldin A (BFA) treatment on the Golgi and COPI markers and on RUSH cargo release

(A-B) Representative images of neurons DIV9-10 transfected with a fill and stained for the cis-GA marker GM130 (A) or the trans-GA marker TGN38 (B) in control and after 30 min of BFA treatment. Images show their presence in control condition, association to GA fragments after BFA treatment and their absence in the axon.

(C-D) Representative images of neurons DIV9-10 co-expressing a fill and COPI components α-COP (C) or β-COP (D) in control and after 30 min of BFA treatment. Images show their localization to the GA in the soma in control, association to GA fragments after BFA treatment and their absence in the axon.

(E-F) Representative images of RUSH-SYT1, RUSH-NF186 and RUSH-L1CAM cargo distribution in the soma and axon after 4h biotin release (E) or pre-treated with BFA for 30 min and released for 4h (F).

(G) Representative images of RUSH-TfR cargo distribution in the soma, dendrite and axon after 4h biotin release or pre-treated with BFA for 30 min and released for 4h.

Scale bars represent 10 µm in (A-G).

Figure S4. (Related to Figure 2). Photoablation efficiently severs axon and blocks soma-axon transport

(A) Representative images of neurons transfected with RUSH-P180ΔCC-SYT1 and LAMP1-RFP which were subjected to photoablation. The blue arrows point to ablation site and the rectangle shows the region of axon where live-cell imaging was acquired.
(B) Time series showing movements of LAMP1 in region described in (A). Arrowheads point to LAMP1-positive compartments not being transported between the somatic and axonal regions. Images were acquired at 1-second intervals for 3 min.
Scale bars represent 20 µm in (A) and 10 µm in (B).

Figure S5. (Related to Figure 3). ERES components are distributed in axon as stationary complexes across developmental stages and inhibition of ERES assembly impairs cargo exit from the ER
(A) Schematic showing essential proteins at the ERES and their organization.
(B) Representative images of axons stained for endogenous SEC31 and Tubulin at DIV2, 4 and 7.
(C) Representative images of neurons expressing a fill and a pORANGE knock-in of SEC16A at DIV7, DIV14 and DIV17.
(D) Representative images of a DIV9 neuron expressing a fill and the SAR1A marker.
(E, F) Representative images of neurons DIV9 expressing a fill and stained for endogenous SEC31A or co-transfected with V5-SEC31A (E). Quantification of endogenous or overexpressed SEC31A puncta per 100 µm axon (F).
(G-L) Time series of neurons transfected with GFP-SEC23A in control (G) or after 30 min BFA treatment (J). Images were acquired at 1-second intervals for 3 min. Arrowheads point to examples of SEC23A puncta. Kymographs of axon segments in (G) and (J) were shown in (H) and (K), respectively. Quantification of number of anterograde, retrograde or stationary SEC23A puncta in the axon in control (I) or after BFA treatment (L).
(M) Representative images of neurons expressing GFP-SEC23A alone, or with SAR1B-H179G mutant.
(N-O) Representative images of neurons expressing RUSH-SYT1 alone or with SAR1B-H79G mutant (N). Quantification of RUSH-SYT1 cargo number in 100 µm axon in control and in condition where SAR1B-H79G was expressed (O).

Data are presented as box-and-whisker plots in (F, O) or as mean values ± SEM in (I, L). Individual data points each represent a neuron, and each color per condition represents an independent experiment. ns = non-significant, ****$p<0.001$ comparing conditions using unpaired t-test in (F) or Mann-Whitney test in (O). Scale bars represent 10 µm in (B, C, D, E, G, J, M and N).

Figure S6. (Related to Figure 4). Validation of SEC12-APEX2 tool, and identification of known proteins present in ERES interactome

(A) Schematic showing procedure for lentiviral infection of cortical neurons with SEC13-V5-APEX2, sample treatment and mass spectrometry analysis.

(B) Representative images of neurons transduced with SEC13-V5-APEX2, treated with biotin-phenol and with or without H_2O_2 as negative control. Expression of SEC13 is visualized with V5 antibody, and biotinylation is detected with conjugated Strep-555.

(C) Immunoblot of SEC13-V5-APEX2 transduced neurons with and without H_2O_2.

(D-E) Volcano plots showing the interactome of SEC13 in neurons. Proteins that are enriched near SEC13 are in yellow, other ERES proteins are shown in blue (D) and ER and GA proteins known to interact with ERES are in orange (E).

(F) Schematic showing the distribution and organization of potential candidates at the ER membrane.

Figure S7. (Related to Figure 5). Validation of shRNA knockdown efficiency with qPCR

(A-D) Quantitative PCR fold change of sh HDLBP (A), sh ZW10 (B), sh NBAS (C) and sh SEC22B (D) to scramble control. All values were normalized to respective GAPDH internal control. At least 2 experiments were done with 3 technological replicates per biological sample.

Supplemental videos

Video S1. Release of RUSH cargos in control and under BFA treatment

Video S2. Release of RUSH cargos with P180ΔCC axonal hook

Video S3. Release of RUSH cargos with P180ΔCC axonal hook in desomatized axons

Video S4. Axonal ERES components are tightly associated with the axonal ER

Video S5. Co-movements of SEC22B with RUSH-SYT1 Golgi-bypassing cargos, ZW10 and NBAS

Supplemental tables

Data Table 1 (Related to Figure 4A and Figure S6D and S6E). Data table containing analyzed proteomics data for SEC13-V5-APEX2 in cortical neurons.

Data Table 2 (Related to Figures 1-7 and Figures S5, S6 and S7). Table with the source/raw data for each quantification and uncropped blots presented in the figures and detailed experimental information including N replicates, n number and statistical tests.

STAR METHODS

KEY RESOURCES TABLE

REAGENT or RESOURCE	SOURCE	IDENTIFIER
Antibodies		
Mouse anti-Puromycin	Merck	MABE343; RRID:AB_2566826
Mouse anti-SMI-312	BioLegend	837904; RRID:AB_2566782
Chicken anti-MAP2	Abcam	Ab5392; RRID:AB_2138153
Rabbit anti-Synaptotagmin-1	Synaptic Systems	105 008; RRID:AB_2832236
Rabbit anti-Neurexin-1alpha	Frontier Institute / Nittobo Medical	MSFR104630; RRID:AB_2571817
Rabbit anti-L1CAM	Proteintech	20659-1-AP; RRID:AB_2878717
Rabbit-anti-TRIM46	van Beuningen et al.[75]	N/A
Mouse anti-V5	Thermo Fisher Scientific	R960-25; RRID:AB_2556564
Rat anti-HA	Roche	11867423001; RRID:AB_390918
Mouse anti-GM130	BD Biosciences	610823; RRID:AB_398142
Sheep anti-TGN38	Bio-Rad	AHP499G; RRID:AB_2203272
Mouse-anti-GFP	Thermo Fisher Scientific	A-11120; RRID:AB_221568
Mouse anti-mCherry	Takara Bio	CL 632543
Rabbit anti-SEC31A	Cell Signaling Technology	13466; RRID:AB_2798228
Mouse anti-β-Tubulin III	Sigma-Aldrich	T8660; RRID:AB_477590
Rabbit anti-HDLBP	Proteintech	15406-1-AP; RRID:AB_2117367
Rabbit anti-NBAS	Proteintech	14683-1-AP; RRID:AB_1959590
Rabbit anti-ZW10	Abcam	Ab21582; RRID:AB_779030
Rabbit anti-Synapsin-I	Millipore	AB1543; RRID:AB_2200400
Mouse anti-RTN4A	R and D systems	MAB3098; RRID:AB_10997139
Mouse anti-Pan-Neurofascin external	UC Davis / NIH NeuroMab	75-172; RRID:AB_2282826
Goat anti-mouse Alexa Fluor 405	Molecular Probes	A31553; RRID:AB_221604
Goat anti-Mouse IgG (H+L) Highly Cross-Adsorbed Alexa Fluor 488	Thermo Fisher Scientific	A-11029; RRID:AB_2534088
Goat anti-mouse Alexa Fluor 568	Thermo Fisher Scientific	A-11031; RRID:AB_144696
Goat anti-rabbit IgG (H + L) Highly cross-absorbed secondary antibody Alexa Fluor 405	Thermo Fisher Scientific	A-31556; RRID:AB_221605
Goat anti-mouse IgG2a cross-absorbed secondary antibody Alexa Fluor 594	Thermo Fisher Scientific	A-21135; RRID:AB_2535774
Goat anti-Mouse IgG (H+L) Highly Cross-Adsorbed Secondary Antibody, Alexa Fluor 647	Thermo Fisher Scientific	A-21236; RRID:AB_2535805
Goat anti-rabbit IgG (H + L) Highly cross-absorbed secondary antibody Alexa Fluor 405	Thermo Fisher Scientific	A-31556; RRID:AB_221605
Goat anti-Rabbit IgG (H+L) Highly Cross-Adsorbed Secondary Antibody, Alexa Fluor 488	Thermo Fisher Scientific	A-11034; RRID:AB_2576217
Goat anti-rabbit IgG (H+L) Highly Cross-Adsorbed CF®594	Sigma-Aldrich	SAB4600110
Goat anti-rabbit IgG (H + L) highly cross-absorbed secondary antibody Alexa Fluor 568	Thermo Fisher Scientific	A-11036; RRID:AB_10563566
Goat anti-Rabbit IgG (H+L) Highly Cross-Adsorbed Secondary Antibody, Alexa Fluor 647	Thermo Fisher Scientific	A-21245; RRID:AB_2535813
Goat anti-chicken IgY (H+L) Secondary Antibody, Alexa Fluor 488	Thermo Fisher Scientific	A-11039; RRID:AB_2534096
Goat anti-Chicken IgY (H+L) Secondary Antibody, Alexa Fluor 568	Thermo Fisher Scientific	A-11041; RRID:AB_2534098

Donkey anti-Sheep IgG (H+L) Cross-Adsorbed Secondary Antibody, Alexa Fluor 488	Thermo Fisher Scientific	A-11015; RRID:AB_2534082
Goat anti-Rat IgG (H+L) Cross-Adsorbed Secondary Antibody, Alexa Fluor 568	Thermo Fisher Scientific	A-11077; RRID:AB_2534121
Alexa-Fluor 555 conjugated Strep	Thermo Fisher Scientific	S21381; RRID:AB_2307336
Atto488 conjugated Fluotag-X4® GFP nanobody	NanoTag Biotechnologies	N0304-At488-L
Atto488 conjugated GFP-Booster nanobody	ChromoTek	gba488
Rabbit anti-mouse immunoglobulins/HRP	Agilent	P0260; RRID:AB_2636929
IRDye 800CW Streptavidin	LI-COR Biosciences	926-32230
Chemicals, peptides, and recombinant proteins		
Puromycin dihydrochloride	Sigma-Aldrich	P8833
Anisomycin	Sigma-Aldrich	9789
Lipofectamine 2000	Thermo Fisher Scientific	11668019
Fluoromount-G Mounting Medium	Thermo Fisher Scientific	00-4958-02
Anhydrous-DMSO	Thermo Fisher Scientific	D12345
Biotin	Sigma-Aldrich	B4501
Biotin-phenol	Iris Biotech	L-S.3500
H_2O_2	Sigma-Aldrich	H1009
Sodium Azide	Merck	K43547688
Sodium L-ascorbate	Sigma-Aldrich	0000374819
Trolox	Sigma-Aldrich	238813
Rapalog (A/C Heterodimerizer)	Takara Bio	635057
NeutrAvidin	Thermo Fisher Scientific	31000
Brefeldin A	Sigma-Aldrich	B5936
NAD+	Sigma-Aldrich	10127965001
Mix-n-Stain CF640R antibody labeling kit	Biotium	92245
Duolink® In Situ Detection Reagents FarRed	Sigma-Aldrich	DUO92013
Polyethylenimine (PEI MAX)	Polysciences	24765
Triton-X-100	Sigma-Aldrich	93433
Halo-JFX554 ligand	Kindly provided by the Lavis lab (Janelia)	N/A
Halo-JFX650 ligand	Kindly provided by the Lavis lab (Janelia)	N/A
Experimental models: Cell lines		
Human iPSCs (KOLF2.1)	Pantazis et al.[76]	N/A
HEK293T	ATCC	CRL-3216
Experimental models: Organisms/strains		
Rat (Wistar)	Janvier	N/A
Recombinant DNA		
FUGW	Kind gift from Dr. David Baltimore	Addgene; plasmid #14883
pLKO.1 puro	Kind gift from Dr. Bob Weinberg	Addgene; plasmid #8453
Str-KDEL_SBP-EGFP-Ecadherin	Kind gift from Dr. Frank Perez	Addgene; plasmid #65286
psPAX2	Kind gift from Dr. Didier Trono	Addgene; plasmid #12260
PMD2.G	Kind gift from Dr. Didier Trono	Addgene; plasmid #12259
pmScarlet-i-C1	Kind gift from Dr. Dorus Gadella	Addgene; plasmid #85044
Halo-TfR-RUSH	Kind gift from Dr. Jennifer Lippincott-Schwartz	Addgene; plasmid #166905
SAR1B-H79G-mOrange2	Kind gift from Dr. Jennifer Lippincott-Schwartz	Addgene; plasmid #166900
PEGFP-SEC22B	Kind gift from Dr. Thierry Gali	Addgene; plasmid #101918
pcDNA3.1-MS2-HA-HsNBAS_AA	Kind gift from Dr. Elisa Izaurralde	Addgene; plasmid #148236

mito-V5-APEX2	Kind gift from Dr. Alice Ting	Addgene; plasmid #72480
pEGFP-SEC23A	Kind gift from Dr. David Stephens	Addgene; plasmid #66609
pEYFP-SEC24D	Kind gift from Dr. David Stephens	Addgene; plasmid #66614
pDEST47-SAR1-GFP	Kind gift from Dr. Richard Kahn	Addgenel plasmid #67409
pORANGE Cloning template vector	Kind gift from Dr. Harold MacGillavry	Addgene; plasmid #131471
H2B-mNeonGreen-IRESpuro2	Kind gift from Dr. Daniel Gerlich	Addgene; plasmid #183745
PEGFP(A206K)-C1	Kind gift from Dr. Jennifer Lippincott-Schwarz	N/A
PEGFP(A206K)-N1	Kind gift from Dr. Jennifer Lippincott-Schwarz	N/A
GW1-GFP-ZW10	Kind gift from Dr. Peter van der Sluijs[77]	N/A
HA-NF186-mRFP-FKBP	Kind gift from Dr. Casper Hoogenraad[78]	N/A
HA-BicD2-FRB	Kind gift from Dr. Lukas Kapitein[79]	N/A
Halo-CLCa	Kind gift from Dr. Harold MacGillavry	N/A
pmCherry-N1	Clontech	N/A
mCherry-C1	Clontech	N/A
PGW2-mCherry	Kind gift from Dr. Lukas Kapitein[79]	N/A
PGW1-BFP	Kind gift from Dr. Lukas Kapitein[79]	N/A
V5-SEC16B	van Leeuwen et al.[80]	N/A
Halo-SEC61β	van Leeuwen et al.[80]	N/A
HA-KIFC1-Strep	Farías et al.[30]	N/A
mCherry-SBP-RTN4	Farías et al.[30]	N/A
P180-ΔCoiled-coil-GFP	Farías et al.[30]	N/A
RUSH-SYT1-mNeonGreen	This study	N/A
RUSH-SYT1-Halo	This study	N/A
RUSH-P180ΔCC-HA-SYT1-mNG	This study	N/A
RUSH-NF186-mNeonGreen	This study	N/A
RUSH-Ii-L1CAM-mNeonGreen	This study	N/A
V5-APEX2-SEC13-mNG	This study	N/A
GFP-SEC16A knock-in	This study	N/A
V5-SEC31A	This study	N/A
Halo-SEC24D	This study	N/A
SAR1B-H79G-GFP	This study	N/A
mCh-SBP-SEC23A	This study	N/A
GFP-SBP-SEC23A	This study	N/A
FLAG-FRB-KIFC1	This study	N/A
mCh-FKBP-SEC23A	This study	N/A
GFP-FKBP-SEC23A	This study	N/A
Halo-NBAS	This study	N/A
Halo-ZW10	This study	N/A
pLKO.1-puro rat scramble; shRNA targeting sequence (5'-gatgaaatattccgcaagtaa-3')	This study	N/A
pLKO-GFP rat scramble; shRNA targeting sequence (5'-gaaacaaatcggaaatctt-3')	This study	N/A
pLKO.1-puro rat HDLBP; shRNA targeting sequence (5'-atggtcaaagacctgattaat-3')	This study	N/A
pLKO.1-puro rat SEC22B; shRNA targeting sequence (5'-tcatcatgctgatagtgtatg-3')	This study	N/A
pLKO.1-puro rat ZW10; shRNA targeting sequence (5'-gactctgtcgtcctaaatttg-3')	This study	N/A

pLKO.1-puro rat NBAS; shRNA targeting sequence (5'-atgaccagaaaggccattaag-3')	This study	N/A
Software and algorithms		
QuantStudio Software V1.3	Applied Biosystems	https://quantstudio-design-analysis-software.software.informer.com/1.3/
MaxQuant (v2.0.1.0)	MPI of Biochemistry	https://www.maxquant.org/maxquant/
Perseus (v1.6.15.0	MPI of Biochemistry	https://maxquant.net/perseus/
R with R Studio (v4.5.0)	Bell Laboratories	https://www.r-project.org/
Fiji/ImageJ (v2.16.0/1.54p)	NIH	https://imagej.net/software/imagej/
GraphPad Prism (v10.1.1)	GraphPad	https://www.graphpad.com/
ComDet	Github	https://github.com/UU-cellbiology/ComDet
NeuronJ	Meijering et al.[81]	https://imagescience.org/meijering/software/neuronj/
MosaicJ	Thévenaz and Unser.[82]	https://bigwww.epfl.ch/thevenaz/mosaicj/

RESOURCE AVAILABILITY

Lead contact

Further information and requests for resources, plasmids and reagents should be directed to and will be fulfilled by the lead contact Ginny G. Farías (g.c.fariasgaldames@uu.nl).

Materials availability

Plasmids in this study will be deposited in Addgene or available upon request as of the date of publication.

Data and code availability

The mass spectrometry proteomics data generated in this study will be deposited to the ProteomeXchange Consortium via PRIDE prior publication. Analyzed proteomic data is available in Table S1. Raw data of all quantifications are available in Table S2. Any other data reported in this paper will be shared by the lead contact upon reasonable request.

EXPERIMENTAL MODEL AND SUBJECT DETAILS

Animals

All experiments were approved by the DEC Dutch Animal Experiments Committee (Dier Experimenten Commissie), performed in line with institutional guidelines of Utrecht University, and conducted in agreement with Dutch law (Wet op de Dierproeven, 1996) and European regulations (Directive 2010/63/EU). The animal protocol has been evaluated and approved by the national CCD authority (license AVD10800202216383). Female pregnant Wistar rats were obtained from Janvier, and embryos (both genders) at E18 stage of development were used for primary cultures of hippocampal neurons. Brains from these female rats were used to obtain protein extracts. At Janvier, rats were housed in a temperature and humidity-controlled facility at a 12h/12h light cycle in cages with spruce bedding with enrichment. Pregnancy was monitored by visual examination and weighing where a significant weight gain meant gestation. Pregnant females were then shipped to the Central Laboratory Animal Research Facility of Utrecht University where they were housed for 4 days in pairs under standard laboratory conditions and received food and water ad libitum. Pregnant females were then

euthanized, and embryos (E18) were harvested for primary neuronal cultures. The animals, pregnant females and embryos have not been involved in previous procedures.

Primary neuronal cultures and transfection

Primary hippocampal neurons were prepared from embryonic day 18 rat brains from which the hippocampi were dissected, dissociated in trypsin for 15 min at 37°C and plated at a density of 100,000/well or 50,000/well (12-well plates) on coverslips coated with poly-L-lysine (37.5 µg/mL; Sigma) and Laminin (1.25 µg/mL; Roche). For proteomics, cortices were dissected and dissociated as hippocampal neurons and plated at a density of 1,000,000/well (6-well plates). For experiments in developing neurons (until DIV11), neurons were maintained in neurobasal medium (NB; Gibco) supplemented with 2% B27 (Gibco), 0.5 mM Glutamine (Gibco), 15.6 µM Glutamate (Sigma), and 1% Penicillin/Streptomycin (Gibco) and incubated under controlled temperature and CO2 conditions (37°C, 5% CO2). For experiments in mature neurons (until DIV18), medium was refreshed at DIV10 by replacing half of the medium with BrainPhys (BP) neuronal medium supplemented with 2% Neurocult SM1 neuronal supplement and 1% Pen/Strep. For all RUSH experiments, B27 was subjected to biotin removal using Zebra™ Dye and Biotin Removal Spin Columns (Invitrogen) according to manufacturer's protocol.

Hippocampal neurons were transfected at day in vitro (DIV)1-2 (for DIV 4 experiments), or DIV7-9 (for DIV10-11 experiments) or DIV11-14 (for DIV16-18 experiments) using Lipofectamine 2000 (Invitrogen). Shortly, DNA (0.05-1.5 µg/well) was mixed with Lipofectamine 2000 (1.5-3.3 µL) in NB (Gibco, 200 µL) and incubated for 20 min at room temperature. Before transfection, half of the original medium from each well was stored (500 uL), and 200 uL was removed. For RUSH experiments, 700 uL of the original medium in each well was removed. The transfection mix was added to the neurons in the remaining NB+ medium and incubated for 1 hour at 37°C in 5% CO2. Then, 500 uL of original medium plus 500 uL of fresh NB or BP medium with supplements were added to each well. For RUSH experiments, neurons were transferred to a new plate containing 1 mL of NB RUSH medium in each well. Neurons were kept at 37°C in 5% CO2 until fixation.

Human iPSC culture and neuronal differentiation

Human iPSCs (KOLF2.1J)[76] were differentiated into cortical neurons (iNeurons) by induced expression of human NGN2, following a previously described protocol[83] with minor adaptations. Briefly, KOLF2.1J iPSCs were cultured in Stemflex medium (Thermo Fisher Scientific, Cat# A3349401) in a 6-well plate coated with Matrigel (Merck, Cat# CLS354277). iPSCs were transfected with PB-TO-hNGN2 (Addgene, #172115) and a plasmid containing EF1a-transposase using Lipofectamine Stem (Thermo Fisher Scientific, Cat# STEM00001), followed by selection with 2 µg/ml puromycin to generate a polyclonal pool of iPSCs with stably integrated tet-inducible human NGN2.

Differentiation towards iNeurons was induced by plating these iPSCs in a Matrigel-coated 6-well plate in induction medium (DMEM/F12 (Thermo Fisher Scientific, Cat# 11330032) with 1x N2 supplement (Thermo Fisher Scientific, Cat# 17502048), 1x non-essential amino acids (Thermo Fisher Scientific, Cat# 11140050), 2 mM L-glutamine (Thermo Fisher Scientific, Cat# 25030081), 2 µg/ml Doxycycline (Stemcell Technologies, Cat# 72742)). After three days, the cells were dissociated with accutase (Thermo Fisher Scientific, Cat# A1110501), and plated on glass coverslips coated with poly-L-lysine (Sigma) in maturation BP medium (Stemcell Technologies, Cat# 05790) supplemented with 1x B27 supplement (Gibco), 10 ng/ml BDNF (Thermo Fisher Scientific, Cat# 17834733), 10 ng/ml NT-3 (Thermo Fisher Scientific, Cat#

17894523), and 1 µg/ml laminin (Roche). iNeurons were cultured until DIV24 with weekly half-medium changes.

HEK293T cell culture, lentivirus packaging and lentiviral transduction

HEK293T cells were maintained in Dulbecco's Modified Eagles Medium (DMEM) high glucose with stable glutamine and sodium pyruvate (Capricorn Scientific) supplemented with 10% fetal bovine serum (GIBCO) and 1% Penicillin-Streptomycin (GIBCO). The cells were maintained at 37°C in 5% CO2.

For mass spectrometry experiments with V5-APEX2-SEC13, lentiviruses were produced by transient transfection of HEK293T cells with transfer vector containing V5-APEX2-SEC13, packaging vector psPAX2 and envelope vector pMD2.G with a ratio of 1:1:1 using PEI Max (Polysciences) according to standard protocols with a 3:1 PEI Max:DNA ratio. PEI Max/DNA complexes were prepared in serum-free Opti-MEM (GIBCO) and added to the cells after 20 min. Medium was completely removed after 4 h and changed to NB supplemented with 0.5 mM glutamine. Supernatants from packaging cells were collected 48–72 h post-transfection, filtered through a 0.45 µm filter, concentrated with Ultra Centrifugal Filter 100 kDa MWCO (AMICON) at 4°C 1000g for 45 min. Concentrated lentivirus was resuspended in appropriate volumes of fresh NB medium and immediately used to transduce DIV4 cortical neurons grown on 6-well plates in NB medium supplemented with 2% B27 (Gibco), 0.5 mM Glutamine (Gibco), 15.6 µM Glutamate (Sigma), and 1% Penicillin/Streptomycin (Gibco). Cells were maintained at 37 °C in 5% CO2 until further processing at DIV9.

For shRNA validation, lentiviruses were produced by transient transfection of HEK293T cells with transfer vector pLKO.1 puro containing shRNA, packaging vector psPAX2 and envelope vector pMD2.G following same protocol as above.

METHOD DETAILS

DNA and shRNA Constructs

The following vectors were used: FUGW was a gift from David Baltimore (Addgene plasmid #14883),[84] pLKO.1 puro was a gift from Bob Weinberg (Addgene plasmid #8453),[85] Str-KDEL_SBP-EGFP-Ecadherin was a gift from Franck Perez (Addgene plasmid #65286),[28] psPAX2 and pMD2.G were gifts from Didier Trono (Addgene plasmids #12260 and #12259), pmScarlet-i-C1 was a gift from Dorus Gadella (Addgene plasmid #85044),[86] Halo-TfR-RUSH and SAR1B-H79G-mOrange2 were gifts from Jennifer Lippincott-Schwartz (Addgene plasmid #166905 and #166900),[69] pEGFP-SEC22B was a gift from Thierry Galli (Addgene plasmid #101918),[87] pcDNA3.1-MS2-HA-HsNBAS_AA was a gift from Elisa Izaurralde (Addgene plasmid #148236), mito-V5-APEX2 was a gift from Alice Ting (Addgene plasmid #72480),[37] pEGFP-SEC23A and pEYFP-SEC24D were gifts from David Stephens (Addgene plasmid #66609 and #66614),[88] pDEST47-SAR1-GFP was a gift from Richard Kahn (Addgene plasmid # 67409),[89] pORANGE Cloning template vector was a gift from Harold MacGillavry (Addgene plasmid #131471),[90] H2B-mNeonGreen-IRESpuro2 was a gift from Daniel Gerlich (Addgene plasmid #183745),[91] pEGFP(A206K)-C1 and pEGFP(A206K)-N1 was a gift from Dr. Jennifer Lippincott-Schwartz, GW1-GFP-ZW10 was a gift from Peter van der Sluijs,[77] HA-NF186-mRFP-FKBP was a gift from Casper Hoogenraad,[78] HA-BicD2-FRB was a gift from Lukas Kapitein,[79] Halo-CLCa was a gift from Harold MacGillavry,[92] pmCherry-N1 and mCherry-C1 (Clontech), pGW2-mCherry and pGW1-BFP were a gift from Dr. Lukas Kapitein.[79]

The following plasmids have been previously described: V5-SEC16B and Halo-SEC61β;[80] HA-KIFC1-Strep, mCherry-SBP-RTN4, P180-ΔCoiled-coil-GFP.[30]

The plasmids generated in this study include:
For RUSH-SYT1-mNeonGreen, The STIM1sp-Strep-KDEL-intron-IRES fragment was PCR amplified from Str-KDEL_SBP-EGFP-Ecadherin (Addgene plasmid # 65286) and inserted in the FUGW vector (Addgene plasmid # 14883) between XbaI and EcoRI restriction sites using Gibson Assembly (New England Biolabs). This created an FUGW-Strep-KDEL-intron-IRES (named FUGW-RUSH). FUGW-RUSH was further digested with EcoRI and BamHI. The SBP-HA fragment was PCR amplified from an SBP-HA-APPwt-mNG construct (a gift from D. Draper, Farías Lab); SYT1 was PCR amplified from rat cortical neuron cDNA; and the mNeonGreen fragment was amplified from the mNeonGreen-N1 vector (Farías lab), flanked by AgeI and SmiI restriction sites. These fragments were further inserted in digested FUGW-RUSH vector by Gibson assembly and flexible linkers were added between SBP-HA and SYT1, as well as between SYT1 and mNeonGreen. The following primers were used to generate this construct:
FUGW-XbaI Fw: 5 – ttgggctgcaggtcgactctagagccaccatggatgtatgcgtccgtc – 3'
FUGW-EcoRI Rv: 5' – gctagcttcgaagaattcttatcatcgtgtttttcaaaggaaaacca – 3'
SBP-HA Fw: 5' – cctttgaaaaacacgatgataaggccaccatgggtagcgacgagaagaccactgg – 3'
SBP-HA Rv: 5' – gctaccgctgccgctaccgc – 3'
SYT1 cDNA Fw: 5' – gtagcggtagcggcagcggtagcatggtgagtgccagtcatcc – 3'
SYT1 cDNA Rv: 5' – gaattcgccagaaccagcagcggagccagcggatcccttcttgacagccagcatgg – 3'
mNeonGreen Fw: 5' – gctgctggttctggcgaattcaccggtatggtgagcaagggcgaggaggataa – 3'
mNeonGreen Rv: 5' – agcttgatatcgaattgttaacgatttaaatttacttgtacagctcgtccatgcc – 3'

To generate RUSH-SYT1-Halo construct, RUSH-SYT1-mNeonGreen was digested with AgeI and SmiI, and mNeonGreen was replaced by a HaloTag fragment, which was PCR amplified from a HaloTag-C1 construct. The following primers were used for HaloTag amplification:
HaloTag Fw: 5' – cgctgctggttctggcgaattcaccggtatggcagaaatcggtactggctttcca – 3'
HaloTag Rv: 5' – tgatatcgaattgttaacgatttaaatttagccggaaatctcgagcgtggacag – 3'

For RUSH-P180ΔCC-HA-SYT1-mNG, the STIM1sp-Strep fragment was PCR amplified from Str-KDEL-SBP-eGFP-Ecadherin (Addgene plasmid #65286). Next, the P180ΔCC fragment was PCR amplified from a P180ΔCC-GFP.[30] The intron-IRES-SBP-HA-SYT1-mNeonGreen fragment was PCR amplified from RUSH-SYT1-mNeonGreen (described above). These fragments were subsequently inserted in the FUGW vector (Addgene plasmid # 14883), between XbaI and EcoRI restriction sites using Gibson assembly. The Kozak sequence was added at the start of the STIM1-sp-Strep fragment and flexible linkers were added between these fragments. The following primers were used to generate this construct:
STIM1sp-Strep Fw: 5' – gcttgggctgcaggtcgact – 3'
STIM1sp-Strep Rv: 5' – ggtgctcgagatctgagtccgctgctggacggcatccagag – 3'
P180ΔCC Fw: 5' – cggactcagatctcgagcaccatggatatttacgacactcaaac – 3'
P180ΔCC Rv: 5' – cagttatctatgcggccgctcaagaagctgactctgtcttttt – 3'
Intron-SBP-HA-SYT1-mNG Fw: 5' – tgagcggccgcatagataac – 3'
Intron-SBP-HA-SYT1-mNG Rv: 5' – acggatccgctagcttcgaagaattcatttaaatttacttgtacagctcgtcc-3'

For RUSH-NF186-mNeonGreen, NF186 signal peptide and NF186 were PCR amplified from HA-NF186-mRFP-FKBP;[78] SBP-HA was PCR amplified from SBP-HA-APP-mNG construct (a gift from D. Draper, Farías Lab); and mNeonGreen was amplified from the mNeonGreen-N1 vector (Farías Lab) with added AgeI and SmiI restriction sites. These fragments were subsequently inserted in FUGW-RUSH vector between EcoRI and BamHI restriction sites by Gibson assembly. Flexible linkers were added between SBP-HA and NF186, as well as

between NF186 and mNeonGreen. The following primers were used to generate this construct:
Kozak-NF186sp Fw: 5' – cctttgaaaaacacgatgataaggccaccatgatggccaggcagcaggcgcc – 3'
Kozak-NF186sp Rv: 5' – ggcccctccgaggctgaggag – 3'
SBP-HA Fw: 5' – tcctcctcagcctcggaggggccggtagcgacgagaagaccactgg – 3'
SBP-HA Rv: 5' – gctaccgctgccgctaccgc – 3'
NF186 Fw: 5' – gtagcggtagcggcagcggtagcattgagattccgatggattacc – 3'
NF186 Rv: 5' –actgcctcgcccttgctcaccataccggtgaattcgccagaaccagcagcggagccagcggatccgg ccagggaatagatggcattgactg – 3'
mNeonGreen Fw: 5' – gctgctggttctggcgaattcaccggtatggtgagcaagggcgaggaggataa – 3'
mNeonGreen Rv: 5' – agcttgatatcgaattgttaacgatttaaatttacttgtacagctcgtccatgcc – 3'

For RUSH-Ii-L1CAM-mNeonGreen, we first generated the FUGW-RUSH-Ii vector. FUGW vector (Addgene plasmid # 14883) was digested with BamHI and EcoRI. Strep-Ii-Intron-IRES was amplified from pIRES-neo3-Strep-Ii-LAMP2-SBP-FKBP-GFP (gift from Judith Klumperman). The resulting PCR product was assembled with digested FUGW using Gibson Assembly to generate FUGW-RUSH-Ii for subsequent cloning purposes.The following primers were used:
Strep-Ii-IRES Fw: 5' – ttgggctgcaggtcgactctagagccaccatgcacaggaggagaagcag – 3'
Strep-Ii-IRES Rv: 5' – gctagcttcgaagaattcttatcatcgtgtttttcaaaggaaaacca – 3'

Next, FUGW-RUSH-Ii was digested with EcoRI and BamHI. L1CAM signal peptide and L1CAM was amplified from GW1-PAGFP-mL1CAM (gift from Casper Hoogenraad). An HA tag with a linker was added between the signal peptide and L1CAM sequence, then mNeonGreen was PCR amplified from H2B-mNeonGreen-IRESpuro2 (Addgene plasmid # 183745) and SBP was PCR amplified from Str-KDEL_SBP_EGFP-Ecadherin (Addgene plasmid # 65286). All fragments were inserted into FUGW-RUSH-Ii between EcoRI and BamHI by Gibson Assembly. The following primers were used to generate this construct:
L1CAM sp Fw: 5' – aaaacacgatgataagaattatggtcgtgatgctgcggta – 3'
L1CAM sp Rv: 5' – ggaacatcgtatgggtagctaccgagcaggcaggggctgca – 3'
HA-Linker-L1CAM Fw: 5' – agattacgctggtagcggtagcggcagcatacagattccagacgaatataaaggac-3'
HA-Linker-L1CAM Rv: 5' – gcagcagatccagcggatccttctagggctactgcaggattg – 3'
mNeonGreen Fw: 5' – ctggctccgctgctggttctggcgaattcgtgagcaagggcgaggagga – 3'
mNeonGreen Rv: 5' – cttgtacagctcgtccatgcc – 3'
SBP Fw: 5' – ggcatggacgagctgtacaagggatccgacgagaagaccactggttgg – 3'
SBP Rv: 5' – gaattgttaacggatcgaattcttatggttcacgttgaccttgtgg – 3'

For V5-APEX2-SEC13-mNG, we first generated vectors FUGW-IRES-mNeonGreen and V5-APEX-C1.
For generation of FUGW-IRES-mNG, FUGW (Addgene plasmid # 14883) was first digested with BamHI and EcoRI. Intron-IRES was amplified from Str-KDEL_SBP_EGFP-Ecadherin (Addgene plasmid # 65286), mNeonGreen was amplified from H2B-mNeonGreen-IRESpuro2 (Addgene plasmid # 183745). All fragments were assembled by Gibson assembly into FUGW vector between BamHI and EcoRI with the EcoRI site destroyed. The following primers were used to generate this construct:
Intron-IRES Fw: 5' – caggtcgactctagaggatcggatccgaattaattcgctgtctgcgag – 3'
Intron-IRES Rv: 5' – gcccttgctcaccatggttatcatcgtgtttttcaaaggaaaaccacg – 3'
mNeonGreen Fw: 5' – acgatgataaccatggtgagcaagggcgag – 3'
mNeonGreen Rv: 5' – tatcgaattgttaacggatcttacttgtacagctcgtccatgcc – 3'

For generation of V5-APEX2-C1 vector, V5-APEX2 was PCR amplified from mito-V5-APEX2 (Addgene plasmid #72480) and inserted into pEGFP(A206K)-C1 vector between BglII and AgeI restriction sites using the following primers:
V5-APEX2-linker Fw: 5' – cgtcagatccgctagcgctaccggtGCCACCATGGGTAAGCCTATC – 3'
V5-APEX2-linker Rv: 5' – aattcgaagcttgagctcgagatctGCTACCGCTGCCGCTACC – 3'

Then, SEC13 sequence was PCR amplified from rat cDNA, and V5-APEX2 with a Kozak sequence in front, was amplified from pV5-APEX2-C1. These amplified sequences were subsequently inserted in FUGW-IRES-mNeoGreen between XbaI and BamHI restriction sites using Gibson assembly. A flexible linker was added in front of the SEC13 sequence. The following primers were used to generate FUGW-V5-APEX2-SEC13:
Kozak-V5-APEX2 Fw: 5'– gcttgggctgcaggtcgactgccaccatgggtaagcctatc – 3'
Kozak-V5-APEX2 Rv: 5' – gccgctgccgctggtgctgccggatcccttggcatcagcaaacccaag – 3'
SEC13 Fw: 5' – aagggatccggcagcaccagcggcagcggcatggtgtcagtaattaacac – 3'
SEC13 Rv: 5'– gcagacagcgaattaattcggaattccgtcattgctcattctgttg – 3'

For generation of GFP-SEC16A knock-in, 20 nt RNA guides were designed and selected using the UCSC genome browser gateway (https://genome-euro.ucsc.edu/), with RGSC5.0/rn5 (Rattus norvegicus) as reference genome and NGG (SpCas9, 3' side) PAM. Target sequences were chosen, taking into consideration the MIT guide specificity score.[93] The chosen targets were inserted in the pORANGE template backbone[90] at BbsI restriction sites. The donor sequence was designed to contain a GFP tag flanked by two Cas9 target sites and PCR amplified from a GFP containing plasmid. To facilitate genomic integration of the donor sequence in the correct orientation, these target sites including PAM sequences were inserted as the reverse complement of the genomic target sequence. This donor sequence was then ligated in the pORANGE vector containing targets at HindIII and XhoI restriction sites. Short linker sequences of at least three amino acids and additional base pairs to make the donor in frame after integration in the genome were introduced between the target sites and the tag sequence. The primers for SEC16A target site and donor were as followed:
SEC16A target Fw: 5' – aaacttataagcagcatctcctgc – 3'
SEC16A target Rv; 5' – caccgcaggagatgctgcttataa – 3'
GFP donor Fw: 5'-ataaagcttgcaggagatgctgcttataaaggcagccaccatggctagcggagtgagcaaggg cgaggag-3'
GFP donor Rv: 5'-atactcgagcctttataagcagcatctcctgcagagcgcttccactcttgtacagctcgtccatgc-3'

For V5-SEC31A, we first generated pCMV-V5-C1 vector by inserting a V5 fragment into pCMV-mScarletii-C1 vector (Addgene plasmid #85044) between AgeI and BsrGI restriction sites. SEC31A fragment was PCR amplified from pEGFP-SEC31A (Addgene plasmid #66612) and inserted into pCMV-V5-C1 vector generated above between BspEI and BamHI restriction sites. A flexible linker (GPKLGSGS) was also included in front of SEC31A sequence. The following primers were used to generated pCMV-V5-C1 and V5-SEC31A:
Kozak-V5-C1 Fw: 5' – cgtcagatccgctagcgctaactgccaccatgggtaag – 3'
Kozak-V5-C1 Rv: 5' – cgagatctgagtccggacttgggccccgtagaatcgag – 3'
SEC31A Fw: 5' – cgattctacggggcccaagttaggcagcggtagtatgaagttaaaggaagtagatc – 3'
SEC31A Rv: 5' – tcagttatctagatccggtgttagacacccagcttattg – 3'

For Halo-SEC24D, we first generated a pHaloTag-C1 vector. Briefly, HaloTag was PCR amplified from Halo-CLCa (a gift from Harold MacGillavry), and inserted in pGFP(A206K)-C1

vector digested with AgeI and BglII restriction enzymes using Gibson Assembly. The following primers were used for amplification of HaloTag:
Halo Fw: 5' – cgtcagatccgctagcgctagccaccatggcagaaatcggtactggc – 3'
Halo Rv: 5' – aattcgaagcttgagctcgagatctgctaccgctgccgctacc – 3'
HaloTag was then PCR amplified from HaloTag-C1 vector and SEC24D was amplified from pEYFP-SEC24D (Addgene plasmid #66614). These fragments were inserted into the pEGFP(A206K)-C1 between AgeI and EcoRI restriction sites. A kozak sequence and a flexible linker were inserted by addition to cloning primers. The following primers were used to generate this construct:
HaloTag Fw: 5' – gatccgctagcgctaccggtcgccaccatggcagaaatcggtactggcttt – 3'
HaloTag Rv: 5' – agaaccagcagcggagccagcggatccgccggaaatctcgagcgtgga – 3'
SEC24D Fw: 5' – cgctggctccgctgctggttctggcgaattcatgagtcaacaaggttacgtggct – 3'
SEC24D Rv: 5' – attcgaagcttgagctcgagagcggatccttaattaagcagctgacagatctcc – 3'

For SAR1B-H79G-GFP, SAR1B-H79G was PCR amplified from SAR1B-H79G-mOrange2 (Addgene plasmid #166900) and inserted into pEGFP(A206K)-N1 between BamHI and BglII restriction sites. A kozak sequence was inserted by addition to cloning primers. The following primers were used to generate this construct:
Sar1B-H79G Fw: 5' – cgctagcgctaccggactcagatctgccaccatgtccttcatattt – 3'
Sar1B-H79G Rv: 5' – ccatggtggcgaccggtggatccgaaccgctgccgctaccatcgatgtactgtgccatc – 3'

For the Strep-SBP heterodimerization system, mCh-SBP-SEC23A or GFP-SBP-SEC23A were generated. The SEC23A fragment was PCR amplified from EGFP-SEC23A (Addgene plasmid #66609) and inserted into either mCh-SBP-C1 or GFP(A206K)-SBP-C1 plasmids[30] between SalI and BamHI restriction sites. The following primers were used:
SEC23A Fw: 5' – caaagcttcgaattctgcagtcgaccggtagcggcagcggtagcatgacaacctatttggaa
ttcattc – 3'
SEC23A Rv: 5' – tcagttatctagatccggtggatcctcaagcagcactggacac – 3'

For the FKBP-FRB heterodimerization system, FLAG-FRB-KIFC1 and mCh-FKBP-SEC23A or GFP-FKBP-SEC23A were generated.
For FLAG-FRB-KIFC1, FUGW vector (Addgene plasmid #14883) was digested with XbaI and EcoRI. KIFC1 was first subcloned from Strep-KIFC1-HA,[30] FRB was subcloned from HA-BicD2-FRB (a gift from Lukas Kapitein),[79] a 20 amino acid linker GSAGSAAGSGAGSAAGSGEF was introduced behind the FRB fragment. An additional FLAG tag was introduced in front of FRB-KIFC1 using primers. All fragments were inserted into restricted FUGW vector by Gibson assembly. These primers were used to generate this construct:
KIFC1 Fw: 5' – tacaaagacgatgacgacaagaccggtatcctctggcatgagatgtggcatgaag – 3'
KIFC1 Rv: 5' – cgctagcttcgaagaattcttacttcctgttggcctgagcagt – 3'
FRB Fw: 5' – tacaaagacgatgacgacaagaccggtatcctctggcatgagatgtggcatgaag – 3'
FRB Rv: 5' – gcagcggagccagcggatccctttgagattcgtcggaacacatgataatagagg – 3'
20aa linker: 5' – gaattcgccagaaccagcagcagatccagcgccagaacctgcagcggagccagcggatcc – 3'
FLAG tag: 5' – gctgcaggtcgactctagagccaccatggactacaaagacgatgacgacaagaccggt – 3'

For mCh-FKBP-SEC23A or GFP-FKBP-SEC23A, SEC23A was PCR amplified from EGFP-SEC23A (Addgene plasmid #66609) and 2x FKBP was amplified from mCh-FKBP2x-RTN4.[30] These fragments were inserted into either mCherry-C1 or GFP(A206K)-C1 vector, between

SalI and BglII restriction sites. A linker was added between FKBP and SEC23A. The following primers were used to generate these constructs:
FKBP2x Fw: 5' – gctgtacaagtccggactcagatctggagtgcaggtggaaaccatc – 3'
FKBP2x Rv: 5' – aggttgtcatgctaccgctgccgctacc – 3'
SEC23A Fw: 5' – cagcggtagcatgacaacctatttggaattcattc – 3'
SEC23A Rv: 5' – atcccgggcccgcggtaccgtcgactcaagcagcactggacac – 3'

For Halo-NBAS and Halo-ZW10, NBAS was PCR amplified from pcDNA3.1-MS2-HA-HsNBAS_AA (Addgene plasmid # 148236), and ZW10 was PCR amplified from GFP-GW1-ZW10.[77] These fragments were inserted separately in HaloTag-C1 vector (described above) digested with BglII and BamHI. The following primers were used to generate these two plasmids:
NBAS Fw: 5' – cggtagcggcagcggtagcagatctatggcggcccccgagtca – 3'
NBAS Rv: 5' – agttatctagatccggtggatcctcacacccagtgctgtgctgc – 3'
ZW10 Fw: 5' – cggtagcggcagcggtagcagatctatggcctcgttcgtgaca – 3'
ZW10 Rv: 5' – cggtagcggcagcggtagcagatctatggcctcgttcgtgaca – 3'

The following rat shRNA-targeting sequences inserted to pLKO.1-puro were used in this study:
scramble shRNA (5'-gatgaaatattccgcaagtaa-3') or
scramble shRNA (5'-gaaacaaatcggaaatctt-3')
HDLBP-shRNA (5'-atggtcaaagacctgattaat-3')
SEC22B-shRNA (5'-tcatcatgctgatagtgtatg-3')
ZW10-shRNA (5'-gactctgtcgtcctaaatttg-3')
NBAS-shRNA (5'-atgaccagaaaggccattaag-3')

The following sequences were used in this study to validate HDLBP, SEC22B, ZW10 and NBAS shRNA-mediated knockdown efficiency:
For HDLBP:
HDLBP qPCR Fw1: 5' – agagaggaaaacccagttcaca – 3'
HDLBP qPCR Rv1: 5' – tcggtctccttggcctctc – 3'
For SEC22B:
SEC22B qPCR Fw2: 5' – agaagcactctcagcattgga – 3'
SEC22B qPCR Rv2: 5' – cttcgcatcctggcggtatt – 3'
For ZW10:
ZW10 qPCR Fw1: 5' – aaatcggagatcggtgggc – 3'
ZW10 qPCR Rv1: 5' – gcagccgctcttctttctgt – 3'
For NBAS:
NBAS qPCR Fw2: 5' – ccagtcaccatgaggtcgag – 3'
NBAS qPCR Rv2: 5' – acaggttgttggctatgacaca – 3'
Primers targeting GAPDH were used as internal control.
GAPDH qPCR Fw: 5' – caactccctcaagattgtcagcaa – 3'
GAPDH qPCR Rv: 5' – ggcatggactgtggtcatga – 3'

Antibodies and reagents

The following primary antibodies were used in this study: mouse anti-Puromycin (Merck Cat# MABE343, RRID: AB_2566826, 1:1000), mouse anti-SMI-312 (BioLegend Cat#837904, RRID:AB_2566782, 1:1000), chicken anti-MAP2 (Abcam Cat#ab5392, RRID:AB_2138153, 1:5000), rabbit anti-Synaptotagmin-1 (Synaptic Systems Cat#105 008, RRID:AB_2832236, 1:1000), rabbit anti-Neurexin-1alpha (Frontier Institute/ Nittobo Medical Cat# MSFR104630,

1:300), rabbit anti-L1CAM (Proteintech Cat# 20659-1-AP, RRID:AB_2878717, 1:250), rabbit-anti-TRIM46 (a gift from Casper Hoogenraad,, 1:500), mouse anti-V5 (Thermo Fisher Scientific Cat# R960-25, RRID:AB_2556564, 1:500), rat anti-HA (Roche Cat# 11867423001, RRID:AB_390918, 1:200), mouse anti-GM130 (BD Biosciences Cat#610823, RRID:AB_398142, 1:1000), sheep anti-TGN38 (Bio-Rad Cat#AHP499G, RRID:AB_2203272, 1:1000), mouse-anti-GFP (Thermo Fisher Scientific Cat#A-11120; RRID:AB_221568, 1:700), mouse anti-mCherry (Takara Bio, Cat#CL 632543, 1:1000), rabbit anti-SEC31A (Cell Signaling Technology Cat#13466, RRID:AB_2798228, 1:300), mouse anti- β-Tubulin III (Sigma-Aldrich Cat#T8660, RRID:AB_477590, 1:1000), rabbit anti-HDLBP (Proteintech Cat#15406-1-AP, RRID:AB_2117367, 1:500), rabbit anti-NBAS (Proteintech Cat#14683-1-AP, RRID:AB_1959590, 1:200), rabbit anti-ZW10 (Abcam Cat#ab21582, RRID:AB_779030, 1:500), rabbit anti-Synapsin-I (Millipore Cat#AB1543, RRID:AB_2200400, 1:500), mouse anti-RTN4A (named NogoA) (R and D Systems Cat# MAB3098, RRID:AB_10997139), mouse anti-Pan-Neurofascin external (clone A12/18; UC Davis/NIH NeuroMab, Cat#75-172, RRID: AB_2282826, 0.18 mg/ml).

The following secondary antibodies were used in this study: goat anti-mouse Alexa405 (Molecular Probes, Cat#A31553, RRID:AB_221604, 1:500), goat anti-Mouse IgG (H+L) Highly Cross-Adsorbed Alexa Fluor 488 (Thermo Fisher Scientific Cat#A-11029, RRID:AB_2534088, 1:1000), goat anti-mouse Alexa568 (Thermo Fisher; Cat#A-11031, RRID:AB_144696, 1:1000). goat anti-rabbit IgG (H + L) Highly cross-absorbed secondary antibody Alexa Fluor 405 (Thermo Fisher Scientific Cat#A-31556, RRID:AB_221605, 1/500), goat anti-mouse IgG2a cross-absorbed secondary antibody Alexa Fluor 594 (Thermo Fisher Scientific Cat#A-21135, RRID:AB_2535774, 1/1000), goat anti-Mouse IgG (H+L) Highly Cross-Adsorbed Secondary Antibody, Alexa Fluor 647 (Thermo Fisher Scientific Cat#A-21236, RRID:AB_2535805, 1/1000), goat anti-rabbit IgG (H + L) Highly cross-absorbed secondary antibody Alexa Fluor 405 (Thermo Fisher Scientific Cat#A-31556, RRID:AB_221605, 1/500), goat anti-Rabbit IgG (H+L) Highly Cross-Adsorbed Secondary Antibody, Alexa Fluor488 (Thermo Fisher Scientific Cat#A-11034, RRID:AB_2576217, 1/1000), goat anti-rabbit IgG (H+L) Highly Cross-Adsorbed CF®594 (Sigma-Aldrich, Cat#SAB4600110, 1:500), goat anti-rabbit IgG (H + L) highly cross-absorbed secondary antibody Alexa Fluor 568 (Thermo Fisher Scientific Cat#A-11036, RRID:AB_10563566, 1/1000), goat anti-Rabbit IgG (H+L) Highly Cross-Adsorbed Secondary Antibody, Alexa Fluor647 (Thermo Fisher Scientific Cat#A-21245, RRID:AB_2535813, 1:500), goat anti-chicken IgY (H+L) Secondary Antibody, Alexa Fluor488 (Thermo Fisher Scientific Cat#A-11039, RRID:AB_2534096, 1/1000), goat anti-Chicken IgY (H+L) Secondary Antibody, Alexa Fluor568 (Thermo Fisher Scientific Cat#A-11041, RRID:AB_2534098, 1/1000), donkey anti-Sheep IgG (H+L) Cross-Adsorbed Secondary Antibody, Alexa Fluor488 (Thermo Fisher Scientific Cat#A-11015, RRID:AB_2534082, 1/1000), goat anti-Rat IgG (H+L) Cross-Adsorbed Secondary Antibody, Alexa Fluor568 (Thermo Fisher Scientific Cat#A-11077, RRID:AB_2534121, 1/500), Alexa Fluor555 conjugated Strep (Thermo Fisher Scientific Cat#s21381, RRID:AB_2307336, 1:1000), Atto488 conjugated Fluotag-X4® GFP nanobody (NanoTag Biotechnologies, Cat#N0304-At488-L, 1:250), Atto488 conjugated GFP-Booster nanobody (ChromoTek, Cat#gba488, 1:250), rabbit anti-mouse immunoglobulins/HRP (Agilent Cat# P0260, RRID:AB_2636929, 1/10000), IRDye 800CW Streptavidin (LI-COR Biosciences, Cat#926-32230, 1/10000).
Other reagents used in this study were: Puromycin dihydrochloride (Sigma-Aldrich, Cat#P8833), Anisomycin (Sigma-Aldrich, Cat#9789), Lipofectamine 2000 (Thermo Fisher Scientific, Cat#1639722), Fluoromount-G Mounting Medium (ThermoFisher Scientific, Cat#00-4958-02), anhydrous-DMSO (Thermo Fisher Scientific, Cat#D12345), biotin (Sigma-

Aldrich, Cat#B4501), biotin-phenol (Iris Biotech, Cat#LS.3500), H_2O_2 (Sigma-Aldrich, Cat#H1009), Sodium Azide (Merck, Cat#K43547688), Sodium L-ascorbate (Sigma, Cat#0000374819), Trolox (Sigma, Cat#238813), rapalog (A/C Heterodimerizer) (Takara Bio, Cat#635057), NeutrAvidin (Thermo Fisher Scientific, Cat#31000), Brefeldin A (Sigma-Aldrich, Cat#B5936), NAD+ (Sigma-Aldrich, Cat# 10127965001), Mix-n-Stain CF640R antibody labeling kit (Biotium, Cat#92245), Duolink® In Situ Detection Reagents FarRed (Sigma-Aldrich, Cat#DUO92013), Polyethylenimine (PEI MAX; Polysciences, Cat#24765), and Triton-X-100 (Sigma, Cat#93433). JFX554 and JFX650 were kindly provided by the Lavis Lab (Janelia).[94]

Drug treatments

BFA was used at 2-2.5 µg/ml for 30 min (Figure 4D, Figures S3A, B, C, D) or 4h 30 min (Figures 2C, 3I, 3N, 4K, 5C, and 5E, and Figures S3F and S3G) for fixed cell experiments. For live-cell experiments, neurons were incubated with BFA 2-2.5 µg/ml for 30 min and transferred to a spinning disk confocal microscope. Samples were imaged for up to 3h (Figure 4M, Figure S5J). BDNF was used at 100 ng/ml for 30 min, after which cells were incubated with puromycin for 10 min (Figures 1B and 1D) or kept for 4h with BFA and biotin (Figures 2C, 3I, 3N, 4K, 5C and 5E) before fixation, or fixed immediately (Figure 3O).

For experiments combining expression of RUSH-SYT1 construct with shRNAs for 4 days, NAD+ (1mM) was added to culture medium to ensure neuron survival in biotin-free medium over long period.

For the Streptavidin/SBP heterodimerization system assay, NeutrAvidin (0.3 mg/ml) was added to neurons immediately after transfection to avoid Strep-SBP uncoupling by the presence of biotin in culture medium. NeutrAvidin was kept in the medium for 48h (Figures 3E, 6B, 6D, 6F and 6H) or 72h (Figure 7A) until fixation.

For drug-induced FKBP/FRB heterodimerization assay, rapalog (500 nM) was added after transfection for 16h before further BFA, biotin and BDNF treatments (Figures 3H, I). Ethanol 0.1% was used as a vehicle in control treatment.

RNA extraction, reverse transcription and quantitative PCR

Rat cortical neurons DIV9 were used to validate knockdown efficiency of HDLBP, ZW10, NBAS, and SEC22B shRNAs. Total RNA from transduced rat cortical neurons was extracted using RNeasy Mini kit (Qiagen, 74104). cDNA was reverse-transcribed using SuperScript III First-Strand Synthesis System (Invitrogen, 18080-051) according to manufacturer's instructions. Quantification of target genes was done by qPCR using Power SYBR Green PCR Master Mix (Applied Biosystems, 4367659) and ViiA 7 Real-Time PCR System (Applied Biosystems). Data was extracted from ViiaA 7 Real-Time PCR system using QuantStudio Software V1.3 (Applied Biosystems).

Mass Spectrometry sample preparation and analysis

Sample preparation

Neurons transduced with lentivirus at DIV4 stably expressing FUGW-APEX2-SEC13-mNG were subjected to APEX2 treatment at DIV9 as previously described.[95] Briefly, neurons were incubated with NB media supplemented with 500µM biotin-phenol (IrisBio-tech) at 37°C for 20 min before addition of 1mM H_2O_2 at room temperature for 1 min to activate peroxidase activity. Biotinylation was immediately quenched by two washes in ice-cold quencher solution (10mM sodium azide, 10mM sodium ascorbate and 5mM Trolox in HBSS) and incubated 10 min on ice in azide-free quencher solution. Cells were scrapped and pooled according to their respective conditions. Pellets were stored at -80°C until all three biological replicates were

collected. Cell pellets were lysed with freshly made quenching-RIPA buffer (150mM NaCl, 50mM Tris-HCl pH7.4, 0.1% SDS, 0.5% sodium-deoxycholate, 1% Triton X-100, 10mM sodium azide, 10mM sodium ascorbate, 5mM Trolox and 1x protease inhibitors (Roche)) on ice for 30 min. Lysates were cleared by centrifuging at 16,000 x g 4°C, supernatants were incubated overnight with pre-equilibrated Pierce magnetic streptavidin beads (Invitrogen) on a rotor at 4°C. Beads were washed three times with detergent-free RIPA buffer (150mM NaCl, 50mM Tris-HCl pH7.4) and three times with freshly prepared 3M Urea buffer (Urea in 50mM ammonium bicarbonate). Beads were resuspended in 10µL of 3M Urea buffer and reduced with 5mM TCEP (Sigma) at room temperature for 30 min, alkylated with 10mM IAA (Sigma) in the dark at room temperature for 20 min and quenched with 20mM DTT (Sigma). Samples were washed three times with 2M Urea buffer and resuspended in 100µL 2M Urea buffer. Suspended beads were first incubated with 1µg LysC for 4 hours at room temperature, followed by adding 1µg Trypsin for digestion at 37°C overnight. Peptides were collected by combining digested supernatant with two subsequent 100µL 2M Urea buffer washes and immediately acidified with 1% trifluoroacetic acid. Digested peptides were desalted on Sep-Pak C18 Cartridges (Waters) and vacuum concentrated for storage until subsequent MS analysis.

Western blot analysis

Cell lysates were prepared as previously described before incubation with beads. 5% of lysates were reserved for immunoblotting. Samples were loaded on a homemade 10% Bis-Acrylamide gels (Bio-Rad) and transferred by wet transfer onto PVDF membranes (Bio-Rad). Membranes were blocked with 5% skimmed milk in TBS-T for 1h at room temperature and were incubated overnight at 4°C with primary antibodies diluted in antibody buffer (3% BSA in TBS-T) on a rotator. Blots were washed 3 times with TBS-T for 5 min each on a shaker and were incubated with anti-mouse HRP-conjugated secondary antibodies in antibody buffer for 45 min at room temperature, then washed three more times with TBS-T. Detection was performed using Clarity Western ECL Substrate (Bio-Rad, Cat#1705060) and imaged on an ImageQuant 800 system (AMERSHAM). To detect biotinylation, membranes were washed 3 times in TBS-T and incubated with IRDye 800CW Streptavidin for 45 min at room temperature. Finally, blots were washed 3 times with TBS-T for 5 min each and twice briefly in TBS before developing on an Odyssey CLx imaging system (LICOR) with Image Studio version 5.2.

MS and data analysis

All samples were reconstituted in 0.1% formic acid and analyzed on a Orbitrap Exploris 480 mass spectrometer (Thermo Fisher Scientific, San Jose, CA, United States) coupled to an UltiMate 3000 UHPLC system (Thermo Fisher Scientific, San Jose, CA, United States). Peptides were loaded onto a trap column (C18 PepMap100, 5 µm, 100 Å, 5 mm × 300 µm, Thermo Fisher Scientific, San Jose, CA, United States) with solvent A (0.1% formic acid in water) at 30 µl/min flowrate and chromatographically separated over the analytical column (Poroshell 120 EC C18, Agilent Technologies, 50 µm x 75 cm, 2.7 µm) using 180 min gradient at 300 nL/min flow rate. The gradient proceeds as follows: 9% solvent B (0.1% FA in 80% acetonitrile, 20% water) for 1 min, 9–13% for 1 min, 13–44% for 155 min, 44–55% for 5 min, 55–99% for 5 min, 99% for 3 min, and finally the system equilibrated with 9% B for 10 min.

The mass spectrometers were used in a data-dependent mode, which automatically switched between MS and MS/MS. After a survey MS scan ranging from 375 to 1600 m/z with 14 s dynamic exclusion time, the most abundant peptides of 120 m/z or higher were subjected to high energy collision dissociation (HCD) for further fragmentation using a 1.4 m/z isolation

window. MS spectra were acquired in high-resolution mode (R > 60,000), whereas MS2 was in high-sensitivity mode (R > 15,000) and 28% normalized collision energy.

For data analysis, raw files were processed using MaxQuant's (Version 2.0.1.0).[96] Andromeda search engine in reversed decoy mode based on rat reference proteome (Uniprot-FASTA, UP000002494, downloaded March 2023) with an FDR of 0.01 at both peptide and protein levels. Digestion parameters were set to specific digestion with trypsin with a maximum number of 2 missed cleavage sites and a minimum peptide length of 7. Oxidation of methionine and amino-terminal acetylation were set as variable and carbamidomethylation of cysteine as fixed modifications. The tolerance window was kept at default. A total of 3 biological replicates with 2 technical replicates each were analyzed. The resulting protein group file was first processed using Perseus (version 1.6.15.0)[97] to filter for common contaminants, reverse site-specific identifications. Proteins with peptide count <2 were excluded. The processed file was migrated to R (Version 4.5.0) for further analysis with a custom script. Briefly, raw intensity was $\log_2$ transformed and only proteins found in at least four replicates in the same condition were retained for analysis. Control and H_2O_2 conditions were separated and missing values within the same condition were imputed using BPCA and median normalized. Next, both conditions were joined back. For data visualization, proteins only found in H_2O_2 but not in control were imputed using QRILC for statistical purposes based on the assumption that these proteins were biologically relevant to SEC13 interactome. APEX2-SEC13 samples were tested using unpaired two sample *t*-test and proteins with a p value < 0.05 and $\log_2$ fold change ≥1 were considered significantly enriched. Data were visualized using R (Version 4.5.0).

Puromycilation assay

To label newly synthesized proteins, neurons were briefly incubated with 10 µM puromycin for 10 min. This duration is commonly used to detect newly made proteins in axons.[17,98] Following the incubation, any unincorporated puromycin was removed by washing neurons twice with NB medium. Neurons were then immediately fixed and processed for immunostaining as detailed below. For control conditions, neurons were pre-treated with 100 µg/ml anisomycin for 40 min.

Puromycilation-proximity ligation assay (Puro-PLA)

Newly synthesized proteins by proximity ligation were detected using anti-puromycin antibody in combination with antibodies recognizing specific POIs. Detection was performed using Duolink® PLA detection reagents (Sigma-Aldrich) according to the manufacturer's protocol. Duolink® PLA probes, including Duolink® In Situ PLA probe anti-mouse PLUS (Sigma-Aldrich, Cat#DUO92001) and anti-rabbit MINUS (Sigma-Aldrich, Cat#DUO92005) were used as secondary antibodies. Duolink® In Situ Detection Reagents FarRed (Sigma-Aldrich, Cat#DUO92013) were used for ligation, amplification and probe binding.

After puromycilation assay, fixation, permeabilization and washing (as described above), cells were blocked in Duolink® Blocking Solution for 1h at 37°C followed by an incubation with primary antibody pairs diluted in Duolink® Antibody Diluent at 4°C overnight. After washing 2 times, 5 min between each with 1X wash buffer A, PLA probes were added in 1:5 dilution in Duolink® Antibody Diluent for 1h at 37°C. After washing, cells were incubated for 30 min with ligation reaction containing the circularization oligos and T4 ligase diluted in Ligation buffer. After brief washes with wash buffer A, amplification and label probe binding was done with Polymerase and the fluorophore-labeled detection oligo diluted Amplification buffer for 100

min at 37°C. Amplification was stopped by 2 washes in 1X wash buffer B and 1 in 0.01X wash buffer B. For signal stability, cells were washed with PBS/MC fixed for 5 min at room temperature with 4% PFA/sucrose and processed further for immunofluorescence.

HaloTag labeling

HaloTag labeling was performed with cell-permeable Halo-JFX554 or Halo-JFX650 ligands (Lavis Lab, Janelia).[94] Ligands were dissolved in DMSO to 50 µM and stored in single-use aliquots at -20°C. HaloTag ligands were diluted in culture medium to a final concentration of 100-200 nM. Cells were incubated with ligands for 10 min in incubator, at 37°C, 5% CO_2. After that, cells were rinsed and put back to the culture medium for subsequent fixation (described below) or used for live cell imaging.

Live HA surface staining

For experiments involving staining for surface HA tag, neurons were incubated with rat anti-HA (Roche) diluted 1:200 in original medium from each well for 30 min, followed by a brief incubation in secondary antibody diluted 1:500 in original medium for 30 min. Incubations were done at 37°C, 5% CO_2. Cells were then washed in NB buffer and followed subsequent fixation and immunofluorescence protocol.

Immunofluorescence staining and confocal imaging

Neurons were fixed in 4% paraformaldehyde supplemented with 4% sucrose in PBS for 7-10 min at RT. Fixed cells were washed 3 times with PBS plus magnesium chloride and calcium chloride (PBS-MC) and subsequently permeabilized with 0.2% Triton X-100 in PBS-MC for 15 min at RT. Neurons were again washed with PBS-MC and then incubated with blocking buffer (0.2% porcine gelatin in PBS-MC) for 30 min at 37°C. Next, cells were incubated with primary antibodies diluted in blocking buffer for 30 min at 37°C or overnight at 4°C, washed 3 times with PBS-MC, incubated with secondary antibodies in blocking buffer for 30 min at 37°C, and washed 3 times with PBS-MC. Coverslips were then briefly dipped in Milli-Q water and mounted in Fluoromount-G mounting medium.

Imaging was done using a confocal laser scanning microscope (LSM900, with Zen (blue edition) imaging software version 3.7.97.07000 (Zeiss)) equipped with Plan-Apochromat ×63 NA 1.40 oil DIC and Plan-Apochromat x40 NA1.30 oil DIC objectives. Each confocal image was a z stack of 5–10 images, each averaged 2 times, covering the entire region of interest from top to bottom. Maximum projection images were obtained from the resulting z stack. For fluorescence intensity comparison, settings were kept the same for all conditions.

Live-cell imaging

Live-cell imaging experiments were conducted using an inverted Nikon Eclipse Ti-E microscope (Nikon) equipped with a Plan Apo VC 100X/NA 1.40 oil objective, an S Fluor 100X/0.5-1.3 oil objective (Nikon) and a Plan Apo VC 60X/NA 1.40 oil objective (Nikon). The system included a Yokogawa CSU-X1-A1 spinning disk confocal unit (Roper Scientific), a Photometrics Evolve 512 EMCCD camera (Roper Scientific), and an incubation chamber (Tokai Hit) mounted on a motorized XYZ stage (Applied Scientific Instrumentation). Coverslips were mounted in a metal ring and imaged using an incubation chamber supplemented with original full medium from neurons. Cells were maintained at optimal conditions of 37°C and 5% CO_2 during imaging. Image acquisition and device control were managed using MetaMorph software (version 7.10.2.240). For single-color imaging, each laser channel was exposed for 100–200 ms, while for dual-color imaging, laser channels were sequentially exposed within the same time range. Time-lapse imaging intervals and total durations varied

by experiment, as specified in the figure and movie legends. To identify axons, neurons were either co-transfected with a fill and identified by morphology or stained for 15 min with a CF640R-conjugated antibody against the axon initial segment (AIS) protein neurofascin (NF-640R).

Axon cutting with photoablation laser

Cells were transfected with P180ΔCC-HA-SYT1-mNG. Experiments were performed using the ILas2 system (Roper Scientific). Neurons were selected and their positions were saved in MetaMorph software. Teem Photonics 355nm Q-switched pulsed laser was used to perform laser-induced severing. 10% 355nm laser with a spot length of 100 points and diameter of 100 pixels was applied at the proximal axon to separate the axon and the soma. Biotin was immediately added, and images were acquired at distal parts of the severed axons at 1 min intervals for 60-90 min.

Live-cell imaging with SoRa microscope

For super-resolution imaging with the SoRa microscope, the experiment was performed using a Nikon Eclipse T2 inverted microscope (Nikon) equipped with a CFI SR HP Apo TIRF 100XAC/ NA 1.49 oil objective. The system included a Yokogawa Spinning Disk Field Scanning Confocal Systems CSU-W1 (Nikon) with an added SoRa (Super Resolution by Optical Pixel Reassignment) mode for approximately 1.4x improvement in resolution, an ORCA-Fusion digital sCMOS camera (Hamamatsu), an incubation chamber (Tokai Hit) to maintain samples at 37°C and 5% CO_2 during image acquisition. Image acquisition and device control were managed by NIS-Elements (v5.21). Each laser channel was exposed for 400 ms and time-lapse imaging was acquired at 1s intervals for 2 min. Deconvolution on acquired images was performed using the 2D Richardson-Lucy (RL) method with 20 iterations for each channel.

Image analysis and quantification

Puro-PLA signal detection and newly synthesized protein number analysis.

To quantify the amount of newly synthesized protein in axons, we acquired multi-channel z-stacks of neurons labelled with puro-PLA signals, endogenous MAP2 for dendrites, and endogenous SMI-312 for axons. Maximum intensity projections were applied to raw images. The SMI-312 signal, excluding the soma plus 20 µm radius from soma edge, was thresholded and this region was added to ROI manager, representing the axonal area. The same region was overlayed on PLA channel, and the ComDet plugin (https://github.com/ekatrukha/ComDet) was used to quantify the number of PLA signals, corresponding to the number of newly synthesized protein. Numbers were normalized to the corresponding area and averaged over multiple cells. Data were presented as number of newly synthesized proteins per 100 μm^2 axon area in Figures 1C, 1E, 1H, 1J and 1L.

For knock-down experiments, the axon was selected as the longest neurite based on a fluorescent protein fill, and a positive signal for the axonal marker SMI-312. A 100-µm axon segment at least 100 µm away from the soma was straightened. The number of newly synthesized proteins was manually quantified (Figure 5B).

Quantification of RUSH cargo number in axon and percentage of cargo fusing with membrane.

To quantify the number of RUSH cargo in the axon, an axon was first identified using the axon initial segment marker TRIM46.[75] A segmented line was traced along the axon, starting at minimum 50 µm away from the soma and straightened for quantifications using Fiji/ImageJ. A 100µm-axon segment was selected, and the number of RUSH cargos was manually quantified

(Figures 2D, 3J, 5D and Figure S5O). To assess the amount of fusion with the PM, we calculated the percentage of RUSH cargos that were also positive for HA surface staining (Figures 3O and 5F).

Quantification of ERES number in axon.
The axon was identified based on morphology, using a fill or staining for β-Tubulin or TRIM46. A 100-µm axon segment was analyzed in which number of ERES were manually counted (Figures 3F, 3L and Figure S5F) or by using ImageJ's build-in Find Maxima function (Figures 6C, 6E). To analyze the colocalization between SEC23A and SEC24D, SEC31A or SEC16B, a 100-µm axon segment was selected for quantification. The ImageJ ComDet plugin (https://github.com/ekatrukha/ComDet) was used on these segments to detect number of puncta and percentage of colocalization between channels (Figure 3B).

Kymograph analysis.
Kymographs were generated from live cell images using Fiji/ImageJ. Segmented lines were drawn and straightened along the axon identified by morphology using a fill and/or using the AIS marker NF-CF640R. Straightened axons were re-sliced followed by z-projection to obtain kymographs. A segment of 30 µm was cropped out for analysis. Anterograde movements were oriented from left to right in all kymographs. Time of recording and length of segments are indicated in each kymograph (Figures S5H and S5K). The number of events for anterograde, retrograde and stationary GFP-SEC23A puncta was manually counted from kymographs (Figures S5I and S5L).

Fluorescence intensity profile plots.
The distribution of different proteins was analyzed using ImageJ. Plot profiles were generated using a line traced along specified markers. Length of traced profile line is indicated in each intensity plot. Representative images and their corresponding plots are shown in each figure (Figure 4F, 4H, 4J, 4L).

ER intensity analysis.
To analyze average ER intensity in the axon, a staining for endogenous RTN4A was performed. Samples were imaged with the same settings for laser power, exposure and gain for all conditions. Axons were identified by using a TRIM46 staining. Segmented lines of approximately 40 µm along the axons were manually drawn and straightened. Mean intensity was measured by tracing a line along the straightened axon using Fiji/ImageJ (Figure 6G).

Axon morphology analysis.
To analyze axon complexity and morphology, images containing the whole axon were used. Neurons were transfected with a cell fill and the axons were identified using the AIS marker TRIM46. Axon length and morphology (Figure 6I, 6J, 6L and 6M) were analyzed using NeuronJ plugin for Fiji/ImageJ.[81] Axons were traced and classified as either primary, secondary or tertiary branch. For axons that could not fit in one field of view, several images were taken and stitched together using MosaicJ plugin.[82] All measurements were saved to an Excel file.

Synaptic bouton quantification.
Presynaptic boutons were identified by swellings along the axon by expressing a cell fill, as described previously.[99,100] Mature boutons were quantified from 3 segments of axons (50 µm each), determined by boutons that were also positive for the endogenous pre-synaptic maker Synapsin-I (Figure 7B and 7D).

Statistical analysis

Data processing and statistical analysis were performed using Microsoft Excel, GraphPad Prism (version 10.1.1), MaxQuant (version 2.0.1.0), Perseus (version 1.6.15.0) and R (version 4.5.0). The assumption of data normality was checked using D'Agostino–Pearson omnibus test. Unpaired t-tests, Mann-Whitney tests, Kruskal-Wallis tests followed by Dunn's multiple comparison test, ordinary one-way ANOVA tests followed by Dunnett's multiple comparisons or Tukey's multiple comparisons test were performed for statistical analysis as indicated in figure legends. See Table S2 for details on number of experiments, type of analysis and statistical test per experiment.

REFERENCES

1. Futerman, A.H., and Banker, G.A. (1996). The economics of neurite outgrowth − the addition of new membrane to growing axons. Trends in Neurosciences *19*, 144‑149. https://doi.org/10.1016/S0166-2236(96)80025-7.

2. Holt, C.E., Martin, K.C., and Schuman, E.M. (2019). Local translation in neurons: visualization and function. Nat Struct Mol Biol *26*, 557‑566. https://doi.org/10.1038/s41594-019-0263-5.

3. Kalil, K., and Dent, E.W. (2014). Branch management: mechanisms of axon branching in the developing vertebrate CNS. Nat Rev Neurosci *15*, 7‑18. https://doi.org/10.1038/nrn3650.

4. Bradke, F. (2022). Mechanisms of Axon Growth and Regeneration: Moving between Development and Disease. J Neurosci *42*, 8393‑8405. https://doi.org/10.1523/JNEUROSCI.1131-22.2022.

5. O’ Donnell, M., Chance, R.K., and Bashaw, G.J. (2009). Axon Growth and Guidance: Receptor Regulation and Signal Transduction. Annu Rev Neurosci *32*, 383‑412. https://doi.org/10.1146/annurev.neuro.051508.135614.

6. Jung, H., Yoon, B.C., and Holt, C.E. (2012). Axonal mRNA localization and local protein synthesis in nervous system assembly, maintenance and repair. Nat Rev Neurosci *13*, 308‑324. https://doi.org/10.1038/nrn3210.

7. Campbell, D.S., and Holt, C.E. (2001). Chemotropic responses of retinal growth cones mediated by rapid local protein synthesis and degradation. Neuron *32*, 1013‑1026. https://doi.org/10.1016/s0896-6273(01)00551-7.

8. Shigeoka, T., Jung, H., Jung, J., Turner-Bridger, B., Ohk, J., Lin, J.Q., Amieux, P.S., and Holt, C.E. (2016). Dynamic Axonal Translation in Developing and Mature Visual Circuits. Cell *166*, 181‑192. https://doi.org/10.1016/j.cell.2016.05.029.

9. Hafner, A.-S., Donlin-Asp, P.G., Leitch, B., Herzog, E., and Schuman, E.M. (2019). Local protein synthesis is a ubiquitous feature of neuronal pre- and postsynaptic compartments. Science *364*. https://doi.org/10.1126/science.aau3644.

10. Zivraj, K.H., Tung, Y.C.L., Piper, M., Gumy, L., Fawcett, J.W., Yeo, G.S.H., and Holt, C.E. (2010). Subcellular Profiling Reveals Distinct and Developmentally Regulated Repertoire of Growth Cone mRNAs. J. Neurosci. *30*, 15464‑15478. https://doi.org/10.1523/JNEUROSCI.1800-10.2010.

11. Jung, J., Ohk, J., Kim, H., Holt, C.E., Park, H.J., and Jung, H. (2023). mRNA transport, translation, and decay in adult mammalian central nervous system axons. Neuron *111*, 650-668.e4. https://doi.org/10.1016/j.neuron.2022.12.015.

12. Taylor, A.M., Berchtold, N.C., Perreau, V.M., Tu, C.H., Li Jeon, N., and Cotman, C.W. (2009). Axonal mRNA in uninjured and regenerating cortical mammalian axons. J Neurosci *29*, 4697‑4707. https://doi.org/10.1523/JNEUROSCI.6130-08.2009.

13. Gumy, L.F., Yeo, G.S.H., Tung, Y.-C.L., Zivraj, K.H., Willis, D., Coppola, G., Lam, B.Y.H., Twiss, J.L., Holt, C.E., and Fawcett, J.W. (2011). Transcriptome analysis of embryonic and adult sensory axons reveals changes in mRNA repertoire localization. RNA *17*, 85‑98. https://doi.org/10.1261/rna.2386111.

14. Cornejo, V.H., Luarte, A., and Couve, A. (2017). Global and local mechanisms sustain axonal proteostasis of transmembrane proteins. Traffic *18*, 255‑266. https://doi.org/10.1111/tra.12472.

15. Horton, A.C., and Ehlers, M.D. (2003). Dual Modes of Endoplasmic Reticulum-to-Golgi Transport in Dendrites Revealed by Live-Cell Imaging. J. Neurosci. *23*, 6188‑6199. https://doi.org/10.1523/JNEUROSCI.23-15-06188.2003.

16. Wang, J., Fourriere, L., and Gleeson, P.A. (2020). Local Secretory Trafficking Pathways in Neurons and the Role of Dendritic Golgi Outposts in Different Cell Models. Front Mol Neurosci *13*, 597391. https://doi.org/10.3389/fnmol.2020.597391.

17. Koppers, M., Özkan, N., Nguyen, H.H., Jurriens, D., McCaughey, J., Nguyen, D.T.M., Li, C.H., Stucchi, R., Altelaar, M., MacGillavry, H.D., et al. (2024). Axonal endoplasmic reticulum tubules control local translation via P180/RRBP1-mediated ribosome interactions. Developmental Cell *59*, 2053-2068.e9. https://doi.org/10.1016/j.devcel.2024.05.005.

18. tom Dieck, S., Kochen, L., Hanus, C., Heumüller, M., Bartnik, I., Nassim-Assir, B., Merk, K., Mosler, T., Garg, S., Bunse, S., et al. (2015). Direct visualization of newly synthesized target proteins *in situ*. Nature Methods *12*, 411‑414. https://doi.org/10.1038/nmeth.3319.

19. Geppert, M., Goda, Y., Hammer, R.E., Li, C., Rosahl, T.W., Stevens, C.F., and Südhof, T.C. (1994). Synaptotagmin I: A major Ca2+ sensor for transmitter release at a central synapse. Cell *79*, 717‑727. https://doi.org/10.1016/0092-8674(94)90556-8.

20. Trotter, J.H., Hao, J., Maxeiner, S., Tsetsenis, T., Liu, Z., Zhuang, X., and Südhof, T.C. (2019). Synaptic neurexin-1 assembles into dynamically regulated active zone nanoclusters. Journal of Cell Biology *218*, 2677‑2698. https://doi.org/10.1083/jcb.201812076.

21. Maness, P.F., and Schachner, M. (2007). Neural recognition molecules of the immunoglobulin superfamily: signaling transducers of axon guidance and neuronal migration. Nat Neurosci *10*, 19‑26. https://doi.org/10.1038/nn1827.

22. Willis, D.E., van Niekerk, E.A., Sasaki, Y., Mesngon, M., Merianda, T.T., Williams, G.G., Kendall, M., Smith, D.S., Bassell, G.J., and Twiss, J.L. (2007). Extracellular stimuli specifically regulate localized levels of individual neuronal mRNAs. J Cell Biol *178*, 965‑980. https://doi.org/10.1083/jcb.200703209.

23. Cagnetta, R., Frese, C.K., Shigeoka, T., Krijgsveld, J., and Holt, C.E. (2018). Rapid Cue-Specific Remodeling of the Nascent Axonal Proteome. Neuron *99*, 29-46.e4. https://doi.org/10.1016/j.neuron.2018.06.004.

24. Koppers, M., and Holt, C.E. (2022). Receptor-Ribosome Coupling: A Link Between Extrinsic Signals and mRNA Translation in Neuronal Compartments. Annu Rev Neurosci *45*, 41‑61. https://doi.org/10.1146/annurev-neuro-083021-110015.

25. Deng, C., Moradi, M., Reinhard, S., Ji, C., Jablonka, S., Hennlein, L., Lüningschrör, P., Doose, S., Sauer, M., and Sendtner, M. (2021). Dynamic remodeling of ribosomes and endoplasmic reticulum in axon terminals of motoneurons. Journal of Cell Science *134*, jcs258785. https://doi.org/10.1242/jcs.258785.

26. Nedozralova, H., Basnet, N., Ibiricu, I., Bodakuntla, S., Biertümpfel, C., and Mizuno, N. (2022). In situ cryo-electron tomography reveals local cellular machineries for axon

branch development. Journal of Cell Biology *221*, e202106086. https://doi.org/10.1083/jcb.202106086.

27. Farías, G.G., Guardia, C.M., Britt, D.J., Guo, X., and Bonifacino, J.S. (2015). Sorting of Dendritic and Axonal Vesicles at the Pre-axonal Exclusion Zone. Cell Rep *13*, 1221‑1232. https://doi.org/10.1016/j.celrep.2015.09.074.

28. Boncompain, G., Divoux, S., Gareil, N., de Forges, H., Lescure, A., Latreche, L., Mercanti, V., Jollivet, F., Raposo, G., and Perez, F. (2012). Synchronization of secretory protein traffic in populations of cells. Nat Methods *9*, 493‑498. https://doi.org/10.1038/nmeth.1928.

29. Lippincott-Schwartz, J., Donaldson, J.G., Schweizer, A., Berger, E.G., Hauri, H.-P., Yuan, L.C., and Klausner, R.D. (1990). Microtubule-dependent retrograde transport of proteins into the ER in the presence of brefeldin a suggests an ER recycling pathway. Cell *60*, 821‑836. https://doi.org/10.1016/0092-8674(90)90096-W.

30. Farías, G.G., Fréal, A., Tortosa, E., Stucchi, R., Pan, X., Portegies, S., Will, L., Altelaar, M., and Hoogenraad, C.C. (2019). Feedback-Driven Mechanisms between Microtubules and the Endoplasmic Reticulum Instruct Neuronal Polarity. Neuron *102*, 184-201.e8. https://doi.org/10.1016/j.neuron.2019.01.030.

31. Aridor, M., and Fish, K.N. (2009). Selective Targeting of ER Exit Sites Supports Axon Development. Traffic *10*, 1669‑1684. https://doi.org/10.1111/j.1600-0854.2009.00974.x.

32. Özkan, N., Koppers, M., van Soest, I., van Harten, A., Jurriens, D., Liv, N., Klumperman, J., Kapitein, L.C., Hoogenraad, C.C., and Farías, G.G. (2021). ER ‑ lysosome contacts at a pre-axonal region regulate axonal lysosome availability. Nat Commun *12*, 4493. https://doi.org/10.1038/s41467-021-24713-5.

33. Aridor, M., Bannykh, S.I., Rowe, T., and Balch, W.E. (1995). Sequential coupling between COPII and COPI vesicle coats in endoplasmic reticulum to Golgi transport. J Cell Biol *131*, 875‑893. https://doi.org/10.1083/jcb.131.4.875.

34. Long, K.R., Yamamoto, Y., Baker, A.L., Watkins, S.C., Coyne, C.B., Conway, J.F., and Aridor, M. (2010). Sar1 assembly regulates membrane constriction and ER export. Journal of Cell Biology *190*, 115‑128. https://doi.org/10.1083/jcb.201004132.

35. Caldeira, M.V., Melo, C.V., Pereira, D.B., Carvalho, R.F., Carvalho, A.L., and Duarte, C.B. (2007). BDNF regulates the expression and traffic of NMDA receptors in cultured hippocampal neurons. Molecular and Cellular Neuroscience *35*, 208‑219. https://doi.org/10.1016/j.mcn.2007.02.019.

36. Zhao, L., Sheng, A.-L., Huang, S.-H., Yin, Y.-X., Chen, B., Li, X.-Z., Zhang, Y., and Chen, Z.-Y. (2009). Mechanism underlying activity-dependent insertion of TrkB into the neuronal surface. Journal of Cell Science *122*, 3123‑3136. https://doi.org/10.1242/jcs.047712.

37. Lam, S.S., Martell, J.D., Kamer, K.J., Deerinck, T.J., Ellisman, M.H., Mootha, V.K., and Ting, A.Y. (2015). Directed evolution of APEX2 for electron microscopy and proximity labeling. Nat Methods *12*, 51‑54. https://doi.org/10.1038/nmeth.3179.

38. Zinnall, U., Milek, M., Minia, I., Vieira-Vieira, C.H., Müller, S., Mastrobuoni, G., Hazapis, O.-G., Del Giudice, S., Schwefel, D., Bley, N., et al. (2022). HDLBP binds ER-targeted mRNAs by multivalent interactions to promote protein synthesis of transmembrane and secreted proteins. Nat Commun *13*, 2727. https://doi.org/10.1038/s41467-022-30322-7.

39. Ooi, Y.S., Majzoub, K., Flynn, R.A., Mata, M.A., Diep, J., Li, J.K., van Buuren, N., Rumachik, N., Johnson, A.G., Puschnik, A.S., et al. (2019). An RNA-centric dissection of host complexes controlling flavivirus infection. Nat Microbiol *4*, 2369‑2382. https://doi.org/10.1038/s41564-019-0518-2.

40. Lee, M.C.S., Miller, E.A., Goldberg, J., Orci, L., and Schekman, R. (2004). Bi-Directional Protein Transport Between the Er and Golgi. Annual Review of Cell & Developmental Biology *20*, 87‑123. https://doi.org/10.1146/annurev.cellbio.20.010403.105307.

41. Farquhar, M.G., and Palade, G.E. (1981). The Golgi apparatus (complex)-(1954-1981)-from artifact to center stage. The Journal of cell biology *91*, 77s‑103s. https://doi.org/10.1083/jcb.91.3.77s.

42. Tagaya, M., Arasaki, K., Inoue, H., and Kimura, H. (2014). Moonlighting functions of the NRZ (mammalian Dsl1) complex. Frontiers in Cell and Developmental Biology *2*.

43. Raote, I., Ortega-Bellido, M., Santos, A.J., Foresti, O., Zhang, C., Garcia-Parajo, M.F., Campelo, F., and Malhotra, V. (2018). TANGO1 builds a machine for collagen export by recruiting and spatially organizing COPII, tethers and membranes. eLife *7*, e32723. https://doi.org/10.7554/eLife.32723.

44. Mancias, J.D., and Goldberg, J. (2007). The Transport Signal on Sec22 for Packaging into COPII-Coated Vesicles Is a Conformational Epitope. Molecular Cell *26*, 403‑414. https://doi.org/10.1016/j.molcel.2007.03.017.

45. Sun, W., Tian, B.-X., Wang, S.-H., Liu, P.-J., and Wang, Y.-C. (2020). The function of SEC22B and its role in human diseases. Cytoskeleton *77*, 303‑312. https://doi.org/10.1002/cm.21628.

46. Cohen, N.R., Taylor, J.S.H., Scott, L.B., Guillery, R.W., Soriano, P., and Furley, A.J.W. (1998). Errors in corticospinal axon guidance in mice lacking the neural cell adhesion molecule L1. Current Biology *8*, 26‑33. https://doi.org/10.1016/S0960-9822(98)70017-X.

47. Wiencken-Barger, A.E., Mavity-Hudson, J., Bartsch, U., Schachner, M., and Casagrande, V.A. (2004). The Role of L1 in Axon Pathfinding and Fasciculation. Cerebral Cortex *14*, 121‑131. https://doi.org/10.1093/cercor/bhg110.

48. Krueger, D.D., Tuffy, L.P., Papadopoulos, T., and Brose, N. (2012). The role of neurexins and neuroligins in the formation, maturation, and function of vertebrate synapses. Curr Opin Neurobiol *22*, 412‑422. https://doi.org/10.1016/j.conb.2012.02.012.

49. Goda, Y., and Davis, G.W. (2003). Mechanisms of synapse assembly and disassembly. Neuron *40*, 243‑264. https://doi.org/10.1016/s0896-6273(03)00608-1.

50. Ziv, N.E., and Garner, C.C. (2004). Cellular and molecular mechanisms of presynaptic assembly. Nature Reviews Neuroscience *5*, 385. https://doi.org/10.1038/nrn1370.

51. Südhof, T.C. (2021). The cell biology of synapse formation. J Cell Biol *220*, e202103052. https://doi.org/10.1083/jcb.202103052.

52. Batista, A.F.R., Martínez, J.C., and Hengst, U. (2017). Intra-axonal Synthesis of SNAP25 Is Required for the Formation of Presynaptic Terminals. Cell Reports *20*, 3085‑3098. https://doi.org/10.1016/j.celrep.2017.08.097.

53. Kim, E., and Jung, H. (2015). Local protein synthesis in neuronal axons: why and how we study. BMB Rep *48*, 139‑146. https://doi.org/10.5483/BMBRep.2015.48.3.010.

54. Greif, K.F., Asabere, N., Lutz, G.J., and Gallo, G. (2013). Synaptotagmin-1 promotes the formation of axonal filopodia and branches along the developing axons of forebrain neurons. Developmental Neurobiology *73*, 27–44. https://doi.org/10.1002/dneu.22033.

55. Sytnyk, V., Leshchyns’ka, I., and Schachner, M. (2017). Neural Cell Adhesion Molecules of the Immunoglobulin Superfamily Regulate Synapse Formation, Maintenance, and Function. Trends in Neurosciences *40*, 295–308. https://doi.org/10.1016/j.tins.2017.03.003.

56. Cui-Wang, T., Hanus, C., Cui, T., Helton, T., Bourne, J., Watson, D., Harris, K.M., and Ehlers, M.D. (2012). Local Zones of Endoplasmic Reticulum Complexity Confine Cargo in Neuronal Dendrites. Cell *148*, 309–321. https://doi.org/10.1016/j.cell.2011.11.056.

57. Hanus, C., Kochen, L., Dieck, S. tom, Racine, V., Sibarita, J.-B., Schuman, E.M., and Ehlers, M.D. (2014). Synaptic Control of Secretory Trafficking in Dendrites. Cell Rep *7*, 1771–1778. https://doi.org/10.1016/j.celrep.2014.05.028.

58. Mikhaylova, M., Bera, S., Kobler, O., Frischknecht, R., and Kreutz, M.R. (2016). A Dendritic Golgi Satellite between ERGIC and Retromer. Cell Reports *14*, 189–199. https://doi.org/10.1016/j.celrep.2015.12.024.

59. Bowen, A.B., Bourke, A.M., Hiester, B.G., Hanus, C., and Kennedy, M.J. (2017). Golgi-independent secretory trafficking through recycling endosomes in neuronal dendrites and spines. eLife *6*, e27362. https://doi.org/10.7554/eLife.27362.

60. Govind, A.P., Jeyifous, O., Russell, T.A., Yi, Z., Weigel, A.V., Ramaprasad, A., Newell, L., Ramos, W., Valbuena, F.M., Casler, J.C., et al. (2021). Activity-dependent Golgi satellite formation in dendrites reshapes the neuronal surface glycoproteome https://doi.org/10.1101/2021.04.06.438745.

61. Andres-Alonso, M., Borgmeyer, M., Mirzapourdelavar, H., Lormann, J., Klein, K., Schweizer, M., Hoffmeister-Ullerich, S., Oelschlegel, A.M., Dityatev, A., and Kreutz, M.R. (2023). Golgi satellites are essential for polysialylation of NCAM and expression of LTP at distal synapses. Cell Reports *42*. https://doi.org/10.1016/j.celrep.2023.112692.

62. Terasaki, M. (2018). Axonal endoplasmic reticulum is very narrow. J Cell Sci *131*, jcs210450. https://doi.org/10.1242/jcs.210450.

63. Cornejo, V.H., González, C., Campos, M., Vargas-Saturno, L., Juricic, M. de los Á., Miserey-Lenkei, S., Pertusa, M., Madrid, R., and Couve, A. (2020). Non-conventional Axonal Organelles Control TRPM8 Ion Channel Trafficking and Peripheral Cold Sensing. Cell Reports *30*, 4505-4517.e5. https://doi.org/10.1016/j.celrep.2020.03.017.

64. Everts, I., Villmann, C., and Hollmann, M. (1997). N-Glycosylation Is Not a Prerequisite for Glutamate Receptor Function but Is Essential for Lectin Modulation. Molecular Pharmacology *52*, 861–873. https://doi.org/10.1124/mol.52.5.861.

65. Kwon, S.E., and Chapman, E.R. (2012). Glycosylation Is Dispensable for Sorting of Synaptotagmin 1 but Is Critical for Targeting of SV2 and Synaptophysin to Recycling Synaptic Vesicles *. Journal of Biological Chemistry *287*, 35658–35668. https://doi.org/10.1074/jbc.M112.398883.

66. Hanus, C., Geptin, H., Tushev, G., Garg, S., Alvarez-Castelao, B., Sambandan, S., Kochen, L., Hafner, A.-S., Langer, J.D., and Schuman, E.M. (2016). Unconventional secretory processing diversifies neuronal ion channel properties. eLife *5*, e20609. https://doi.org/10.7554/eLife.20609.

67. Budnik, A., and Stephens, D.J. (2009). ER exit sites – Localization and control of COPII vesicle formation. FEBS Letters *583*, 3796–3803. https://doi.org/10.1016/j.febslet.2009.10.038.

68. Downes, K.W., and Zanetti, G. (2025). Mechanisms of COPII coat assembly and cargo recognition in the secretory pathway. Nat Rev Mol Cell Biol, 1–16. https://doi.org/10.1038/s41580-025-00839-y.

69. Weigel, A.V., Chang, C.-L., Shtengel, G., Xu, C.S., Hoffman, D.P., Freeman, M., Iyer, N., Aaron, J., Khuon, S., Bogovic, J., et al. (2021). ER-to-Golgi protein delivery through an interwoven, tubular network extending from ER. Cell *184*, 2412-2429.e16. https://doi.org/10.1016/j.cell.2021.03.035.

70. Cai, H., Reinisch, K., and Ferro-Novick, S. (2007). Coats, Tethers, Rabs, and SNAREs Work Together to Mediate the Intracellular Destination of a Transport Vesicle. Developmental Cell *12*, 671–682. https://doi.org/10.1016/j.devcel.2007.04.005.

71. Sztul, E., and Lupashin, V. (2009). Role of vesicle tethering factors in the ER-Golgi membrane traffic. FEBS Lett *583*, 3770–3783. https://doi.org/10.1016/j.febslet.2009.10.083.

72. Raote, I., and Malhotra, V. (2019). Protein transport by vesicles and tunnels. Journal of Cell Biology *218*, 737–739. https://doi.org/10.1083/jcb.201811073.

73. Wang, X., Li, X., Wang, J., Wang, J., Hu, C., Zeng, J., Shi, A., and Lin, L. (2022). SMGL-1/NBAS acts as a RAB-8 GEF to regulate unconventional protein secretion. Journal of Cell Biology *221*, e202111125. https://doi.org/10.1083/jcb.202111125.

74. Kamiguchi, H. (2007). The Role of Cell Adhesion Molecules in Axon Growth and Guidance. In Axon Growth and Guidance Advances in Experimental Medicine and Biology., D. Bagnard, ed. (Springer), pp. 95–102. https://doi.org/10.1007/978-0-387-76715-4_7.

75. van Beuningen, S.F.B., Will, L., Harterink, M., Chazeau, A., van Battum, E.Y., Frias, C.P., Franker, M.A.M., Katrukha, E.A., Stucchi, R., Vocking, K., et al. (2015). TRIM46 Controls Neuronal Polarity and Axon Specification by Driving the Formation of Parallel Microtubule Arrays. Neuron *88*, 1208–1226. https://doi.org/10.1016/j.neuron.2015.11.012.

76. Pantazis, C.B., Yang, A., Lara, E., McDonough, J.A., Blauwendraat, C., Peng, L., Oguro, H., Kanaujiya, J., Zou, J., Sebesta, D., et al. (2022). A reference human induced pluripotent stem cell line for large-scale collaborative studies. Cell Stem Cell *29*, 1685-1702.e22. https://doi.org/10.1016/j.stem.2022.11.004.

77. van Vlijmen, T., Vleugel, M., Evers, M., Mohammed, S., Wulf, P.S., Heck, A.J.R., Hoogenraad, C.C., and van der Sluijs, P. (2008). A unique residue in rab3c determines the interaction with novel binding protein Zwint-1. FEBS Letters *582*, 2838–2842. https://doi.org/10.1016/j.febslet.2008.07.012.

78. Kuijpers, M., van de Willige, D., Freal, A., Chazeau, A., Franker, M.A., Hofenk, J., Rodrigues, R.J.C., Kapitein, L.C., Akhmanova, A., Jaarsma, D., et al. (2016). Dynein Regulator NDEL1 Controls Polarized Cargo Transport at the Axon Initial Segment. Neuron *89*, 461–471. https://doi.org/10.1016/j.neuron.2016.01.022.

79. Kapitein, L.C., Schlager, M.A., van der Zwan, W.A., Wulf, P.S., Keijzer, N., and Hoogenraad, C.C. (2010). Probing Intracellular Motor Protein Activity Using an Inducible

Cargo Trafficking Assay. Biophysical Journal *99*, 2143–2152. https://doi.org/10.1016/j.bpj.2010.07.055.

80. van Leeuwen, W., Nguyen, D.T.M., Grond, R., Veenendaal, T., Rabouille, C., and Farías, G.G. (2022). Stress-induced phase separation of ERES components into Sec bodies precedes ER exit inhibition in mammalian cells. J Cell Sci *135*. https://doi.org/10.1242/jcs.260294.

81. Meijering, E., Jacob, M., Sarria, J.-C.F., Steiner, P., Hirling, H., and Unser, M. (2004). Design and validation of a tool for neurite tracing and analysis in fluorescence microscopy images. Cytometry A *58*, 167–176. https://doi.org/10.1002/cyto.a.20022.

82. Thévenaz, P., and Unser, M. (2007). User-friendly semiautomated assembly of accurate image mosaics in microscopy. Microsc. Res. Tech. *70*, 135–146. https://doi.org/10.1002/jemt.20393.

83. Flores, E.L., Qi, A., Reilly, L., Santiana, M., Ward, M., and Cookson, M. (2023). iNDI Transcription Factor-NGN2 differentiation of human iPSC into cortical neurons Version 2.

84. Lois, C., Hong, E.J., Pease, S., Brown, E.J., and Baltimore, D. (2002). Germline Transmission and Tissue-Specific Expression of Transgenes Delivered by Lentiviral Vectors. Science *295*, 868–872. https://doi.org/10.1126/science.1067081.

85. Stewart, S.A., Dykxhoorn, D.M., Palliser, D., Mizuno, H., Yu, E.Y., An, D.S., Sabatini, D.M., Chen, I.S.Y., Hahn, W.C., Sharp, P.A., et al. (2003). Lentivirus-delivered stable gene silencing by RNAi in primary cells. RNA *9*, 493–501. https://doi.org/10.1261/rna.2192803.

86. Bindels, D.S., Haarbosch, L., van Weeren, L., Postma, M., Wiese, K.E., Mastop, M., Aumonier, S., Gotthard, G., Royant, A., Hink, M.A., et al. (2017). mScarlet: a bright monomeric red fluorescent protein for cellular imaging. Nat Methods *14*, 53–56. https://doi.org/10.1038/nmeth.4074.

87. Gallo, A., Danglot, L., Giordano, F., Hewlett, B., Binz, T., Vannier, C., and Galli, T. (2020). Role of the Sec22b–E-Syt complex in neurite growth and ramification. Journal of Cell Science *133*, jcs247148. https://doi.org/10.1242/jcs.247148.

88. Stephens, D.J., Lin-Marq, N., Pagano, A., Pepperkok, R., and Paccaud, J.P. (2000). COPI-coated ER-to-Golgi transport complexes segregate from COPII in close proximity to ER exit sites. J Cell Sci *113 (Pt 12)*, 2177–2185. https://doi.org/10.1242/jcs.113.12.2177.

89. Kerr, S.C., and Kahn, R.A. (2015). Tool box: Plasmids for the expression or knockdown of human ARF Family GTPases (ARF/ARL/SAR) and their co-expression in bacteria with N-myristoyltransferases. Cellular Logistics *5*, e1090523. https://doi.org/10.1080/21592799.2015.1090523.

90. Willems, J., Jong, A.P.H. de, Scheefhals, N., Mertens, E., Catsburg, L.A.E., Poorthuis, R.B., Winter, F. de, Verhaagen, J., Meye, F.J., and MacGillavry, H.D. (2020). ORANGE: A CRISPR/Cas9-based genome editing toolbox for epitope tagging of endogenous proteins in neurons. PLOS Biology *18*, e3000665. https://doi.org/10.1371/journal.pbio.3000665.

91. Cuylen, S., Blaukopf, C., Politi, A.Z., Müller-Reichert, T., Neumann, B., Poser, I., Ellenberg, J., Hyman, A.A., and Gerlich, D.W. (2016). Ki-67 acts as a biological

surfactant to disperse mitotic chromosomes. Nature *535*, 308‑312. https://doi.org/10.1038/nature18610.

92. Catsburg, L.A., Westra, M., Van Schaik, A.M., and MacGillavry, H.D. (2022). Dynamics and nanoscale organization of the postsynaptic endocytic zone at excitatory synapses. eLife *11*, e74387. https://doi.org/10.7554/eLife.74387.

93. Hsu, P.D., Scott, D.A., Weinstein, J.A., Ran, F.A., Konermann, S., Agarwala, V., Li, Y., Fine, E.J., Wu, X., Shalem, O., et al. (2013). DNA targeting specificity of RNA-guided Cas9 nucleases. Nat Biotechnol *31*, 827‑832. https://doi.org/10.1038/nbt.2647.

94. Grimm, J.B., Xie, L., Casler, J.C., Patel, R., Tkachuk, A.N., Falco, N., Choi, H., Lippincott-Schwartz, J., Brown, T.A., Glick, B.S., et al. (2021). A General Method to Improve Fluorophores Using Deuterated Auxochromes. JACS Au *1*, 690‑696. https://doi.org/10.1021/jacsau.1c00006.

95. Li, C.H., Kersten, N., Özkan, N., Nguyen, D.T.M., Koppers, M., Post, H., Altelaar, M., and Farias, G.G. (2024). Spatiotemporal proteomics reveals the biosynthetic lysosomal membrane protein interactome in neurons. Nat Commun *15*, 10829. https://doi.org/10.1038/s41467-024-55052-w.

96. Cox, J., and Mann, M. (2008). MaxQuant enables high peptide identification rates, individualized p.p.b.-range mass accuracies and proteome-wide protein quantification. Nat Biotechnol *26*, 1367‑1372. https://doi.org/10.1038/nbt.1511.

97. Tyanova, S., Temu, T., Sinitcyn, P., Carlson, A., Hein, M.Y., Geiger, T., Mann, M., and Cox, J. (2016). The Perseus computational platform for comprehensive analysis of (prote)omics data. Nat Methods *13*, 731‑740. https://doi.org/10.1038/nmeth.3901.

98. Cioni, J.-M., Lin, J.Q., Holtermann, A.V., Koppers, M., Jakobs, M.A.H., Azizi, A., Turner-Bridger, B., Shigeoka, T., Franze, K., Harris, W.A., et al. (2019). Late Endosomes Act as mRNA Translation Platforms and Sustain Mitochondria in Axons. Cell *176*, 56-72.e15. https://doi.org/10.1016/j.cell.2018.11.030.

99. Spangler, S.A., Schmitz, S.K., Kevenaar, J.T., de Graaff, E., de Wit, H., Demmers, J., Toonen, R.F., and Hoogenraad, C.C. (2013). Liprin-α2 promotes the presynaptic recruitment and turnover of RIM1/CASK to facilitate synaptic transmission. J Cell Biol *201*, 915‑928. https://doi.org/10.1083/jcb.201301011.

100. Lindhout, F.W., Cao, Y., Kevenaar, J.T., Bodzęta, A., Stucchi, R., Boumpoutsari, M.M., Katrukha, E.A., Altelaar, M., MacGillavry, H.D., and Hoogenraad, C.C. (2019). VAP-SCRN1 interaction regulates dynamic endoplasmic reticulum remodeling and presynaptic function. The EMBO Journal *38*, e101345. https://doi.org/10.15252/embj.2018101345.

Figure 1

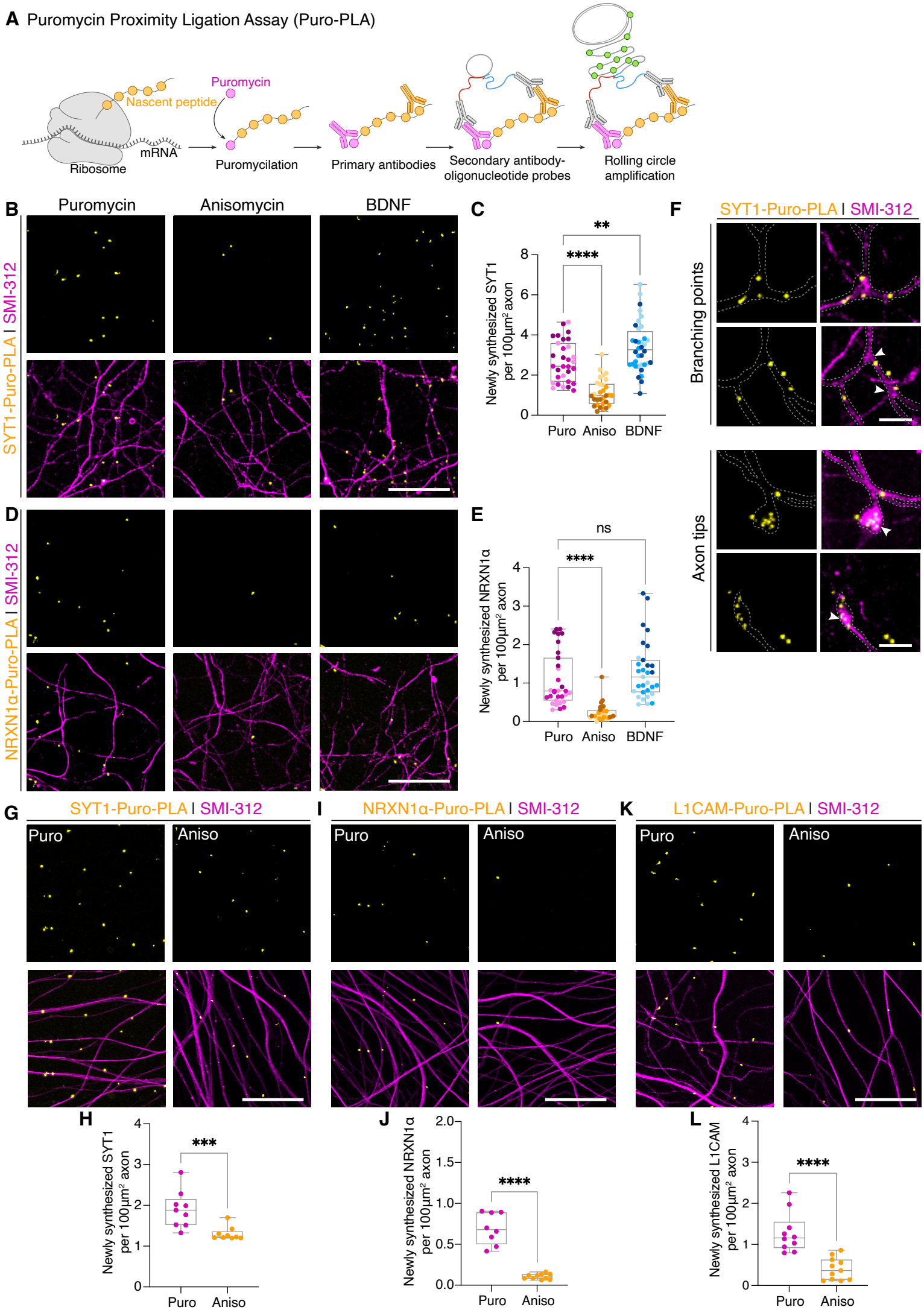
A Puromycin Proximity Ligation Assay (Puro-PLA)
Puromycin
Nascent peptide
mRNA
Ribosome
Puromycilation
Primary antibodies
Secondary antibody-oligonucleotide probes
Rolling circle amplification
B
Puromycin
Anisomycin
BDNF
SYT1-Puro-PLA | SMI-312
C
Newly synthesized SYT1 per 100μm² axon
Puro
Aniso
BDNF
**
****
D
NRXN1α-Puro-PLA | SMI-312
E
Newly synthesized NRXN1α per 100μm² axon
ns
****
F
SYT1-Puro-PLA | SMI-312
Branching points
Axon tips
G
SYT1-Puro-PLA | SMI-312
Puro
Aniso
H
Newly synthesized SYT1 per 100μm² axon
***
I
NRXN1α-Puro-PLA | SMI-312
J
Newly synthesized NRXN1α per 100μm² axon
****
K
L1CAM-Puro-PLA | SMI-312
L
Newly synthesized L1CAM per 100μm² axon
****

Figure 2

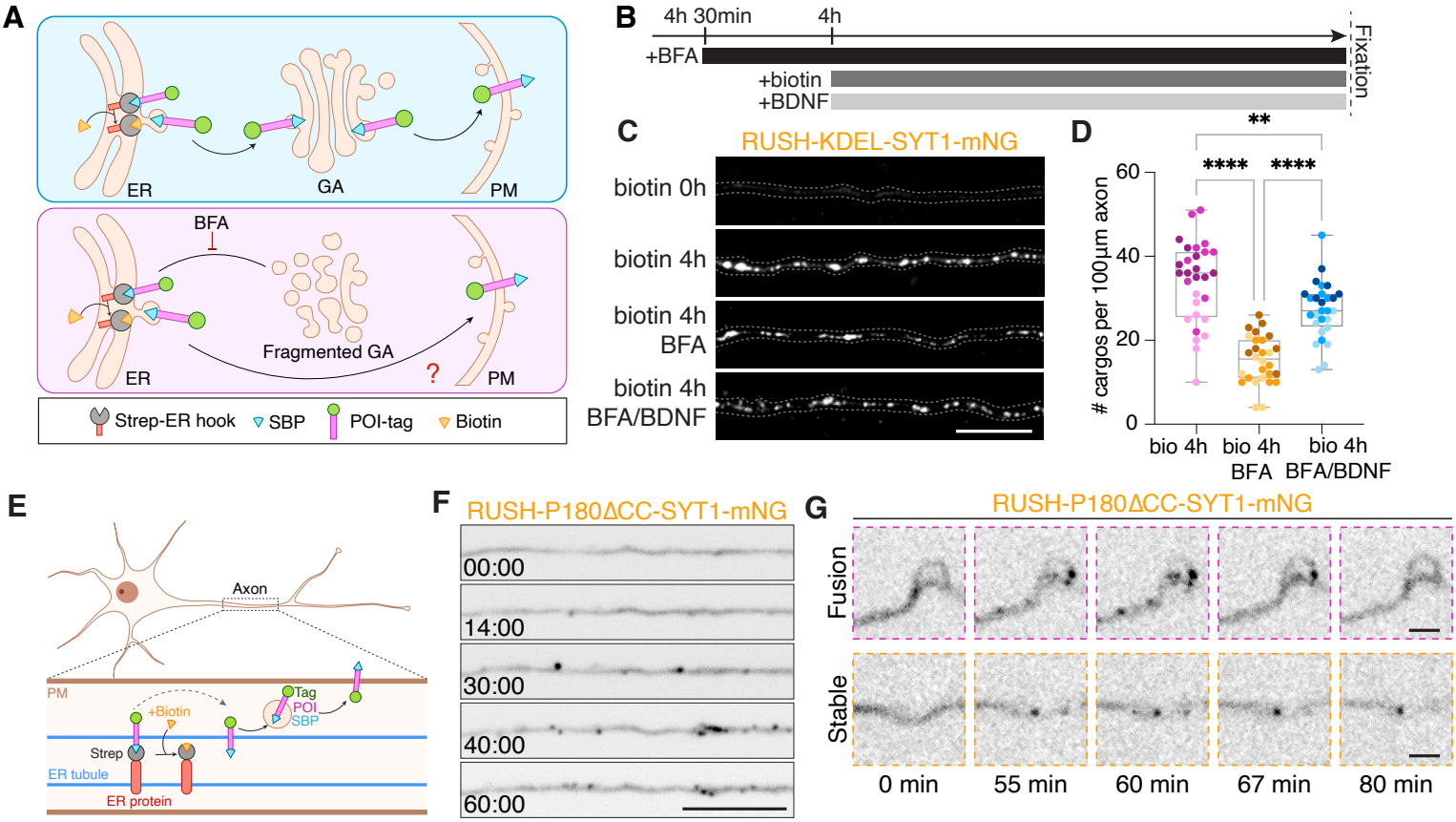
A
ER
GA
PM
BFA
Fragmented GA
?
Strep-ER hook
SBP
POI-tag
Biotin
B
4h 30min
4h
+BFA
+biotin
+BDNF
Fixation
C
RUSH-KDEL-SYT1-mNG
biotin 0h
biotin 4h
biotin 4h BFA
biotin 4h BFA/BDNF
D
**
****
****
cargos per 100µm axon
60
40
20
0
bio 4h
bio 4h BFA
bio 4h BFA/BDNF
E
Axon
PM
+Biotin
Tag
POI
SBP
Strep
ER tubule
ER protein
F
RUSH-P180ΔCC-SYT1-mNG
00:00
14:00
30:00
40:00
60:00
G
RUSH-P180ΔCC-SYT1-mNG
Fusion
Stable
0 min
55 min
60 min
67 min
80 min

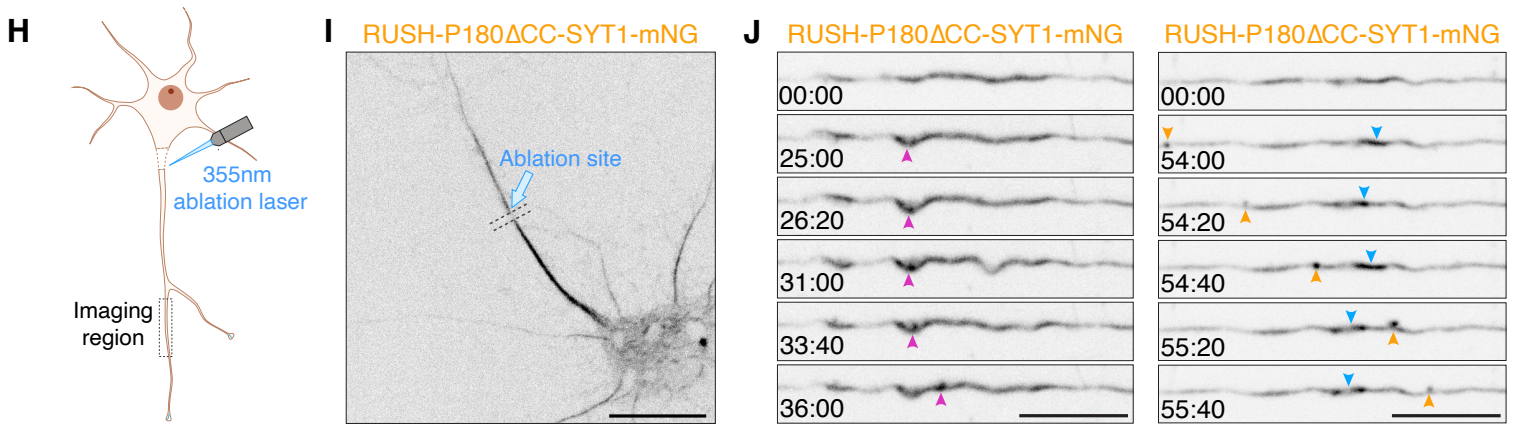
H
355nm ablation laser
Imaging region
I
RUSH-P180ΔCC-SYT1-mNG
Ablation site
J
RUSH-P180ΔCC-SYT1-mNG
00:00
25:00
26:20
31:00
33:40
36:00
RUSH-P180ΔCC-SYT1-mNG
00:00
54:00
54:20
54:40
55:20
55:40

Figure 3

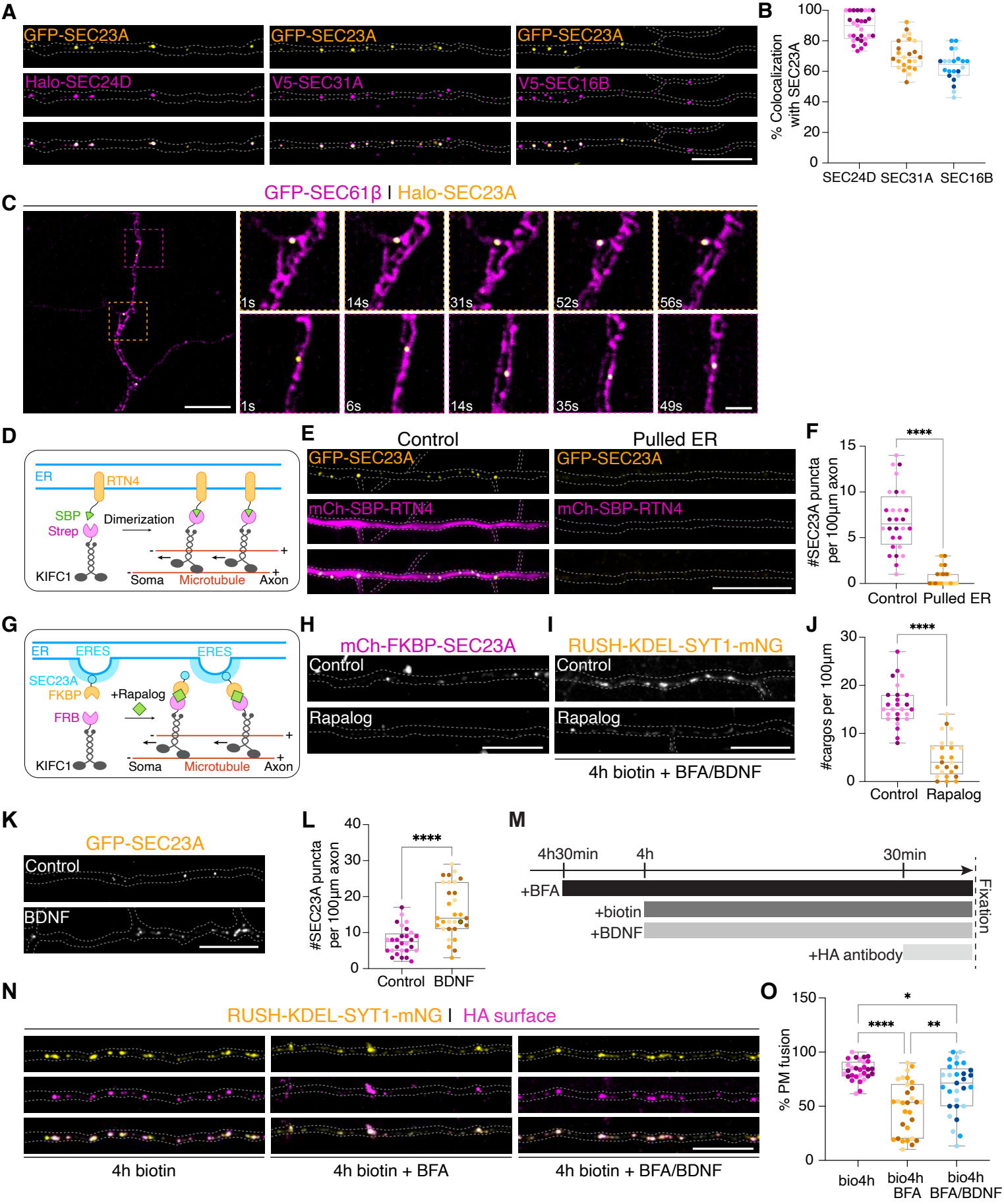
A
GFP-SEC23A
GFP-SEC23A
GFP-SEC23A
Halo-SEC24D
V5-SEC31A
V5-SEC16B
B
% Colocalization with SEC23A
100
80
60
40
20
0
SEC24D
SEC31A
SEC16B
C
GFP-SEC61β | Halo-SEC23A
1s
14s
31s
52s
56s
1s
6s
14s
35s
49s
D
ER
RTN4
SBP
Strep
Dimerization
KIFC1
Soma
Microtubule
Axon
E
Control
Pulled ER
GFP-SEC23A
GFP-SEC23A
mCh-SBP-RTN4
mCh-SBP-RTN4
F
#SEC23A puncta per 100µm axon
****
15
10
5
0
Control
Pulled ER
G
ER
ERES
ERES
SEC23A
FKBP
+Rapalog
FRB
KIFC1
Soma
Microtubule
Axon
H
mCh-FKBP-SEC23A
Control
Rapalog
I
RUSH-KDEL-SYT1-mNG
Control
Rapalog
4h biotin + BFA/BDNF
J
#cargos per 100µm
****
30
20
10
0
Control
Rapalog
K
GFP-SEC23A
Control
BDNF
L
#SEC23A puncta per 100µm axon
****
40
30
20
10
0
Control
BDNF
M
4h30min
4h
30min
+BFA
+biotin
+BDNF
+HA antibody
Fixation
N
RUSH-KDEL-SYT1-mNG | HA surface
4h biotin
4h biotin + BFA
4h biotin + BFA/BDNF
O
% PM fusion
150
100
50
0
*
****
**
bio4h
bio4h BFA
bio4h BFA/BDNF

Figure 4

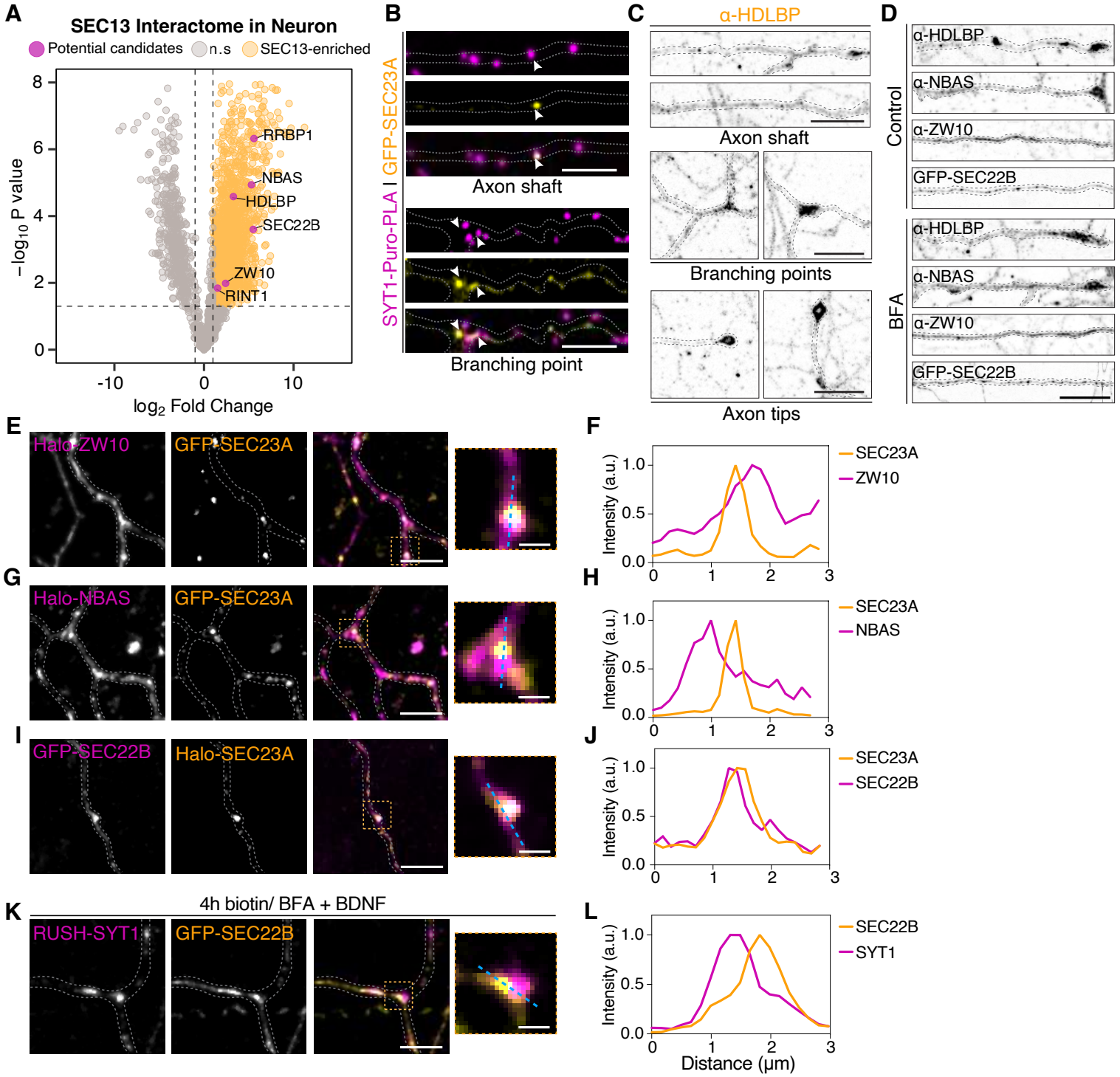
A
SEC13 Interactome in Neuron
Potential candidates
n.s
SEC13-enriched
RRBP1
NBAS
HDLBP
SEC22B
ZW10
RINT1
−log10 P value
log2 Fold Change
B
SYT1-Puro-PLA | GFP-SEC23A
Axon shaft
Branching point
C
α-HDLBP
Axon shaft
Branching points
Axon tips
D
Control
BFA
α-HDLBP
α-NBAS
α-ZW10
GFP-SEC22B
E
Halo-ZW10
GFP-SEC23A
F
SEC23A
ZW10
Intensity (a.u.)
G
Halo-NBAS
GFP-SEC23A
H
SEC23A
NBAS
I
GFP-SEC22B
Halo-SEC23A
J
SEC23A
SEC22B
K
4h biotin/ BFA + BDNF
RUSH-SYT1
GFP-SEC22B
L
SEC22B
SYT1
Distance (μm)
M
RUSH-SYT1 | GFP-SEC22B
N
Halo-ZW10 | GFP-SEC22B
O
Halo-NBAS | GFP-SEC22B

Figure 5

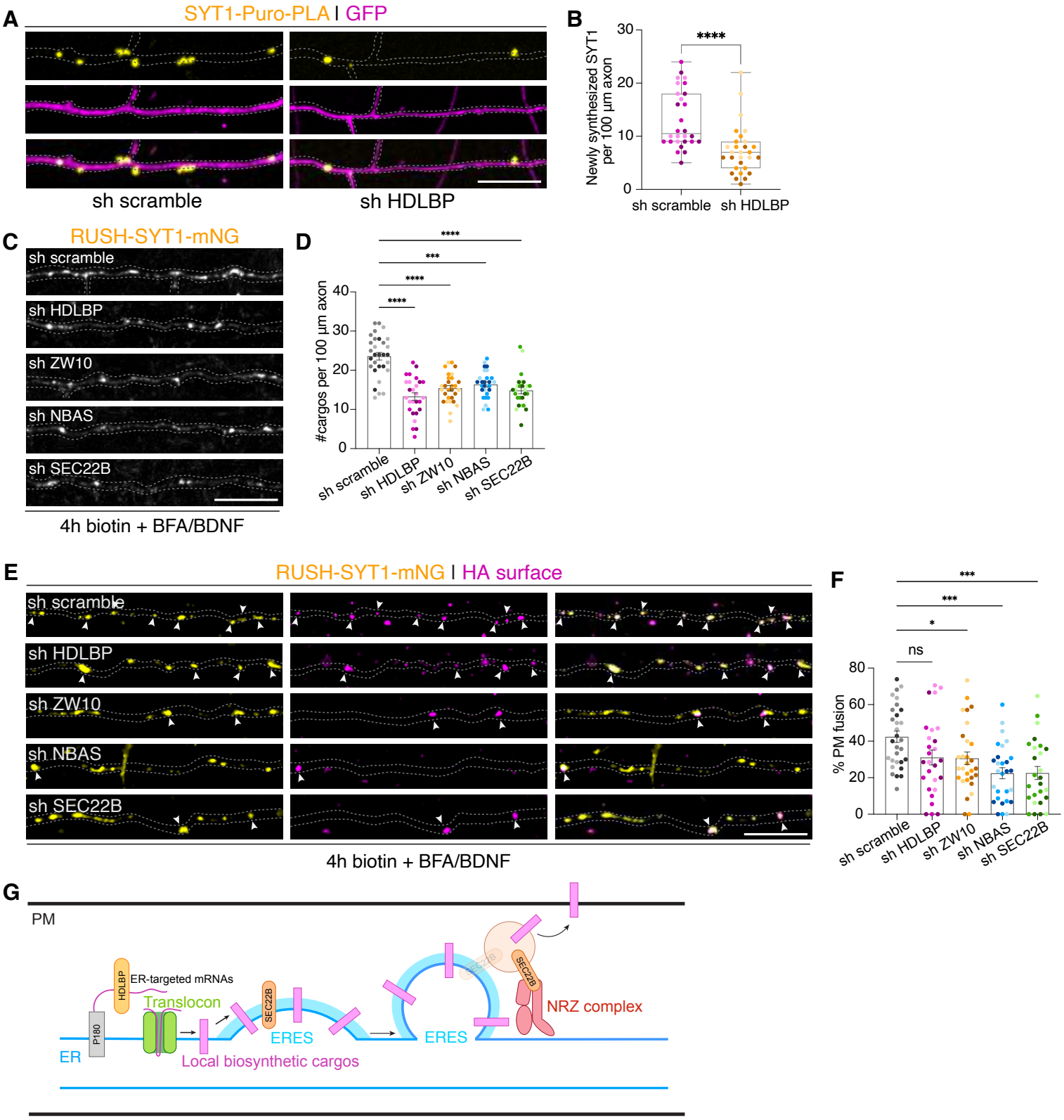
A
SYT1-Puro-PLA | GFP
sh scramble
sh HDLBP
B
Newly synthesized SYT1 per 100 µm axon
****
sh scramble
sh HDLBP
C
RUSH-SYT1-mNG
sh scramble
sh HDLBP
sh ZW10
sh NBAS
sh SEC22B
4h biotin + BFA/BDNF
D
#cargos per 100 µm axon
****
***
****
****
sh scramble
sh HDLBP
sh ZW10
sh NBAS
sh SEC22B
E
RUSH-SYT1-mNG | HA surface
sh scramble
sh HDLBP
sh ZW10
sh NBAS
sh SEC22B
4h biotin + BFA/BDNF
F
% PM fusion
***
***
*
ns
sh scramble
sh HDLBP
sh ZW10
sh NBAS
sh SEC22B
G
PM
HDLBP
ER-targeted mRNAs
Translocon
P180
ER
Local biosynthetic cargos
SEC22B
ERES
ERES
SEC22B
NRZ complex

Figure 6

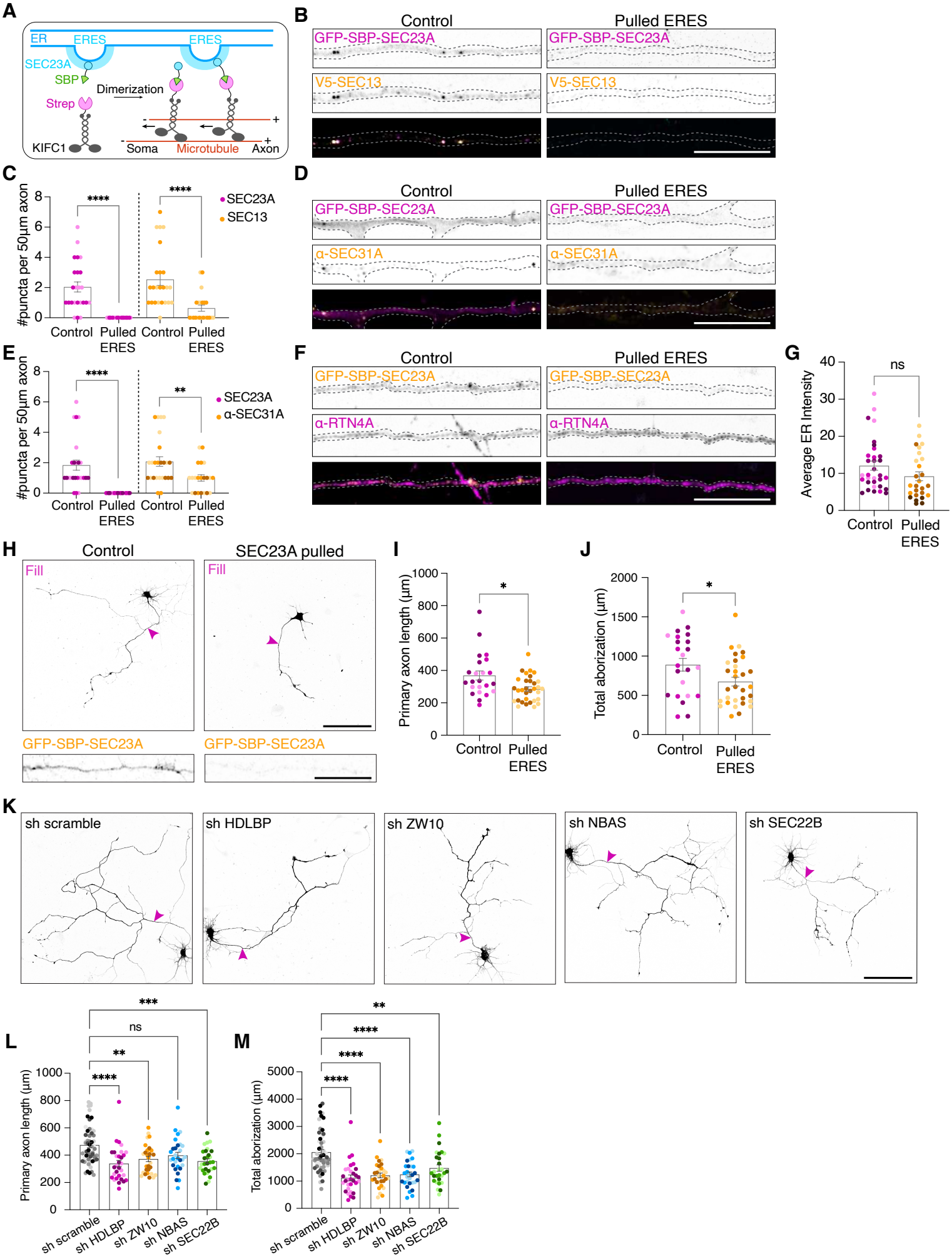
A
ER
ERES
ERES
SEC23A
SBP
Dimerization
Strep
KIFC1
Soma
Microtubule
Axon
B
Control
Pulled ERES
GFP-SBP-SEC23A
V5-SEC13
C
#puncta per 50µm axon
SEC23A
SEC13
Control
Pulled ERES
D
α-SEC31A
E
α-SEC31A
F
α-RTN4A
G
Average ER Intensity
ns
H
SEC23A pulled
Fill
I
Primary axon length (µm)
J
Total aborization (µm)
K
sh scramble
sh HDLBP
sh ZW10
sh NBAS
sh SEC22B
L
M

Figure 7

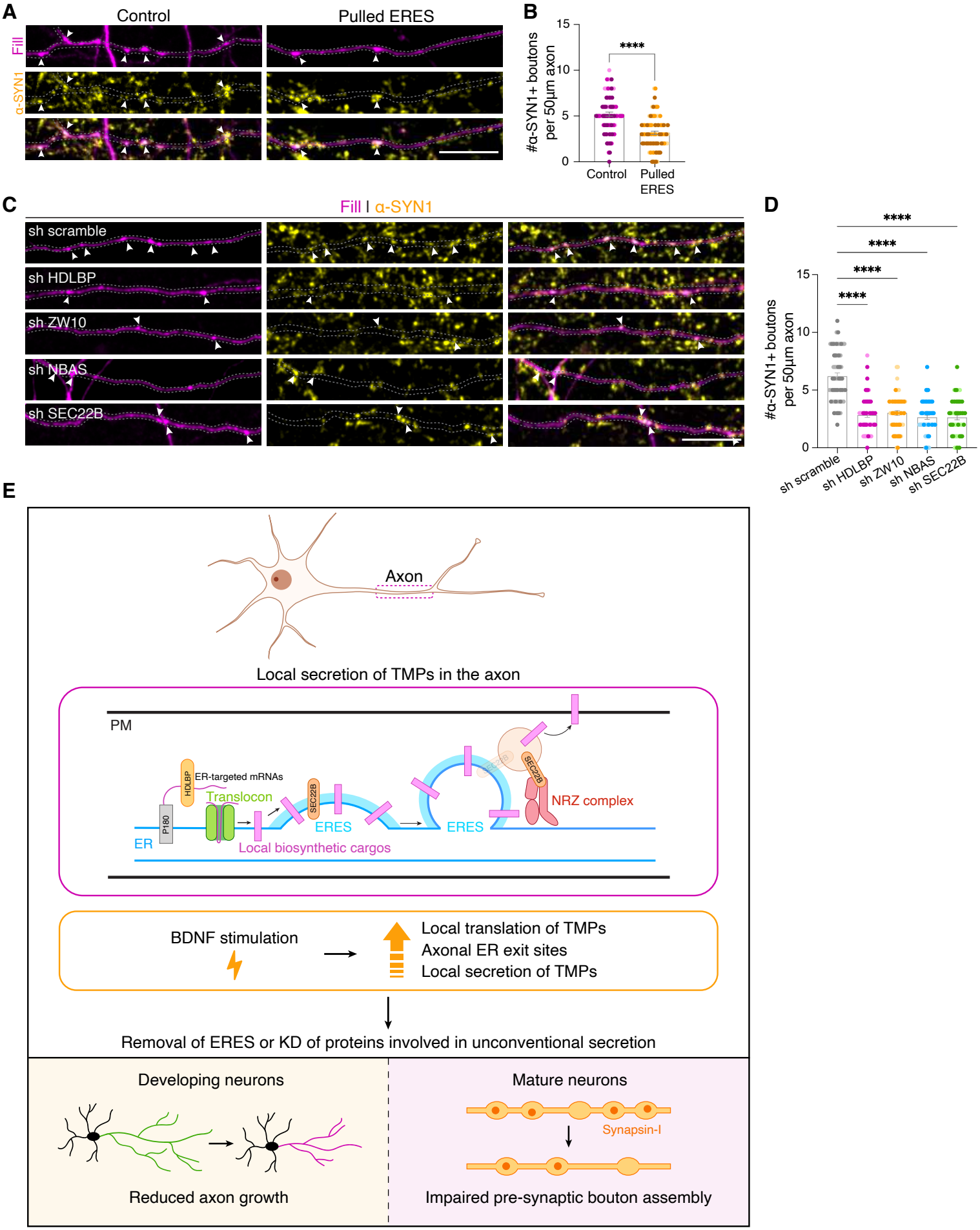
A
Control
Pulled ERES
Fill
α-SYN1
B
#α-SYN1+ boutons per 50µm axon
15
10
5
0
****
Control
Pulled ERES
C
Fill | α-SYN1
sh scramble
sh HDLBP
sh ZW10
sh NBAS
sh SEC22B
D
#α-SYN1+ boutons per 50µm axon
15
10
5
0
****
****
****
****
sh scramble
sh HDLBP
sh ZW10
sh NBAS
sh SEC22B
E
Axon
Local secretion of TMPs in the axon
PM
ER-targeted mRNAs
HDLBP
Translocon
P180
ER
SEC22B
ERES
ERES
SEC22B
NRZ complex
Local biosynthetic cargos
BDNF stimulation
Local translation of TMPs
Axonal ER exit sites
Local secretion of TMPs
Removal of ERES or KD of proteins involved in unconventional secretion
Developing neurons
Reduced axon growth
Mature neurons
Synapsin-I
Impaired pre-synaptic bouton assembly

Figure S1

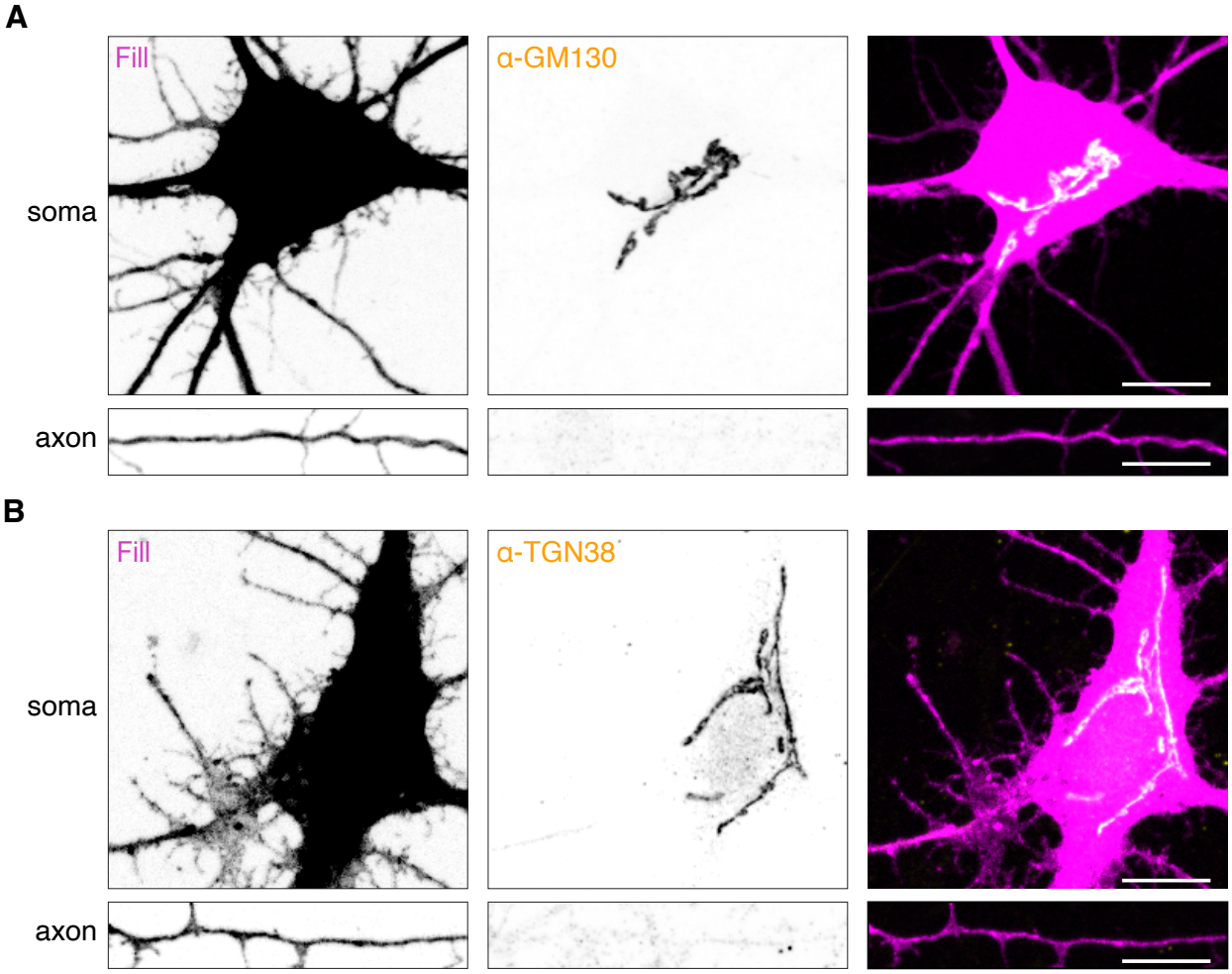

Figure S2

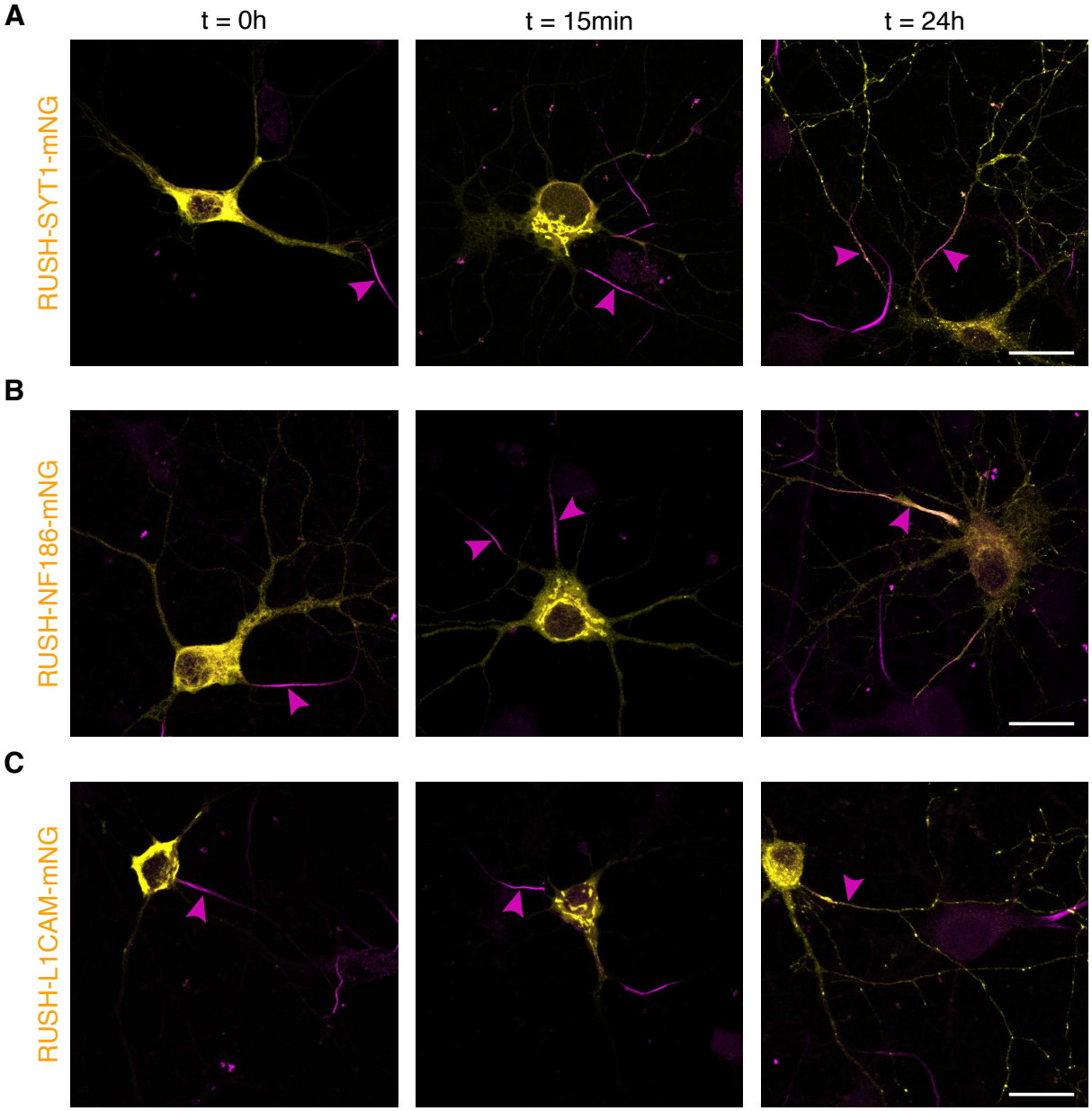
A
t = 0h
t = 15min
t = 24h
RUSH-SYT1-mNG
B
RUSH-NF186-mNG
C
RUSH-L1CAM-mNG

Figure S3

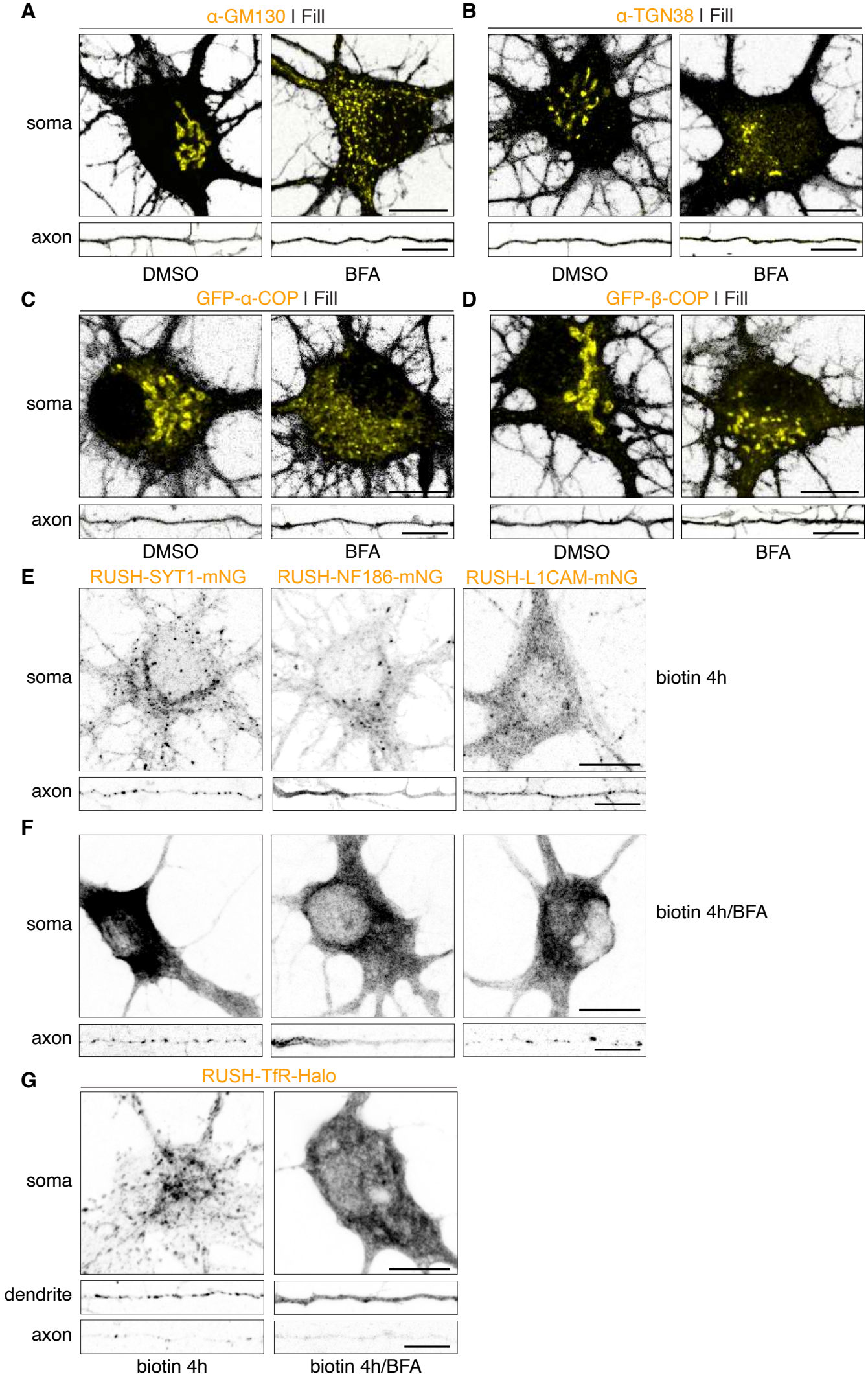
A
α-GM130 I Fill
soma
axon
DMSO
BFA
B
α-TGN38 I Fill
DMSO
BFA
C
GFP-α-COP I Fill
soma
axon
DMSO
BFA
D
GFP-β-COP I Fill
DMSO
BFA
E
RUSH-SYT1-mNG
RUSH-NF186-mNG
RUSH-L1CAM-mNG
soma
axon
biotin 4h
F
soma
axon
biotin 4h/BFA
G
RUSH-TfR-Halo
soma
dendrite
axon
biotin 4h
biotin 4h/BFA

Figure S4

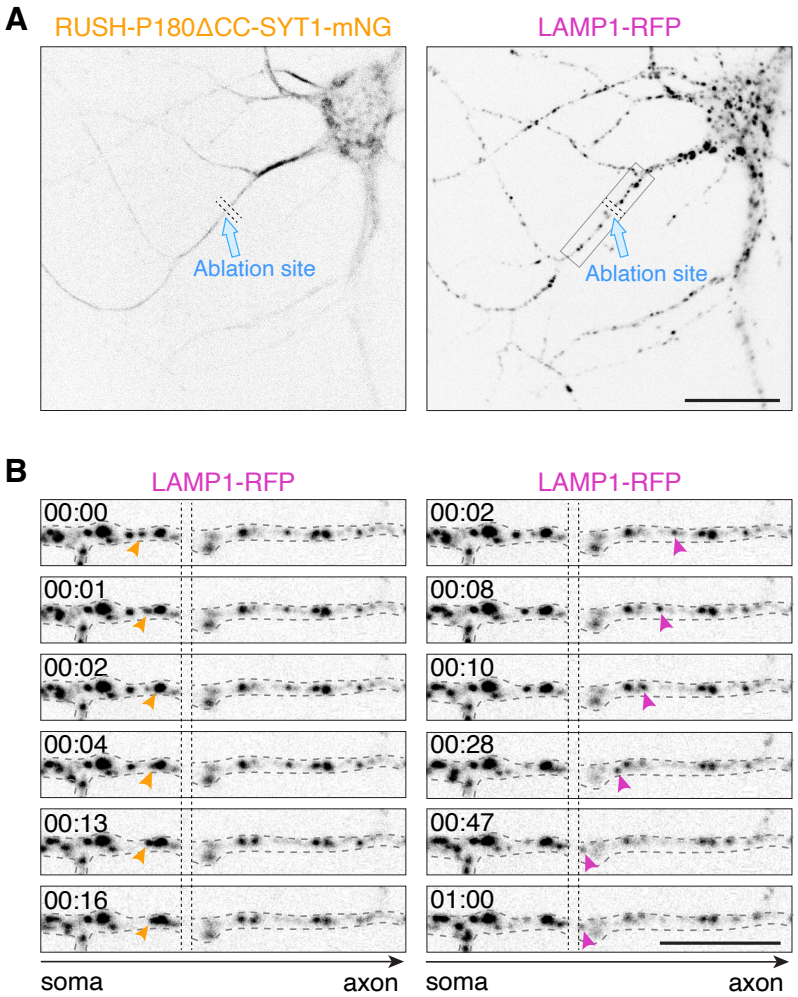
A
RUSH-P180ΔCC-SYT1-mNG
LAMP1-RFP
Ablation site
Ablation site
B
LAMP1-RFP
LAMP1-RFP
00:00
00:01
00:02
00:04
00:13
00:16
00:02
00:08
00:10
00:28
00:47
01:00
soma
axon
soma
axon

Figure S5

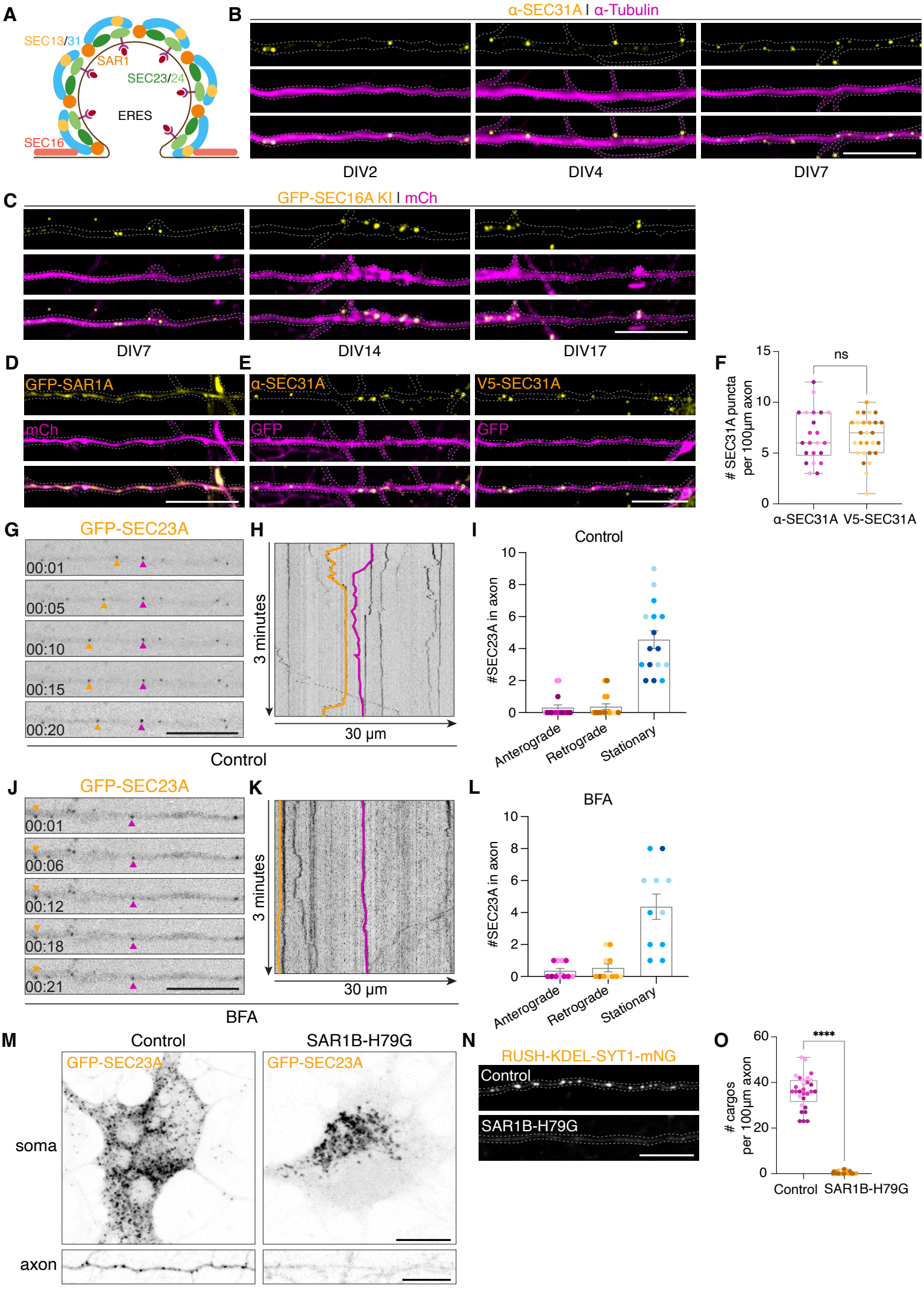
A
SEC13/31
SAR1
SEC23/24
ERES
SEC16
B
α-SEC31A | α-Tubulin
DIV2
DIV4
DIV7
C
GFP-SEC16A KI | mCh
DIV7
DIV14
DIV17
D
GFP-SAR1A
mCh
E
α-SEC31A
GFP
V5-SEC31A
GFP
F
ns
SEC31A puncta per 100µm axon
α-SEC31A
V5-SEC31A
G
GFP-SEC23A
00:01
00:05
00:10
00:15
00:20
H
3 minutes
30 µm
Control
I
Control
#SEC23A in axon
Anterograde
Retrograde
Stationary
J
GFP-SEC23A
00:01
00:06
00:12
00:18
00:21
K
3 minutes
30 µm
BFA
L
BFA
#SEC23A in axon
Anterograde
Retrograde
Stationary
M
Control
SAR1B-H79G
GFP-SEC23A
GFP-SEC23A
soma
axon
N
RUSH-KDEL-SYT1-mNG
Control
SAR1B-H79G
O
****
cargos per 100µm axon
Control
SAR1B-H79G

Figure S6

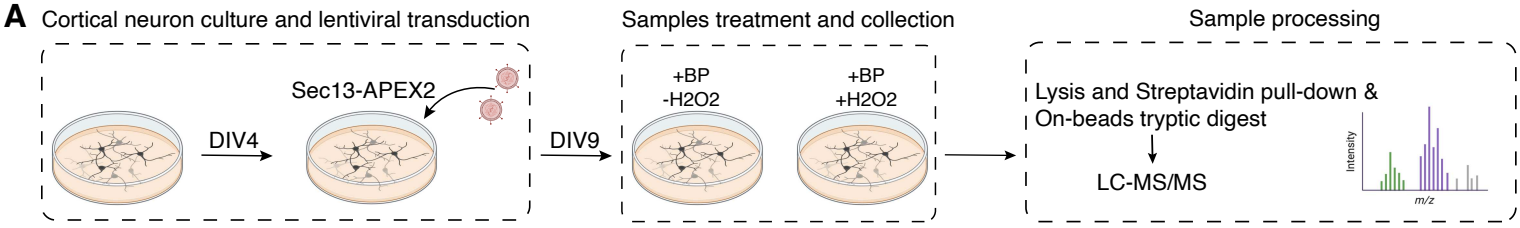
A
Cortical neuron culture and lentiviral transduction
Sec13-APEX2
DIV4
DIV9
Samples treatment and collection
+BP
-H2O2
+BP
+H2O2
Sample processing
Lysis and Streptavidin pull-down &
On-beads tryptic digest
LC-MS/MS
Intensity
m/z

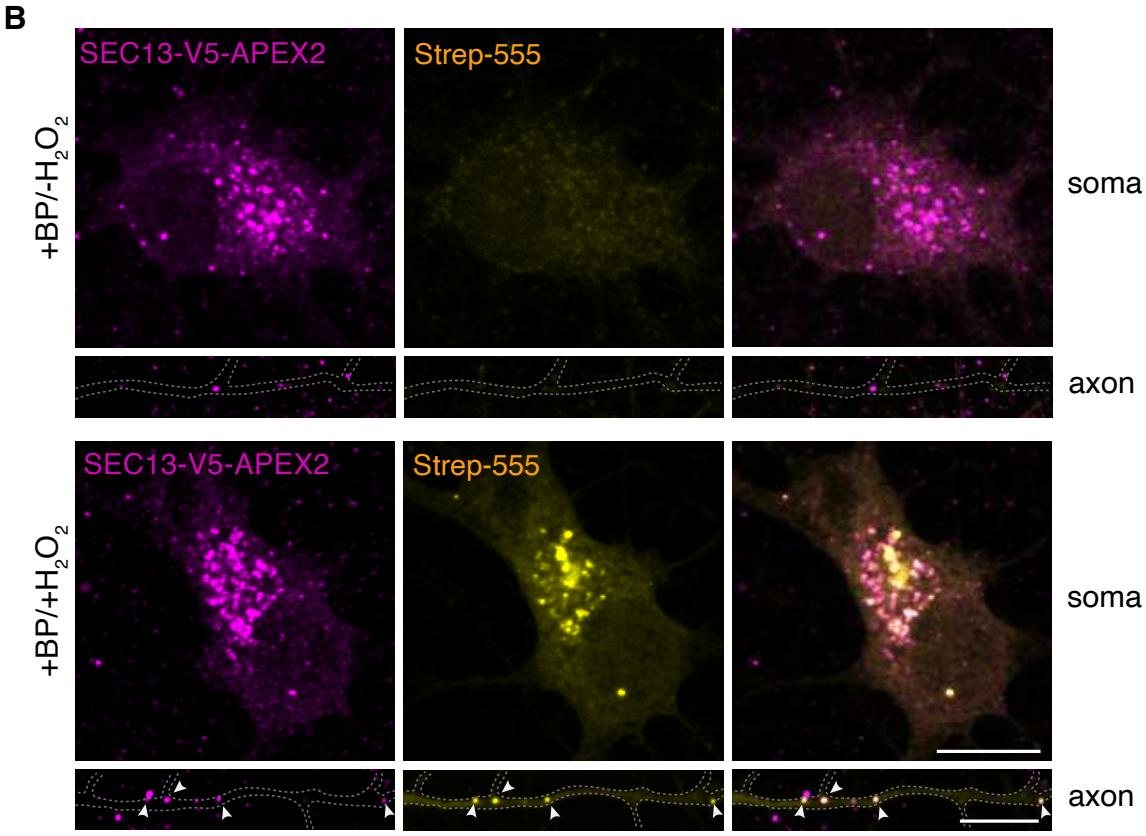
B
SEC13-V5-APEX2
Strep-555
+BP/-H2O2
+BP/+H2O2
soma
axon

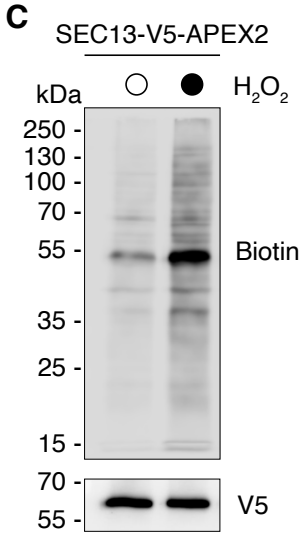
C
SEC13-V5-APEX2
kDa
H2O2
250
130
100
70
55
35
25
15
Biotin
V5

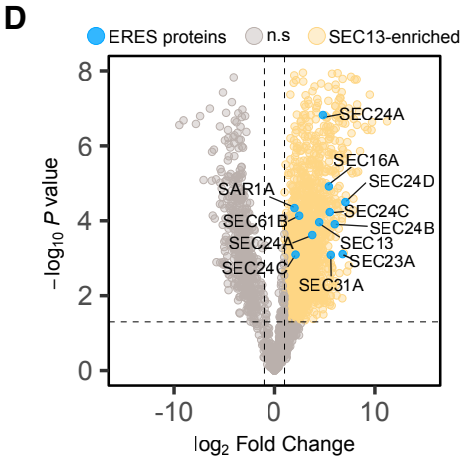
D
ERES proteins
n.s
SEC13-enriched
SEC24A
SEC16A
SEC24D
SAR1A
SEC24C
SEC61B
SEC24B
SEC24A
SEC13
SEC23A
SEC24C
SEC31A
−log10 P value
log2 Fold Change

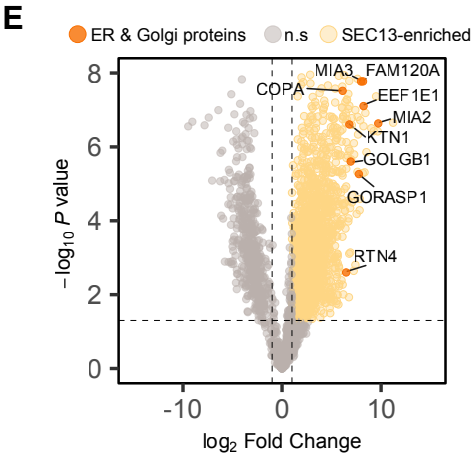
E
ER & Golgi proteins
n.s
SEC13-enriched
MIA3
FAM120A
COPA
EEF1E1
MIA2
KTN1
GOLGB1
GORASP1
RTN4
−log10 P value
log2 Fold Change

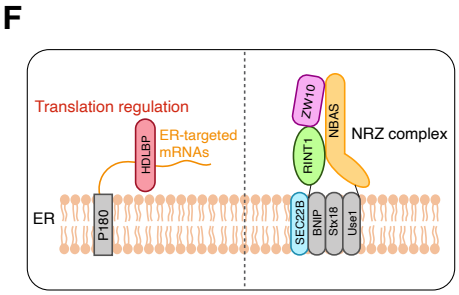
F
Translation regulation
ER-targeted
mRNAs
HDLBP
ZW10
NBAS
NRZ complex
RINT1
ER
P180
SEC22B
BNIP
Stx18
Use1

Figure S7

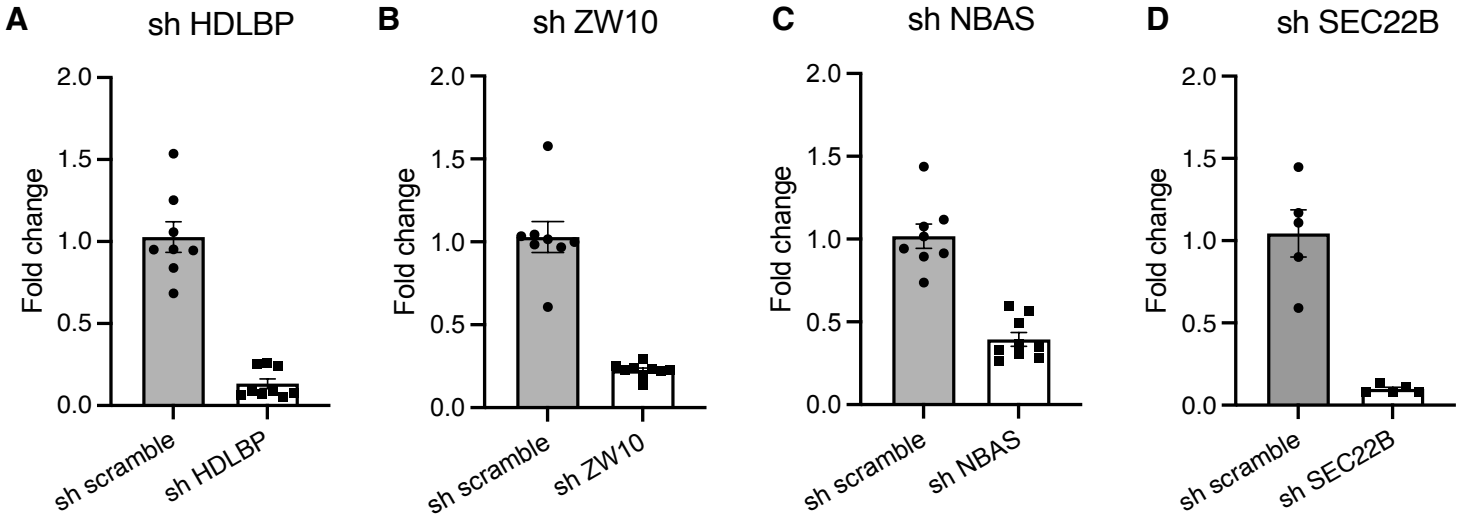
A
sh HDLBP
B
sh ZW10
C
sh NBAS
D
sh SEC22B
Fold change
2.0
1.5
1.0
0.5
0.0
sh scramble
sh HDLBP
sh ZW10
sh NBAS
sh SEC22B